2. The Results of Space Research of the Institutes in 2008-2009

2.1. The Results of the Completed Flight Scientific Programmes of Investigation and Observation

2.1.1. Space Research Institute of the RAS

2.1.1.1. Nature of the Galactic ridge X-ray emission.

Earlier, in our works in 2006-2008 it was shown that the map of the Galactic ridge X-ray emission (a puzzling emission, which have all properties of extremely hot plasma, but according to our knowledge of the Galaxy, can not be kept within the galactic disk) well traces the distribution of stars in the Galaxy. Study of statistics of X-ray sources in the vicinity of the Sun allowed us to make an estimate of contribution of known types of sources (accreting white dwarfs and active stars) and to show that the Ridge emission can be created by these sources. The key experiment which was made to prove or disprove our hypothesis was the ultra-deep survey of the sky area close to the Galactic center (Chandra Bulge Field, CBF), performed by CHANDRA observatory in 2008. We have analized all obtained data and confirmed our previous claims. In particular:We have detected discrete galactic sources with surface densities as high as 1e5 per sq.deg. We have resolved 88 +/-12 % of emission at energies 6-7 keV into contribution of discrete sources, detected in the survey. We have shown that the number-flux function of detected sources agrees well with the that predicted basing on our knowledge of X-ray sources in the Solar vicinity. This allows us to claim that the stellar sources, contributing to the ridge emission is not very young.

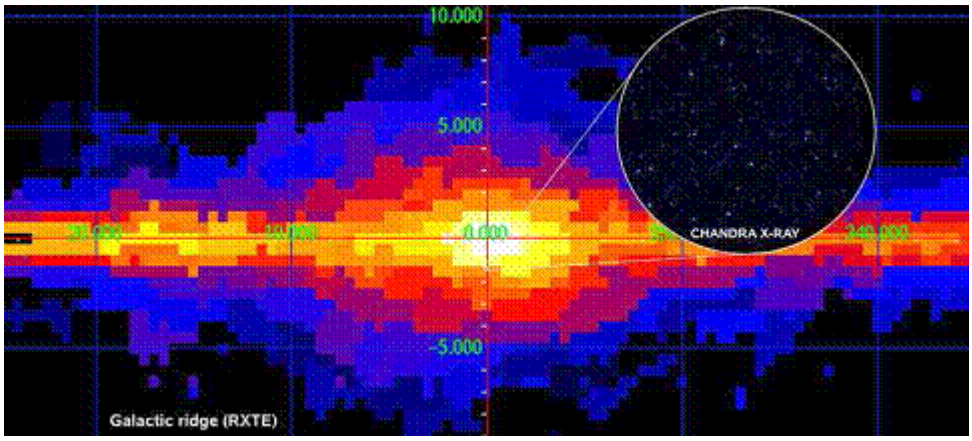

Fig.1.

These results are presented in:

M. Revnivtsev, S. Sazonov, E. Churazov, W. Forman, A. Vikhlinin, R. Sunyaev, "Discrete sources as the origin of the Galactic X-ray ridge emission", 2009, Nature, v. 458, p. 1142

2.1.1.2. The estimation of the parameters of the "Dark Energy" equation of state

In 2009, international group of scientists led by researches from the Space Research Institute has presented results of the Dark Energy nature study based on the growth rate of the large scale structure in the Universe. The deceleration of the growth of clusters of galaxies during the last few billions of years was measured reliably for the first time. The phenomenon provides a new prove of

the existence of the Dark Energy in the Universe and allows to improve its empirical properties significantly (~2 times). For instance, the joint analysis of the X-ray data with the data from cosmic microwave background experiments and super nova Ia data has nailed the errors of the Dark Energy equation of state at the 5% level. The measured equation of state parameter, w0 =-0.99+-0.045, is in agreement with the expected value for the Einstein's cosmological constant (w0 = -1). It is interesting to note also, that the given measurements are very close to the boundary of the w0 range of values corresponding to Dark Energy density growth resulting in the destruction of the large structure in future (so called "Big Rip").

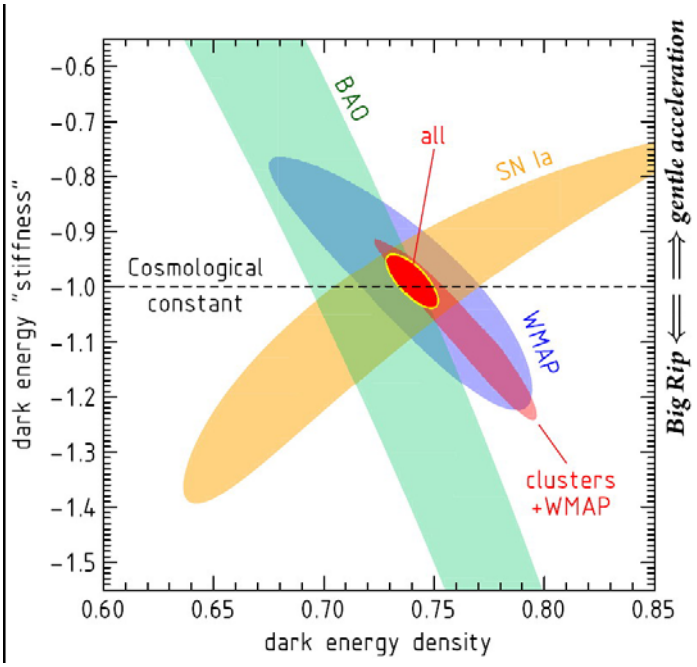

Fig.2. Constraints on the value of Dark Energy equation of state. The values inferred from different methods are shown by different colors. The red region with a gold contour shows the value obtained in joint analysis of all experimental data. The dashed line corresponds to Einstein's cosmological constant.

These results are presented in:

A. Vikhlinin, R. A. Burenin, H. Ebeling, W. R. Forman, A. Hornstrup, C. Jones, A. V Kravtsov., S. S. Murray, D. Nagai, H. Quintana, A. Voevodkin, ``Chandra Cluster Cosmology Project. II. Samples and X-Ray Data Reduction", The Astrophysical Journal, v. 692, p. 1033 (2009)

A. Vikhlinin, A. V. Kravtsov, R. A. Burenin, H. Ebeling, W. R. Forman, A. Hornstrup, C. Jones, S. S.Murray, D. Nagai, H. Quintana, A. Voevodkin, ``Chandra Cluster Cosmology Project III: cosmological parameter constraints", The Astrophysical Journal, v. 692, p. 1060 (2009)

F. Schmidt, A. Vikhlinin, W. Hu, «Cluster constraints on f(R) gravity», Physical Review D, v. 80, id. 083505

Sun, G. M. Voit, M. Donahue, C. Jones, W. Forman, and A. Vikhlinin, «Chandra Studies of the X-Ray Gas Properties of Galaxy Groups», The Astrophysical Journal, v. 693, p. 1142

A. Vikhlinin, «Studies of Dark Energy with Chandra», Chandra's First Decade of Discovery, Proceedings of the conference held 22-25 September, 2009 in Boston, MA. Edited by Scott Wolk, Antonella Fruscione, and Douglas Swartz

2.1.1.3. Measuring the non-thermal pressure in early-type galaxy atmospheres

The distributions of stars and hot (tens of millions Kelvins) gas, observed in X-ray band, trace the properties of the gravitation potential wells both of elliptical galaxies and central galaxies of groups and clusters of galaxies. The gravitation potentials of galaxies NGC 4486 (M87) and NGC 1399 unfired from X-ray and optical data are compared. The comparison shows that the joint contribution of the cosmic rays, magnetic fields, and micro-turbulence is approximately 10-20% of

the thermal pressure. It put constraints not only on the cosmic rays energy density at present time but also onto the evolution of the hot gas if the cosmic ray protons evolve adiabatically with a suppressed diffusion into surrounding space.

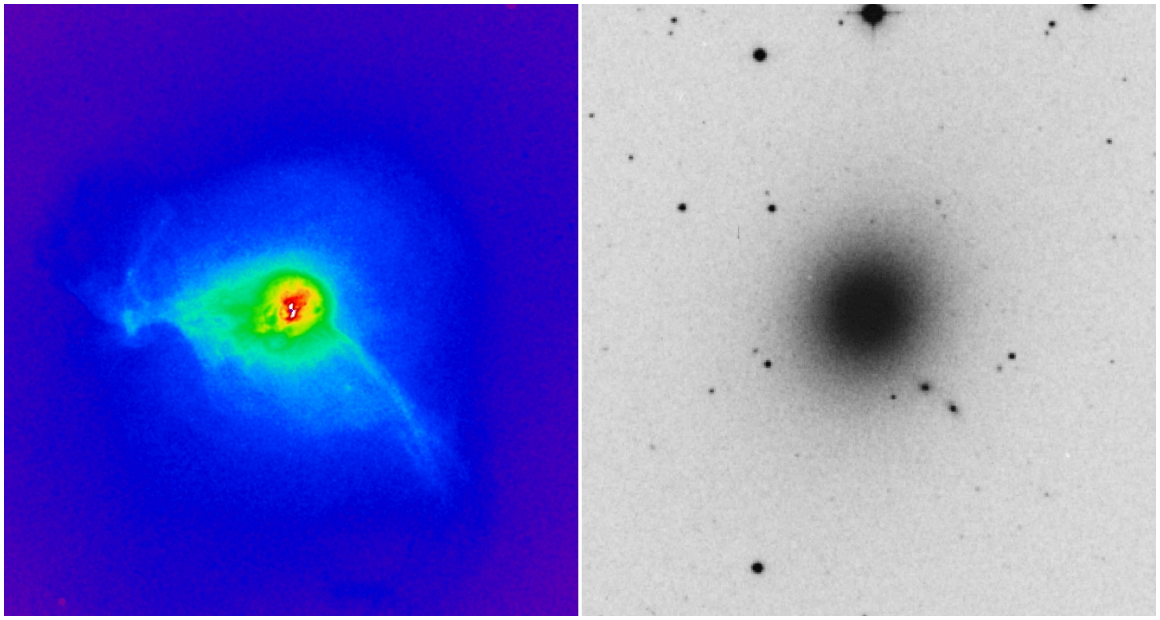

Fig.3. X-ray (left) and optical (right) images of the galaxy M87. The comparison of the stellar and gas distributions in the joint gravitation potential well allows to measure the contribution of the non thermal component into the total gas pressure.

Churazov E., Forman W., Vikhlinin A., Tremaine S., Gerhard O., Jones C., 2008. "Measuring the non-thermal pressure in early-type galaxy atmospheres: a comparison of X-ray and optical potential profiles in M87 and NGC 1399." MNRAS, 388, 1062-1078.

2.1.1.4. Discovery of oprtical afterglows New SGR and bright GRB as a result of creation and support observational network of cosmic gamma-ray bursts on the telescopes in CIS

In the frame of the network of telescopes in CIS the observations of localization regions for 28 GRB were done. 19 of them were made in the first night after GRB? For 12 of them the afterglows were observed. GCN circulars were published (http://gcn.gsfc.nasa.gov/gcn3_archive.html)

GCN: ## 8455 8461 8576 8558 8576 8590 8594 8596 8608 8615 8626 8630, 8175, 8160, 8105, 8094, 7976, 7975, 7891, 7890, 7887, 7883, 7857, 7833, 7739, 7655, 7556, 7534, 7519, 7401, 7400, 7333, 7332, 7331, 7241, 7187.
Observations of telescope BTA (SAO RAN) and ZTSH (Crimea) register and confirm optical component of new (fifth) soft gamma repeater SGR 0501+4516.
GCN circ. #8160, GCN SGR 0501+4516: Detection of possible optical counterpart, T. Fatkhullin (SAO-RAS Nizhnij Arkhyz), A. de Ugarte Postigo (ESO Santiago), A. J. Castro-Tirado, J. Gorosabel and M. Jelínek (IAA-CSIC Granada), V. Sokolov (SAO-RAS), S. Guziy (Nikolaev State Univ.), A. Pozanenko (IKI-RAS Moscow), E. Sonbas (Cukurova Univ.) and D. Pérez-Ramírez (U. Leicester).
GCN circ. #8461, SGR 0501+4516: optical observations in August, V. Rumyantsev, S. Artemenko (CrAO), A. Pozanenko (IKI), A. J. Castro-Tirado (IAA-CSIC Granada).
The optical afterglow for GRB 081126 was discovered (telescope TC-600, Terscol) and later confirmed by observations on foreign telescopes.

GCN circ. #8858, GRB 081126: optical observations, Andreev M., Sergeev A., (Terskol Branch of Institute of Astronomy), A. Pozanenko (IKI)

A.S.Pozanenko cand of sci. 333-45-88 apozanen@iki.rssi.ru

2.1.1.5. Research of magnetorotational supernova explosion for the different initial parameters.

The numerical simulation of the magnetorotational supernova explosion was done for the different initial parameters. It was shown that explosion energy grows with the growth of core mass and initial rotational energy. The magnetorotational mechanism allows to get explosion energy 0.5-2.6 10(51) erg.

The Magnetorotational (MR) supernova explosion mechanism in 2D case was simulated for the different initial core masses and initial rotational energy. The simulations were done for initial core mass between 1.2 - 1.7 Sun mass. At the moment of turning on the magnetic field the specific rotational energy was varied in the following limits 0.19x10(19) erg/g - 0.4x10(19) erg/g. It was shown that the MR mechanism allows get explosion energy 0.5-2.6x10(51) erg, which corresponds to observational data. Supernova explosion energy grows when core mass and initial rotational energy grows. The simulations of MR supernova explosion show that the magnetorotational instability (exponential growth of all components of the magnetic field) develops. We are developing the code for the simulation of MR explosions with the new equation of state (Shen et al.).

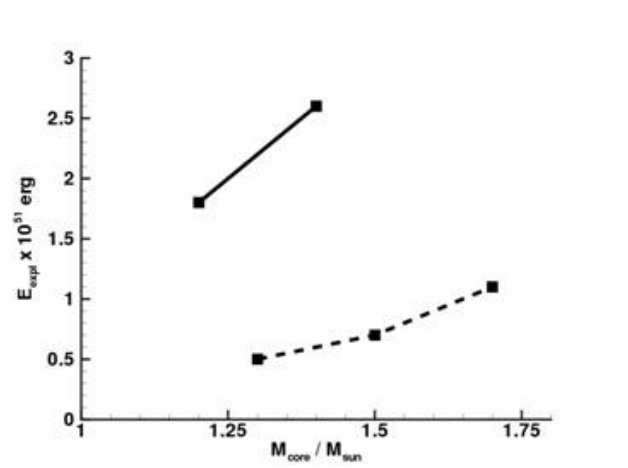

Fig.4. Dependence of MR supernova on initial core mass aand different values of the initial rotational energy before the start of the evolution of the magnetic field. Erot/Mcore ~ 0.39-0.40x10(19) erg/g (solid line) and Erot/Mcore ~ 0.19-0.23x10(19) erg/g (dashed line) (before collapse).

G.S.Bisnovatyi-Kogan doctor of sci. 333-45-88 gkogan@iki.rssi.ru
S.G.Moiseenko doctor of sci. 333-45-88 moiseenko@iki.rssi.ru

Bisnovatyi-Kogan G.S., Moiseenko S.G., Ardeljan N.V. Different magnetorotational sulernovae Astronomy reports v.85, N.12, 1109-1121, 2008

2.1.1.6. SS433 X-ray Spectrum Modelling

X-ray spectrum of SS433 was modelled using Monte Carlo techniques.

X-ray spectrum of SS433 was obtained through numerical simulation.

A model of X-ray emitting region was created based on observational evidence.Also, a code was developed allowing Monte Carlo modelling of the source's X-ray spectrum. Simlations resulted in SS433 spectrum in the range 3-100 keV. Comparison of the model spectrum with INTEGRAL data allows to infer physical properties of the source. The work is completed, the paper about simulations is accepted to Monthly Notices of the Royal Astronomical Society.

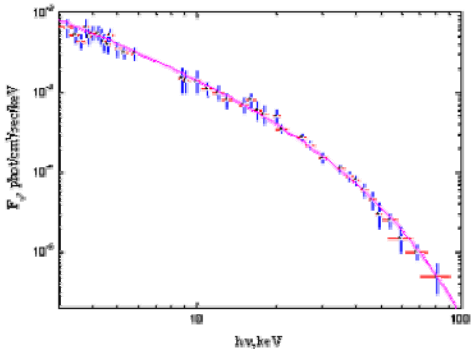

Fig.5. The figure shows comparison of simulations with INTEGRAL observational data.

G.S. Bisnovatyi-Kogan, Sc.D., 333-45-88 gkogan@iki.rssi.ru

Yu.M. Krivosheyev, Ph.D. stud., 333-45-88 krivosheev@iki.rssi.ru

Yu.M. Krivosheyev, G.S. Bisnovatyi-Kogan, A.M. Cherepashchuk and K.A. Postnov “Monte-Carlo simulations of the broadband X-ray continuum of SS433”, Monthly Notices of the Royal Astronomical Society (accepted)

2.1.1.7. Gravitational lensing by gravitational wave

Non-zero shift of photon trajectory as a result of gravitatinal lensing by gravitational wave.

Gravitatinal lensing by gravitational wave was investigated. It was found that though the initial and final photon momentum dirctions coincide, a shift between the initial and final trajectories occur. The value of the shift was calculated analytically for plane gravitational wave pulse. Observational estimates were made.

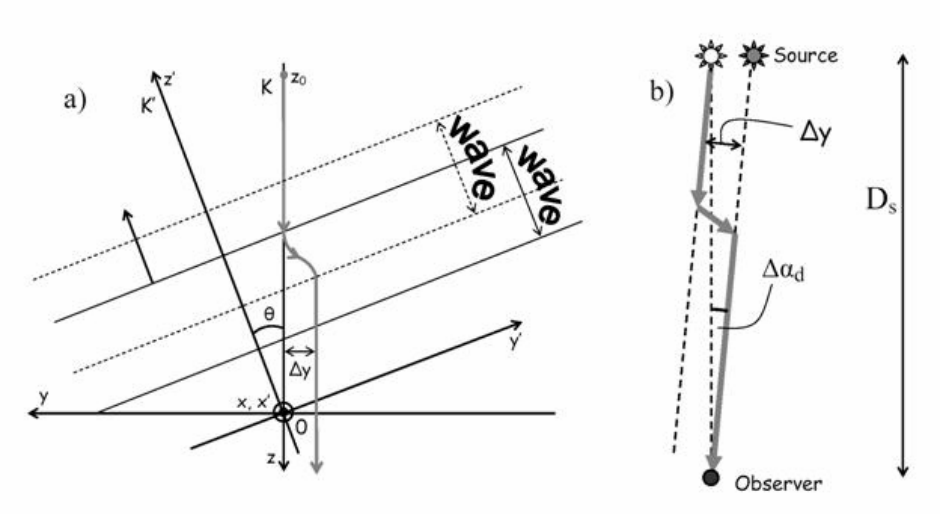

Fig.6. a) shift of photon trajectory as a result of lensing, b) observational effect, misplacement of the source's angular position.

G.S. Bisnovatyi-Kogan, Sc.D., 333-45-88 gkogan@iki.rssi.ru

O.Yu. Tsupko, Ph.D., 333-45-88 tsupko@iki.rssi.ru

Bisnovatyi-Kogan G.S. and Tsupko O.Yu., Gravitation and Cosmology, Gravitational lensing by gravitational waves, No. 3 (55), 226-229. 2008.

2.1.1.8. Gravitational lensing in plasma

A model of gravitational lensing in plasma was developed. Formulas for photon deflection angle in plasma are derived. If a gravitational lens is surrounded by plasma, photon trajectory is dependent on its frequency because of plasma's dispersive properties. It was demonstrated that even in the case of homogenious plasma the lensing angle depends on the photon's frequency, it leads us to conclusion that gravitational lens acts like gravitational radiospectrometer. An analytical formula was obtained for lensing angle in Schwarzschild space-time in homogenious plasma. Possible observational effects are discussed, which are at their strongest when the photon frequency approaches plasma frequency, corresponding to very long radiowaves.

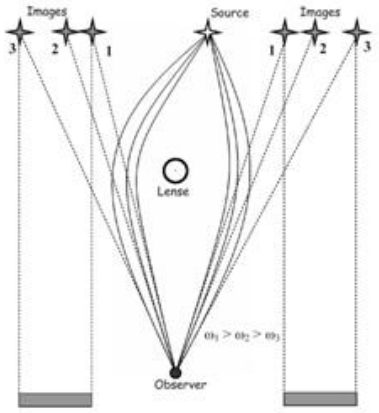

Fig.7. Lensing of point source by point Schwarzschild lens. Instead of two images in vacuum case we observe two linear images. Pairs of images, corresponding to equal photon frequency have the same numbers. Number 1 pair of images correspond to vacuum case.

G.S. Bisnovatyi-Kogan, Sc.D., 333-45-88 gkogan@iki.rssi.ru
O.Yu. Tsupko, Ph.D., 333-45-88 tsupko@iki.rssi.ru
Bisnovatyi-Kogan G.S. and Tsupko O.Yu., Gravitation and Cosmology, Gravitational radiospectrometer, in press.

2.1.1.9. Dynamical stabilization of non-spherical bodies against unlimited collapse

We solve equations of approximate Newtonian dynamics of self-gravitating non-rotating spheroid after its loss of dynamical stability. We obtain that compression to a singularity is possible only in the case of pure spherical collapse, if there are deviations from spherical symmetry, the compression is stopped due to stabilizing effect of nonlinear non-spherical oscillations. In reality, the collapse does not stop due to energy loss to emission, shock wave generation and viscosity. A detailed analysis is performed using Poincare diagram technique. The diagram below shows regions of regular and chaotic oscillations.

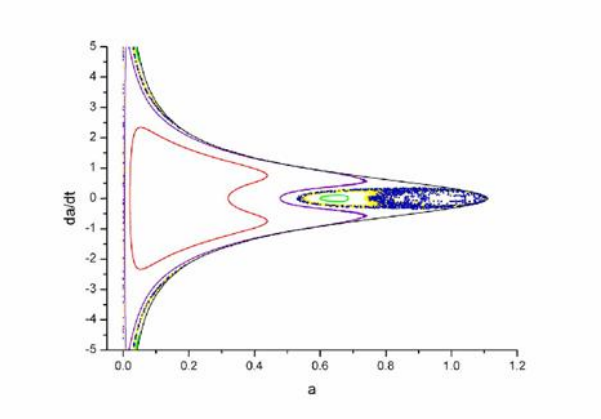

Fig.8. Poincare diagram for spheroid compression with negative total energy and with adiabatic index equal to 4/3. Three regular and two chaotic trajectories are presented.

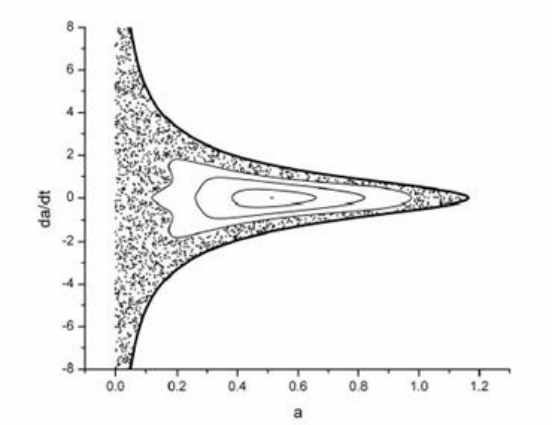

Fig.9. Poincare diagram for spheroid compression with total negative energy and with adiabatic index equal to 6/5. Four regular and one chaotic trajectories are presented.

G.S. Bisnovatyi-Kogan, Sc.D., 333-45-88 gkogan@iki.rssi.ru
O.Yu. Tsupko, Ph.D., 333-45-88 tsupko@iki.rssi.ru
G.S. Bisnovatyi-Kogan, O.Yu. Tsupko Dynamic stabilization of non-spherical bodies against unlimited collapse Mon. Not. R. Astron. Soc. 386, 1398–1403 (2008)

2.1.1.10. Accretion on the magnetize black hole.

Accretion of matter on the black hole with large scale magnetic field was investigated. The disc is considered as turbulent with radiative outer layers, where currents are generated when the matter moves towards the black hole and large scale magnetic field is increasing. The approximate solutions was found when the conductivity is approximated by continuous function which grows rapidly near disc surface.

G.S.Bisnovatyi-Kogan professor 333-45-88 gkogan@iki.rssi.ru
R.V.E. Lovelace, D.M. Rothstein, G.S.Bisnovatyi-Kogan, Advection/Diffusion of Large Scale Magnetic Field in Accretion Disks. Proc. Conf.
Protostellar Jets in Context 7-12 July 2008, island of Rhodes, Greece. 5 pages

2.1.1.11. Observations of gamma-ray bursts

Observations of GRB 081028 were made on ZTSH(Crimea) and multicolor photometry was made starting from 15 minutes after GRB and it lasted for 5 days. The maximum in the afterglow was found in the interval of 1 day while the optical radiation immediately after GRB was not registered. Observation of this event undoubtedly will help to the understanding of the nature <dark> GRB. i.e. GRBs with anomalously small relation of fluxes in optical and X-ray bands.
Obseravtions of the following GRBs were made: GRB 080319b, GRB 061126, GRB 060526. GRB920925C
Extended radiation of the short gamma ray burts SPI-ACS INTEGRAL., P.MInaev, A.Pozanenko, V.Loznikov,

A.S.Pozanenko cand of sci. 333-45-88 apozanen@iki.rssi.ru

2.1.1.12. Diffusion and heavy metals abundance in the ICM in clusters of galaxies

The phenomenon of elements diffusion in the ICM in clusters of galaxies is revisited. The diffusion is driven by gravity, concentration and temperature gradients. The former, sedimentation of heavy elements under the action of gravity, has been appreciated long ago. On the other hand the thermal diffusion driven by temperature gradients has been traditionally excluded from the consideration in clusters of galaxies. The effect of the latter is to evacuate heavy and highly charged species from the cool regions of the gas. We consider the full problem of diffusion based on the Burgers' equations and demonstrate that the temperature gradients present in clusters of galaxies may successfully compete with gravity, evacuating metals from cooler regions. Under the combined action of gravity and temperature gradients, complicated metallicity profiles with several peaks and depressions may be formed. For a typical cool core cluster, the thermal diffusion may significantly reduce and even reverse the gravitational sedimentation of metals, resulting in the depression in their abundance in the core. This may have implications for diagnostics of the low-temperature plasma in the centers of clusters of galaxies.

P.Shtykovskiy, M.Gilfanov, "Thermal diffusion in the intergalactic medium of clusters of galaxies", 2010, MNRAS, 401, 1360

2.1.1.13. Aperiodic time variability of emission of accreting binaries in X-ray and in optical energy ranges and its usage for determination of physical parameters of the accreting objects.

We studied the power spectra of aperiodic variability of accreting binaries with truncated accretion disks (in particular, accreting pulsars). We have shown that all these sources have a characterictic break in the power spectra of their time variability, which we show is a sign of transition of the accreting matter from the disk flow to the magnetospheric flow in the binary system. We have shown that the value of the break frequency can be used to deduce the inner radius of the truncated accretion disk, which is in turn can be used to estimate the magnetic fields of the accreting compact objects (neutron stars and white dwarfs)

Revnivtsev M., Churazov E., Postnov K., Tsygankov S., 2009, Astronomy & Astrophysics, 507, 1211, "Quenching of the accretion disk strong aperiodic variability at the magnetospheric boundary",

2.1.1.14. Internal structure of the active galactic nuclei, basing on study of a sample of INTEGRAL detected AGNs.

All sky survey, which INTEGRAL observatory continues to perform (Krivonos et al. 2007), allowed us to obtain a unique sample of nearby AGNs, practically free from biases due to absorption in the line of sight. This statistically full sample of AGN allows us to make systematic study of AGN characteristics as a function of their luminosity, mass of their black hole, their mass accreting rate etc. This, in turn, gives us information about the structure of the dusty torus around the black hole, and the structure of the region creating narrow emission lines.

In course of this project we have obtained ana analized the number of observations of AGNs in optical (telescope RTT150) and infrared (SPITZER orbital observatory) spectral bands. We have detected tight correlation of their infrared and hard X-ray fluxes. We have concluded that the hot coronae of AGNs contain significant and almost constant fraction of the bolometric luminosity of accreting supermassive black holes. At the same time, the typical opening angle of the dusty torus around the black hole, strongly depends on AGN luminosity. We have not detected strong correlation between fluxes of AGNs in narrow emission lines and their fluxes in hard X-rays.

These results are presented on conference “The Extreme Sky: Sampling the Universe above 10 keV“, Otranto, Italy, Oct.13-17, 2009.

2.1.1.15. CI Cam outburst.

We have computed a spherically symmetric model for the interaction of matter ejected during the outburst of a classical nova with the stellar wind from its optical component.This model is used to describe the intense X-ray outburst (the peak 3-20 keV flux was ~2 Crab) of the binary system CI Camelopardalis in 1998. According to our model, the stellar wind from the optical component heated by a strong shock wave produced when matter is ejected from the white dwarf as the result of a thermonuclear explosion on its surface is the emission source in the standard X-ray band. Comparison of the calculated and observed time dependences of the mean radiation temperature and luminosity of the binary system during its outburst has yielded very important characteristics of the explosion. We have been able to measure the velocity of the ejected matter immediately after the onset of the explosion for the first time: it follows from our model that the ejected matter had a velocity of ~2700 km/s even on 0.1-0.5 day after the outburst onset and it flew with such a velocity for the first 1-1.5 day under an external force, possibly, the radiation pressure from the white dwarf. Subsequently, the matter probably became transparent and began to decelerate. The time dependence of the mean radiation temperature at late expansion phases has allowed us to estimate the mass of the ejected matter, ~ 10^{-7}-10^{-6} Msun. The mass loss rate in the stellar wind required to explain the observed peak luminosity of the binary system during its outburst has been estimated to be dM/dt~(1-2)*10^{-6}Msun/yr.

Filippova E., Revnivtsev M., Lutovinov A. "Diagnostics of the early explosion phase of a classical nova using its X-ray emission: A model for the X-ray outburst of CI Camelopardalis in 1998". Astronomy Letters 34,797 (2008)

The results of the timing analysis of ten bright X-ray pulsars (with fluxes >100 mCrab in the 20-100 keV energy band) that fell into the INTEGRAL field of view from 2003 to 2007 were reviewed in details. The dependence of the pulse profile on the energy and intrinsic source luminosity has been investigated; an especial attention has been paid for the searching of changes in the pulse profile near the cyclotron frequency. The dependence of the pulsed fraction on the X-ray pulsar luminosity and energy band has been studied in detail for the first time. The evolution of pulsars' spectral parameters at different luminosities was a subject of a special interest. The analysis of the data obtained with the RXTE observatory during a powerful outburst of the X-ray pulsar V0332+53 in 2004-2005 was presented in Tsygankov et al. (2010). Observational data covering the outburst brightening phase were analyzed in detail for the first time. A comparison of source parameters and their evolution during the brightening and fading phases shows no evidence for any hysteresis behavior. It was found that the dependences of the energy of the cyclotron absorption line on the luminosity during the brightening and fading phases are almost identical. The complete data sequence including the outburst brightening and fading phases made it possible to impose the more stringent constraints on the magnetic field in the source. The pulse profile and pulsed fraction were studied as functions of the luminosity and photon energy.

Lutovinov, A. A.; Tsygankov, S. S. "Timing characteristics of the hard X-ray emission from bright X-ray pulsars based on INTEGRAL data". Astronomy Letters, V. 35, pp.433-456, 2009

Lutovinov A., Tsygankov S. "X-RAY PULSARS: A VIEW FROM CURRENT COSMIC OBSERVATORIES", Proceedings of XXI Rencontres de Blois "Windows in the Universe", 2009

Tsygankov S. S., Lutovinov A. A., Serber A. V. "Completing the puzzle of the 2004-2005 outburst in V0332+53: the brightening phase included". MNRAS, v. 401, pp. 1628-1635, 2010

2.1.1.16. Measurements and synthesis of Cosmic X-ray background

In order to verify the widely accepted but not fully proved hypothesys of formation of CXB as a cumulative emission of all active galactic nuclei (AGN) in the Universe we have performed measurements of all nearby AGNs in broad energy band 3-300 keV. We have constructed the spectrum of combined emission of AGNs in the local (z<0.1) Universe. The resulted spectrum has clear maximum at energies 50-80 keV and rollovers at energies lower than 20 keV and at energies higher than 100-200 keV. Shape and the amplitude of the obtained spectrum well agrees with an assumption that intrinsic spectrum of AGNs remained universal for AGNs at all redshifts, but their cumulative luminosity density changed with time. Results strongly support the idea, that the hard X-ray CXB indeed is constructed of emission of a large number of AGNs.

Analysis of mission-livetime RXTE archive allowed us to construct the high quality map of the CXB, average over large angular scales. We have detected 2% variations of the CXB on angular scales as large as 20-40 deg. These variations correlate with local large scale structure of the Universe, which allowed us to make an estimate of the total volume luminosity density of the nearby Universe in energy band 2-10 keV (8+/-4)10^38 erg/sec/Mpc^3. Detected variations have hard spectral shape, similar that of CXB. This indicates that the contribution of emission of normal (non-active) galaxies and clusters of galaxies to the total emissivity of the local Universe is minor, does not exceed ~15%. Main part of the detected anysotropy is caused by emission of low luminosity AGNs.

In course of measuring the CXB spectrum with the help of INTEGRAL observations of Earth (used as a shiled to cover the fields of view of INTEGRAL instruments from the CXB flux), we have calculated the reflection of CXB emission from the Earth atmosphere in energy band 1-1000 keV, taking into account chemical abundances, compton scattering and fluorescent X-ray emission. The method of calculations was also applied to estimate the reflected emission from the Mars and the Sun. It is predicted that these objects can be used by future hard X-ray instruments for calibration purposes.

Sazonov S., Krivonos R., Revnivtsev M., Churazov E., Sunyaev R. "Cumulative hard X-ray spectrum of local AGN: a link to the cosmic X-ray background" Astronomy and Astrophysics 482, 517 (2008)

Revnivtsev M., Molkov S., Sazonov S. "Large-scale variations of the cosmic X-ray background and the X-ray emissivity of the local Universe" Astronomy and Astrophysics 483, 425 (2008)

Churazov E., Sazonov S., Sunyaev R., Revnivtsev M. "Earth X-ray albedo for cosmic X-ray background radiation in the 1-1000 keV band" Monthly Notices of the Royal Astronomical Society 385, 719 (2008)

2.1.1.17. Ultra deep observation of the Galaxy in X-ray energy band

In 2008 CHANDRA observatory have finished the long campaign of accumulating the large exposure (1 Msec) on a region close to the Galactic Center (so called Chandra Bulge Field), initiated upon our request. We started to analize the data. As a preliminary work, required to extract maximum information from X-ray data, we have studied this area in infrared spectral band. The main goal of the performed work was to obtain map of the interstellar extinction in the direction of the Chandra Bulge field basing on 2MASS stellar photometry

M.Revnivtsev, R. Burenin, S. Sazonov "Interstellar extinction in the direction of ultra-deep galactic field of CHANDRA observato

2.1.1.18. Formation of current density profile in tilted current sheets

The simple model of strongly tilted sheets (flapping events) in the magnetotail. In accordance with the simple model of slip deformation (vertical differential displacement of neighboring flux tubes), the Jy current density component in the tilted sheet remains constant and equal to that in the horizontal undisturbed sheet. However, a substantial Jz component appears proportional to the local sheet tilt. Slip-type variations, having smaller scale than the full crossing, locally change the tilt and Jz and may thus create a variety of non-classical (bifurcated, asymmetric
etc) current density profiles.
A.A.Petrukovich, W.Baumjohann, R.Nakamura, A.Runov, Formation of current density profile in tilted current sheets Ann. Geophys., 26, 2008, 3669–3676.

2.1.1.19. Tailward and earthward flow onsets observed by Cluster in a thin current sheet

a Cluster survey of the magnetotail during 2001–2007 distribution of plasma flow onsets was investigated, basing on 49 episodes of thin current sheet observations ending with plasma sheet activity onsets. The onsets were defined as flow bursts and/or electric current decrease and/or Bz increase after a period of local quietness (in many cases with signatures of growth phase). Such onsets at 17–20 RE of radial distance were accompanied mainly by tailward flows with negative Bz. At 11–17 RE, earthward flows dominated, except the premidnight sector, where flows of both directions were observed. Tailward velocities were often rather small, within 200–300 km/s. We interpret such tailward flows as reconnection pulses occurring on the closed field lines in the stretched magnetic configuration. Ten activity onsets were not accompanied by plasma flows (faster than 100 km/s). Preonset current density was larger on average in the premidnight and midnight sector in comparison with the postmidnight.
Petrukovich, A. A., W. Baumjohann, R. Nakamura, and H. Reme, Tailward and earthward flow onsets observed by Cluster in a thin current sheet, J. Geophys. Res., 114, A09203, doi:10.1029/2009JA014064, 2009

2.1.1.20. Dipole tilt effects in plasma sheet By: statistical model and extreme values

With 11 years of Geotail measurements we construct a model of plasma sheet By , depending on IMF By , coordinates X, Y , and geodipole tilt angle. At midnight and pre-midnight local times By is positively correlated with tilt (positive in summer). Thus in summer By is shifted towards positive values and in winter towards negative values, so that up to several nT could be added to the IMF influence. The dawn side plasma sheet By generally does not exhibit any tilt dependence, but within 15RE the weaker negative correlation with tilt was revealed. The tilt dependence is just a useful parametrization and several mechanisms actually affecting plasma sheet By were previously suggested. In particular, similar coupling between tilt and IMF By was earlier found in the ionospheric convection patterns. Besides this average response, extreme By (|By |>5 nT, By>IMF By) were often observed (up to 20–25% of cases during solar maximum and in the pre-midnight sector within 20RE). They can not be explained by our statistical model and are preliminary interpreted as an “over-reaction” of the magnetosphere in some individual events. Large By field radically changes dynamics of the current sheet and has to be taken into account during substorm-related studies.
A.A.Petrukovich, Dipole tilt effects in plasma sheet By: statistical model and extreme values Ann. Geophys., 27, 1343–1352, 2009

2.1.1.21. Variability of magnetic field spectra in the Earth's magnetotail

Variability of magnetic fluctuation spectra below 1 Hz in the Earth's plasma sheet using specially selected long observation intervals by Geotail spacecraft is investigated. The spectra can be generally described by a negative power law with two kinks. The range between kinks _0.02–0.2 Hz has the most stable power law index _2.4–2.6. Indices at the lower and the higher frequencies are more variable and generally increase with power of fluctuations. In the sub-second range fluctuations are strongly localized and indices are closer to 3. At the lower-frequency end indices are about 1.5. The lower kink is usually well defined on average spectra and its frequency tends to increase with activity. Combination of spectrum index alpha and fractal dimension delta is expected to follow the Berry relation alpha+2delta =5, but actually is approximately 5.5.

A.A. Petrukovich and D.V. Malakhov, Variability of magnetic field spectra in the Earth's magnetotail, Nonlin. Processes Geophys., 16, 691–698, 2009

2.1.1.22. The boundary layer characteristic

We demonstrate co-existence of the separation of the mutually moving plasma by turbulent barriers with the superdiffusion concentrated plasma jets in the barriers.

Analysis of the Interball and Cluster data demonstrated that the high-latitude turbulent boundary layer over the polar cusps and plasma mantle in the singular point on the magnetopause, represents a kind of barrier (obstacle), which effectively separated moving magnetosheath plasma from that of the stagnant polar cusps.

Simultaneously, the character of dependence of the average squared displacement in the normal direction to the barriers, is compatible with the superdiffusion. The latter is, most probably, carried by the plasma jets, having concentrated kinetic energy density as compared with that of the unshocked solar wind.

This unusual combination of the transport properties in the transport barriers looks to be applicable for the study of the fusion plasma confinement, where the statistical properties of the boundary layers occurred to be rather similar to that of the magnetospheric ones, including the superdiffusion.

Amata E., S.P. Savin, D.Ambrosino, Y. Bogdanova, R. Treumann, M. F. Marcucci, S. Romanov, A.Skalsky, High kinetic energy density jets in the Earth's magnetosheath: a case study. Planetary and Space Science, submitted 2009.

Savin,S.,et al., ROY-A multiscale magnetospheric mission. Planet. Space Sci. (2010), doi: 10.1016 / j.pss.2010.05.001

2.1.1.23. Magneto rotational processes in core collapse supernovae.

The research of magnetohydrodynamical core collapse supernova explosion was continued on the base of 2D numerical simulations with Lagrangean MHD code on triangular grid of variable structure. We debugged 2D MHD code for the equation of state for high temperatures and densities (Shen et al.) for the case when the part of electrons Ye is constant in the matter. For small temperatures the equation of state (Shen et al.) was smoothly interpolated with equation of state and expression for the internal energy of cold matter. We continue debugging of the code for self consistent simulations of the Ye and approximate calculations of neutrino losses. We start to develop the code for the simulations of the neutrino radiative transfer equations by MonteCarlo method for non spherical collapse.

G.S.Bisnovatyi-Kogan doctor of sci.333-45-88 gkogan@iki.rssi.ru
S.G.Moisenko doctor of sci. 333-45-88 moiseenko@iki.rssi.ru

S.G.Moiseenko, G.S.Bisnovatyi-Kogan, N.V.Ardeljan Magnetorotational processes in core collapse supernovae Proseedings of Gamov memorial meeting 2009 Odessa AIP Conference proceedings, 2009, v.1206, pp.282-293

2.1.1.24. Observations of the comet C/2004 Q2

On the basis of our observations of the comet C/2004 Q2 (Machholz) in near infra-red spectral bands it is shown that the substance from a comet surface expires not in the form of a dust and gas, but in the form of fragments which break up to a dust and gas during of one-two days. This result is important from the point of view of an estimation of mass of substance lost by a comet and for understanding of structure of its external layers. The conclusion is drawn about friable character of a external layers of comets, both during the present epoch, and during an epoch of their formation. Taking into account that terrestrial oceans, probably, have resulted from bombardment of the Earth by comets, the hypothesis about stochastic formation on a surface of comets the complex organic molecules, from which the life on the Earth was generated, is formulated. The hypothesis is based on following facts: (1) on surfaces with a friable microstructure in space conditions at low temperature are effectively formed complex organic molecules; (2) their formation is stimulated in many cases with presence of quanta with high energy which are present at the interstellar environment; (3) accruing, at comet formation, the external layer of substance protects the formed molecules from destruction by the same quanta, (4) the big interval of time for formation of complex organic chemistry before its appearing in hothouse conditions on the Earth.

Maslov I.A., IKI, imaslov@iki.rssi.ru

2.1.1.25. Mercury researches

Suggested at the Space research institute (Moscow) and for the first time realized in 1999, the method of observation of the planet Mercury by millisecond expositions became an effective means of obtaining of the resolved images of unknown side of the planet. Using the millisecond expositions method, in 1999-2008 observations at different ground based observatories have been fulfilled. Thousands of electronic photos of the unknown side of Mercury (not covered by shooting from Mariner-10 in 1973-75 and Messenger in 2008) have been collected. Based on the received observant data together with the image processing codes, synthesizing image of the surface of unknown areas have been produced. The synthesized images are comparable to photos obtained from a spacecraft approaching the planet, from distances about 1 million km. In a limited overlapped part they have been compared to photos of the Messenger spacecraft.

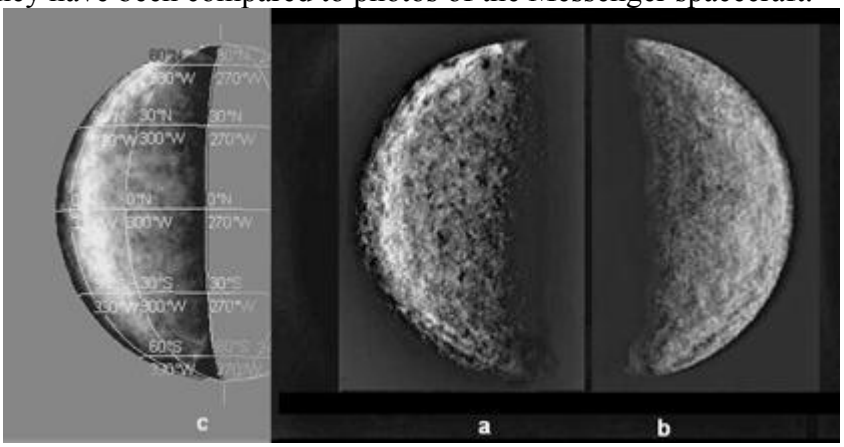

The images obtained allow, with a certain care, to assert, that large details of a relief are asymmetrically distributed on the Mercury surface just as it is observed on other planets of terrestrial group, on the Moon and satellites of giant planets.

Ksanfomality L.V., IKI, ksanf@iki.rssi.ru

2.1.1.26. Research of cosmic GRB

Search and observations of optical afterglows of GRBs in optical band on Russian and foreign telescopes have been performed. The following GRB were observed: GRB090817, GRB081203, GRB 051008, 081028, 081126

A.S.Pozanenko cand of sci. 333-53-66 apozanen@iki.rssi.ru

S. B. Pandey, A. J. Castro-Tirado, M. Jelinek, Atish P. Kamble, J. Gorosabel, A. de Ugarte Postigo, S. Prins, R. Oreiro, V. Chantry, S. Trushkin, M. Bremer, J. M. Winters, A. Pozanenko, Yu. Krugly, I. Slyusarev, G. Kornienko, A. Erofeeva, K. Misra, A. N. Ramprakash, V. Mohan, D. Bhattacharya, A. Volnova, J. Pl, M. Ibrahimov, M. Im, A. Volvach, R. A. M. J. Wijers, (2009), Multi-wavelength observations of the GRB080319B afterglow and the modeling constraints, Astronomy and Astrophysics (2009), 504, 45.

G. Stratta, A. Pozanenko, J-L. Atteia, A. Klotz, S. Basa, B. Gendre, F. Verrecchia, M. Boer, S. Cutini, M. Henze, S. Holland, M. Ibrahimov, F. Ienna, I. Khamitov, S. Klose, V. Rumyantsev, V. Biryukov, D. Sharapov, F. Vachier, S. Arnouts, D.A. Perley, A multiwavelength study of Swift GRB 060111B constraining the origin of its prompt optical emission, (2009) Astronomy and Astrophysics, 503, 783

Melandri, A.; Guidorzi, C.; Kobayashi, S.; Bersier, D.; Mundell, C. G.; Milne, P.; Pozanenko, A.; Li, W.; Filippenko, A. V.; Urata, Y.; Ibrahimov, M.; Steele, I. A.; Gomboc, A.; Smith, R. J.; Tanvir, N. R.; Rol, E.; Huang, K. Evidence for energy injection and a fine-tuned central engine at optical wavelengths in GRB 070419A,(2009), Monthly Notices of the Royal Astronomical Society, Volume 395, Issue 4, pp. 1941

2.1.1.27. Close binaries as GRB sources.

One of the possible mechanism for the explanation of long GRB is Blandford_Zhnaek magnetic mechanism. The numerical simulations confirmed a possibility of the explosion by Blandford_Zhnaek magnetic mechanism, but it requiresveryr large magnetic flux at the black hole horizon about 10^{28}Gcm^2.

It was simulated a possibility of a long GRBs formation due to collision of a compact companion with an ordinary star. In this case it was found a possibility of the formation of a very long living accretion disk (>10 000 c) and very long action of the central machine which can explain slow phase of decreasing of flux, which was observed by Swift.

Magnetic acceleration of ultrarelativistic jets in gamma-ray burst sources Komissarov S.S., Vlahakis N., Königl A., Barkov M.V. 2009 MNRAS 394 1182 Activation of the Blandford-Znajek mechanism in collapsing stars Komissarov S.S., Barkov M.V. 2009 MNRAS 397 1153

M.V.Barkov cand. of sci. 333-45-88 barmv05@gmail.com

2.1.1.28. Radiation transfer in presence of strong gravitation

For the first time the profiles of the lines were calculated for spherically symmetrical relativistic ejections in the strong gravitational field of compact objects. It was shown that the strong gravitational field leads to the formation of three types of profiles: modified P-Cygni, saw-toothed, and W-type.

The code for 3D simulation of radiation transfer in X-ray spectral lines was developed. The X-ray lined spectra were calculated for 2.5 dimensional radiative -hydrodynamic models of ejections from a gas-dust torus in AGNs.

Dorodnitsyn, A., Kallman, T., An Axisymmetric Hydrodynamical Model for the Torus Wind in Active Galactic Nucleus. III. Spectra from Three-Dimensional Radiation Transfer Calculations
ApJ 2009, 703, 1797
Dorodnitsyn, A. Gravitationally distorted P Cygni profiles from outflows near compact objects
MNRAS, 2009, Volume 393, Issue 4, pp. 1433-1448
A.V.Dorodnitsyn Cand. of sci. 333-45-88 dora@iki.rssi.ru

2.1.1.29. Gravitational Lensing in Plasma

A model of gravitational lensing in plasma was developed. If a gravitational lens is surrounded by plasma, photon trajectory is dependent on its frequency because of plasma's dispersive properties. It was demonstrated that even in the case of homogenious plasma the lensing angle depends on the photon's frequency, it leads us to conclusion that gravitational lens acts like gravitational radiospectrometer. An analytical formula was obtained for lensing angle in Schwarzschild space-time in homogenious plasma. Possible observational effects are discussed, which are at their strongest when the photon frequency approaches plasma frequency, corresponding to very long radiowaves.

G.S. Bisnovatyi-Kogan, O.Yu. Tsupko, «Gravitational radiospectrometer», Gravitation and Cosmology, v. 15. no. 1, p. 20, 2009.
G.S. Bisnovatyi-Kogan, O.Yu. Tsupko, «Relativistic images due to Schwarzschild gravitational lensing», Gravitation and Cosmology, v. 15, no. 2, p. 184, 2009.
G.S. Bisnovatyi-Kogan, Sc.D., 333-45-88 gkogan@iki.rssi.ru
O.Yu. Tsupko, Ph.D., 333-45-88 tsupko@iki.rssi.ru

2.1.1.30. SS433 X-ray Spectrum Modelling

A model of emission region of Galactic microquasar SS433 was created based on observational evidence. A code was developed for Monte Carlo modelling of the source's observational X-ray spectrum. Based on this model various parameters of the emission region were inferred through comparison of simulations with INTEGRAL data. Energetic balance of SS433 jet was also investigated.

Yu.M. Krivosheyev, G.S. Bisnovatyi-Kogan, A.M. Cherepashchuk and K.A. Postnov, “Monte-Carlo simulations of the broadband X-ray continuum of SS433”, Monthly Notices of the Royal Astronomical Society, 394, 1674-1684 (2009)
G.S. Bisnovatyi-Kogan, Sc.D., 333-45-88 gkogan@iki.rssi.ru
Yu.M. Krivosheyev, Ph.D. stud., 333-45-88 krivosheev@iki.rssi.ru

2.1.1.31. Accretion on the magnetize black hole.

Numerical models of turbulent accretion disks with radiative outer layers have been constructed.

Lovelace, R. V. E., Rothstein, D. M., Bisnovatyi-Kogan, G. S.
Advection/Diffusion of Large-Scale B Field in Accretion Disks
ApJ 2009, 701, 885

2.1.2. V.N. Pushkov Institute of Terrestrial Magnetism, Ionosphera and Radiowaves Porpogation of the RAS

2.1.2.1. CORONAS-F: Solar and Solar-Terrestrial Physics

The processing of data obtained on board the CORONAS-F mission in the period of its orbital operation in 2001-2005 was continued during 2007-2008. CORONAS-F observed the Sun and recorded the manifestations of solar activity in the Earth's space environment.

Helioseismic Experiment DIFOS/CORONAS-F

Helioseismic data obtained with the DIFOS/CORONAS-F instrument have been used to demonstrate the potentialities of the newly developed method for processing the observation time series with the aim of determining the precise mean frequencies of the split lines of p-modes of the global solar oscillations and studying the origin of nonrotational splitting in the p-mode oscillation spectrum.

Precise determination of the p-mode frequencies is the main goal of the global helioseismology. The accuracy of determining the frequency defines the accuracy of solution of the inverse problem. To solve this problem, ground-based observational networks and space stations have been created for continuous monitoring of the Sun, since the accuracy of the frequency measurements depends on the duration of observations. However, it was revealed that the spectral lines of the p-mode oscillations were subject to splitting that had no connection with the solar rotation. As a result, measuring the line frequencies involves certain difficulties. Various averaging methods have been used, but they yield incongruous results. Thus, the efforts made to develop a system of continuous observations were not properly rewarded. A new method of the time series analysis has been developed and tested using the CORONAS-F/DIFOS data. The method is a generalization of the concept of the analytical signal. It permits finding the instant amplitude, phase and frequency of the signal, as well as estimating separately the contribution of the amplitude and frequency fluctuations to the line broadening.

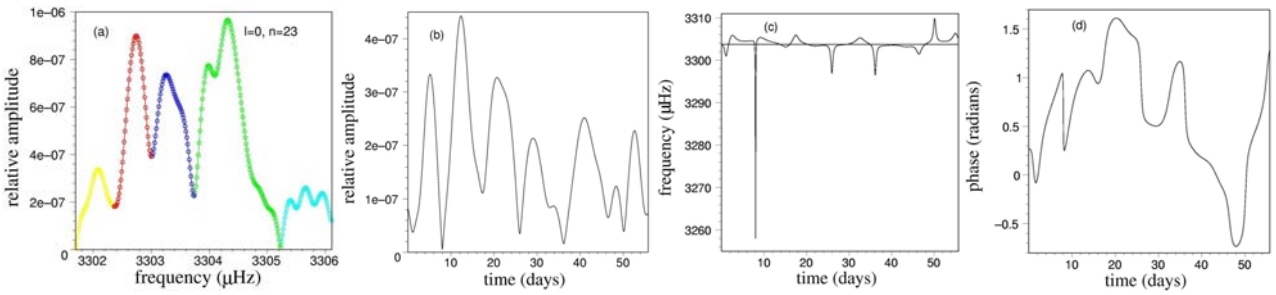

Fig.1. (a) Splitting of the line profile of the global p-mode (l=0,n=23) in the components shown by different colors. (b,c,d) Instant amplitude, frequency, and phase of the p-mode as a function of time.

Fig.1 illustrates the results of processing the CORONAS-F/DIFOS data by the method proposed above. A two-month series of observation of the brightness fluctuations in the wavelength range of 350 nm has been analyzed. Fig.1a shows the nonrotational splitting of the spectral line of the global p-mode with l=0. The beats due to the occurrence of the line components result in time variations of the amplitude (Fig.1б). Spikes of the instant frequency (Fig.1c) occur at the amplitude minima to confirm that the amplitude variations are produced by the component beating. Spikes of the instant frequency manifest the phase jumps at the amplitude minima. The analytical signals obtained for each line component are shown with different colors in Fig.1a. The instant amplitudes, frequencies, and phases of the line components are shown in Figs.2a,b,c. The occurrence of the

frequency spikes and phase jumps suggests that the line components consist of subcomponets, which are unresolved because of insufficient length of the time series. The variances of the amplitude and frequency fluctuations of the line components, as well as the variances of the entire spectral line are shown in Fig.2d. In all cases, the variance of amplitude exceeds that of frequency by a factor of 10-100; i.e., the line width depends entirely on amplitude fluctuations, while the p-mode frequencies are very stable. Thus, the new method for analyzing the time series permits us to find the mean frequency of the split spectral line of the p-mode with a high degree of accuracy. Unusual features of the line components have been revealed that are hard to explain in terms of the theory of stochastic excitation of p-mode oscillations of the Sun.

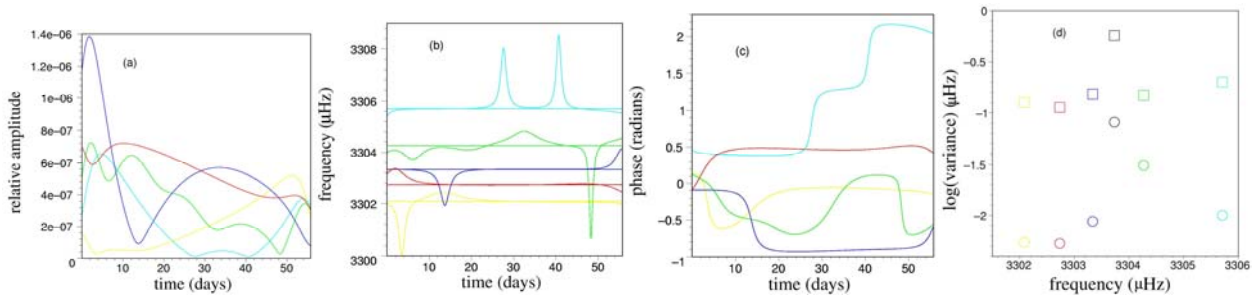

Fig.2. (a,b,c) Instant amplitudes, frequencies, and phases of the line components marked with different colors in Fig.1a. (d) Variances of the amplitude (squares) and frequency (circles) fluctuations of the line components. Variance of the amplitude and frequency of the entire line is marked black.

CORONAS-F/SPIRIT experiment results

Monochromatic solar X-ray images were obtained in the SPIRIT experiment on board CORONAS-F satellite. Spectroheliograph Mg XII of the SPIRIT apparatus, which utilized bend crystal mirror, registered monochromatic images in spectral line λ=8.42 Å (resonance line of H-like ion Mg XII). The emission of the spectral line is formed under relatively high (for solar corona) temperatures T > 5 MK. Thus, Mg XII spectroheliograph allowed for the first time to obtain direct images of hot (flare) solar plasma free from emission of colder plasma of quiet sun.

A comprehensive study of solar flare events based on soft X-ray (SXR) monochromatic Mg XII images as well as SXR flux have been carried out. New data about important characteristics of solar flare plasma – electron temperature, density, their spatial and temporal distributions was obtained. The methods are based on monochromatic X-ray images λ=8.42 (SPIRIT) and simultaneous X-ray fluxes in relatively wide spectral ranges 1-8 Å and 0.5-4 Å (measured on GOES). Also, solar hard X-ray measurements obtained on RHESSI were used to verification of the developed methods.

The method for determination of temperature distribution (Differential Emission Measure) is based on flux intensities in different SXR spectral ranges. The data for 8.42 Å spectral line (SPIRIT) and two wide-band ranges 1-8 Å and 0.5-4 Å (GOES) were used. The method has been applied for reconstruction of DEM temporal profile during February 2002, when the SPIRIT data was obtained with high cadence (1.5 min). It was shown, that during long-last flare events considerable amount of flare plasma has relatively low (for flaring plasma) – 1-4 MK and moderate 4-10 MK temperatures (see fig.3).

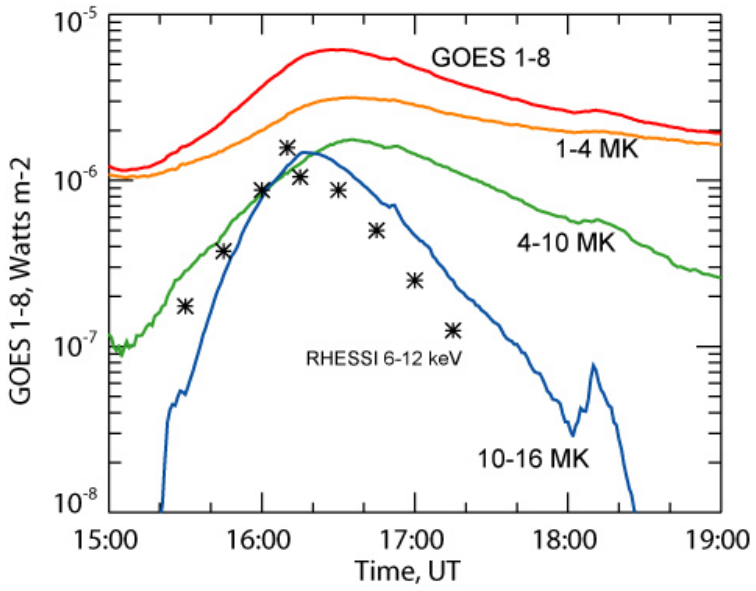

Fig.3.Flux temporal profile measured on 26th Feb 2002 by GOES 1–8 Å (red line) and its distribution to emission fluxes of low-temperature (orange line), mid-temperature (greed line) and hot-temperature (blue line) plasma. Asterisk – normalized flux measured by RHESSI 6– 12 keV X-ray channel.

Monochromatic images and simultaneous DEM distribution were used for modeling of spatial T_e and n_e distributions in flare plasma region. Long-last flare event of 26th Feb 2002 was modeled under assumption spherical symmetry (as suggested by corresponding SXR Mg XII image). The flare had relatively hot core with temperature ranging from 5 up to 16 MK, with the density being increased slightly – from $1.5*10^9$ cm^{-3} in the periphery to $2.5*10^9$ cm^{-3} in the center.

Temporal DEM profiles, obtained with the SXR flux data, were used to overlay monochromatic Mg XII and hard X-ray RHESSI images (see fig.4). The composed image allowed to determine boundaries of hot plasma and ultimately check the spatial modeling of T_e and n_e distributions.

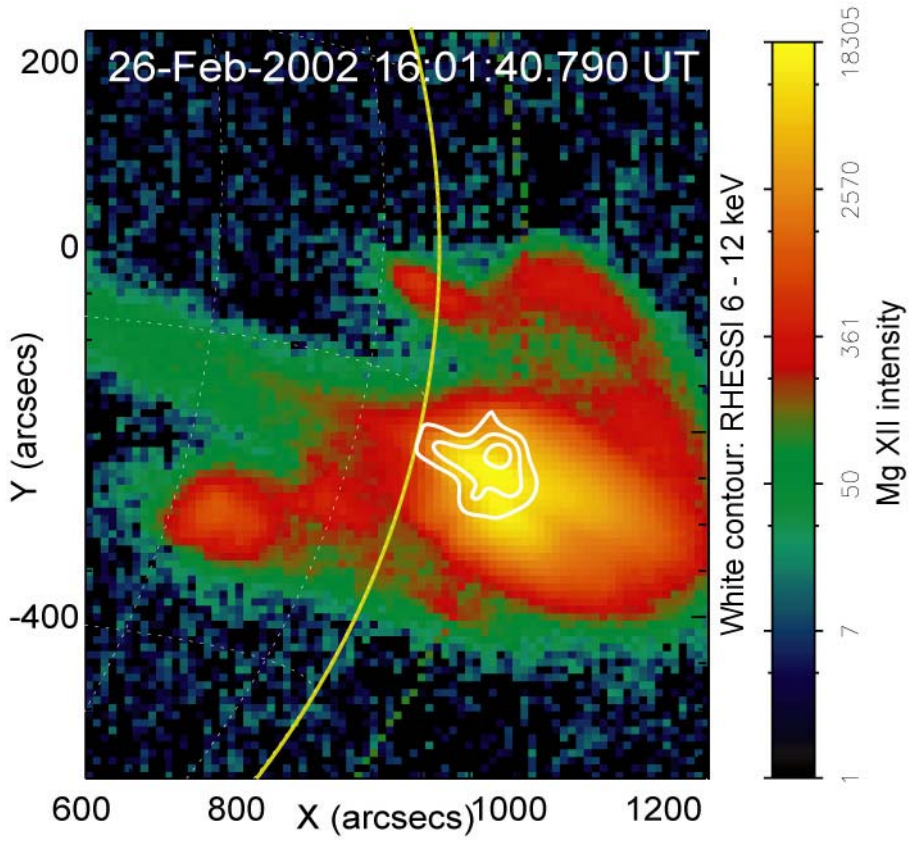

Fig.4.Mg XII image overlaid with RHESSI 612 keV contours.

The obtained information about density and emission measure could be used to test different heating model for flare plasma. It was shown that high amount of cold plasma during the flare and low density in it's core are in accordance with fast shock wave heating and thin target models.

High-temperature plasma in the solar corona.

During a solar flare, the impulsive release of energy stored in the magnetic field efficiently accelerates particles and heats the plasma. Observations carried out using the SXT telescope onboard the Yohkoh satellite (Masuda et al., 1994; Tsuneta et al., 1997) have shown that a hot plasma can be produced during flares in both the chromosphere and the solar corona. Currently, the spatial and temporal parameters of the high-temperature coronal plasma are studied with the RES-K X-ray spectroheliograph, which is part of the SPIRIT complex operated onboard the CORONAS-F satellite (Oraevsky et al., 2002). The RES-K spectroheliograph provides monochromatic images of the full solar disk in the Mg XII 8.42 A line with a temperature of T = 5-15 MK (Zhitnik et al., 2003). This makes it possible to directly observe the hot coronal plasma, whereas the data of the Yohkoh satellite can be used to reveal the high-temperature plasma only indirectly, by comparing SXT images obtained with various filters. We study here the structure and dynamics of the hot coronal plasma during solar flares and between them based on RES-K observations in the Mg XII line.

The SPIRIT instrumentation onboard the CORONAS-F satellite is designed to obtain full-disk images of the Sun in soft-X-ray and extreme-UV spectral channels and lines (for a technical description of the SPIRIT instrumentation, see Zhitnik et al., 2003). We analyze the series of successive images of the NOAA 9830 active region that was obtained using the RES-K spectroheliograph in the Mg XII 8.42 A channel from 21:40 UT on February 21, 2002, to 08:00 UT on February 22, 2002, during a period approximately coincident with a flare of class M4.4, according to the GOES (Geostationary Operational Environmental Satellite) scale. Fig.5 shows a time profile of the Mg XII emission obtained by integrating the emission of all fragments, together

with the simultaneous emission curves obtained in the 25-50 keV range onboard the RHESSI (Ramaty High Energy Solar Spectroscopic Imager) satellite and in the 1 to 8 A range onboard the GOES satellite. The profile of hard X-ray emission should correlate with the injection rate of accelerated electrons.

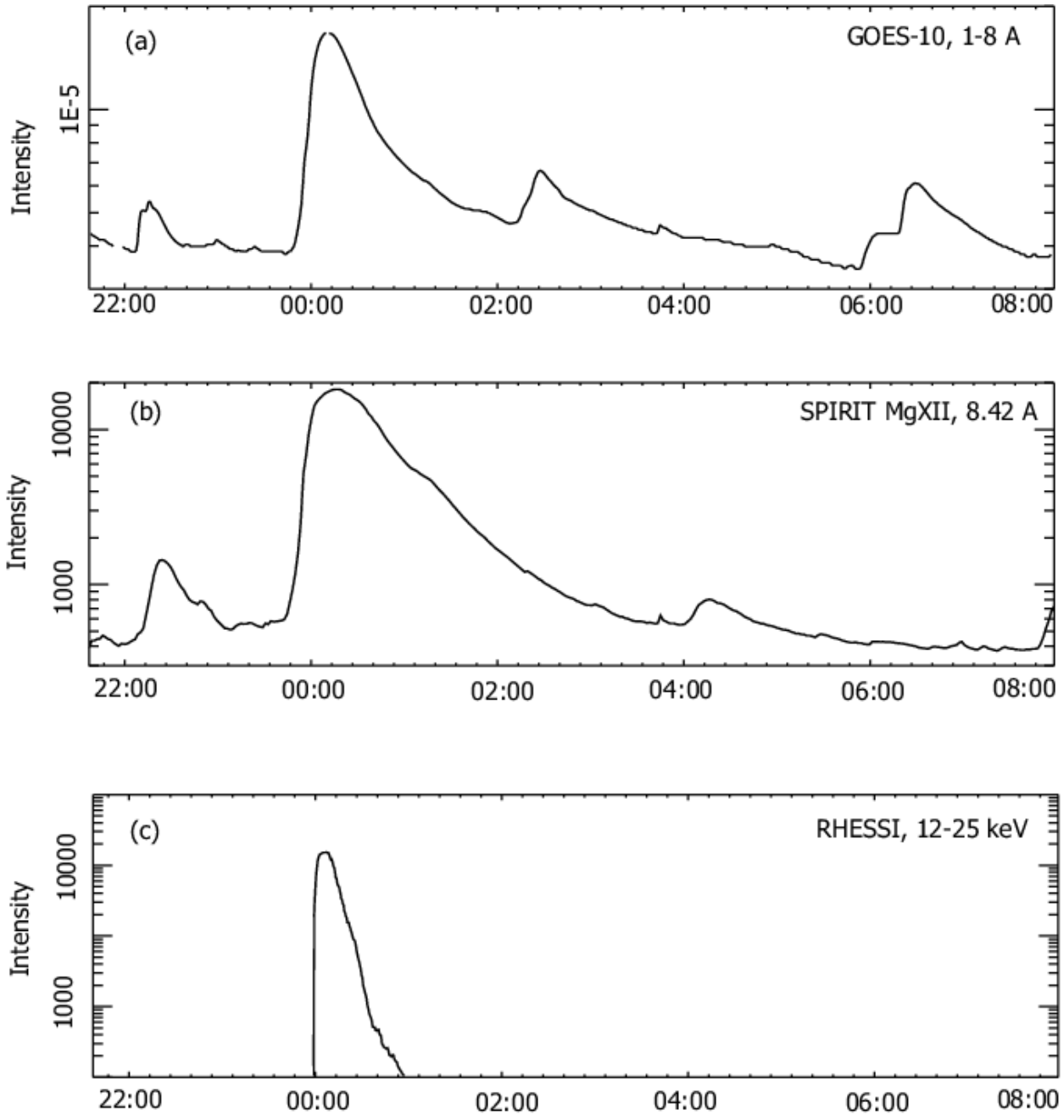

Fig.5.Time profiles of emission: (a) integrated solar emission in the 1-8 A range according to GOES data; (b) MgXII 8.42 A emission of the high-temperature plasma in the core; and (c) hard X-ray emission of the flare in the 25-50 keV range according to RHESSI data.

The structure of the active region in the photosphere and corona is shown in Fig.6 by images in various emission ranges. All these images are reduced to the same scale and, in addition, compensation for their displacement due to solar rotation is applied. Upon analyzing the SOHO/EIT and TRACE images, we selected four groups of magnetic loops, which are denoted in the figure as A1-A4. In the bottom panels, these loop systems are superimposed onto the pattern of high-

temperature emission sources that we detected in the Mg XII SPIRIT images. A comparison between the panels in Fig.6 shows that the location of hot-plasma regions observed in the Mg XII line corresponds to systems of coronal loops, and the plasma-emission intensity is maximal near the apices of the loops.

During the considered series of SPIRIT observations, a class~M4.4 flare occurred. Its onset in the Mg XII line was observed at about 23:45 UT in core R2, whose position is shown in Fig.6. At the time of the flare, cores R2--R4 merged into one in the SPIRIT images, which prevented separate study of the dynamics of each of them. Core R1 was at a large distance from the flare center and could be identified in the images as a separate emission source even at the flare maximum. Fig.7 shows time profiles in the R2--R4 flare area (dashed) and in the distant core R1 (solid). It is remarkable that the time profiles exhibit a correlation, which can be noted at many intervals. In particular, some time after the onset of the flare (dashed curve), an emission outburst was also observed in the distant core R1, although it was weaker. Based on the time delay of the second outburst, 5 min, and the distance between the cores, 2105 km, the speed of the disturbance propagation from the center of the flare can be estimated to be 650 km/s.

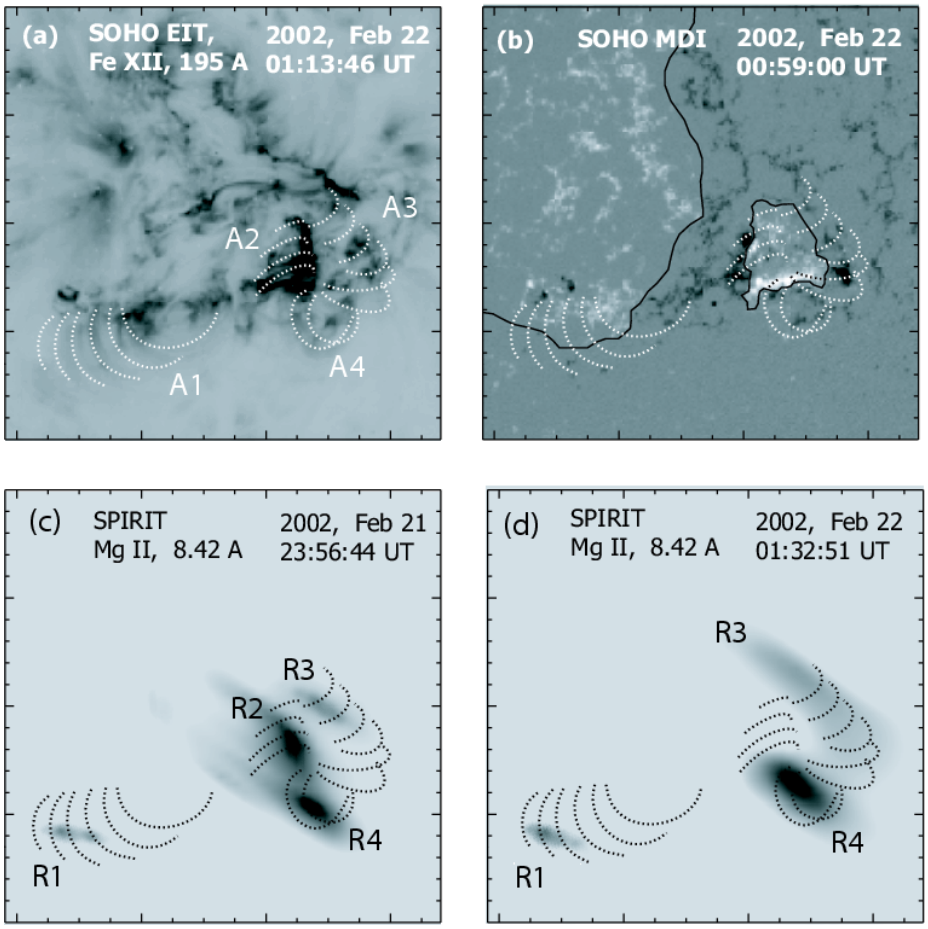

Fig.6.Active region NOAA 9830: (a) SOHO/EIT image in the 195 A line; (b) SOHO/MDI magnetogram and the schematized neutral line of the photospheric magnetic field; (c) location of high-temperature-plasma sources (R1--R4) before the flare (SPIRIT image in the MgXII 8.42 A line); and (d) distribution of high-temperature plasma after the flare. The loop systems observed on the TRACE satellite are marked with dotted curves and A1-A4 symbols.

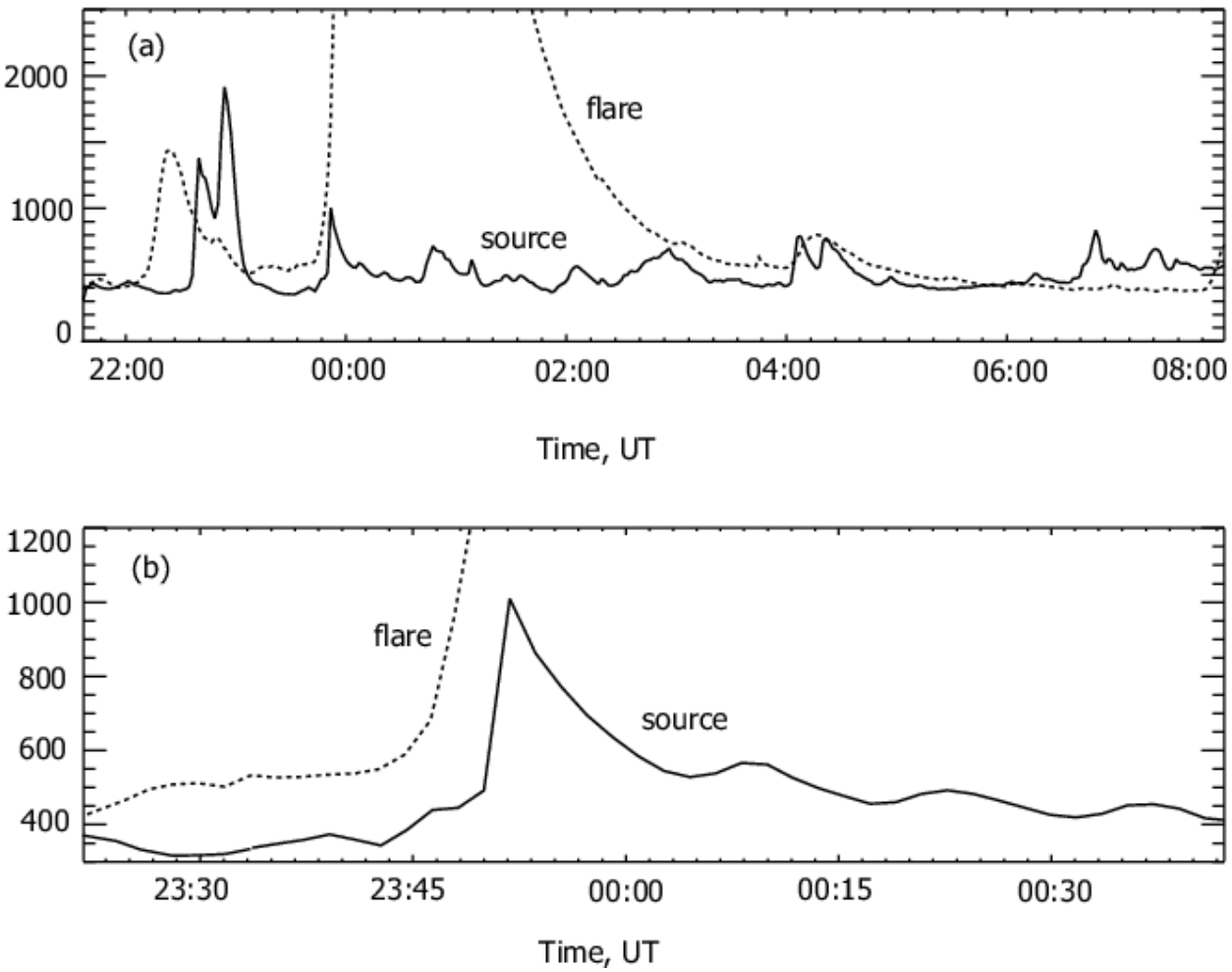

Fig.7.Comparison of the emission profiles of high-temperature plasma in the core of the flare (dotted curve) and in the distant source R1 (solid curve).

EUV corona.

The SPIRIT telescope aboard the CORONAS-F satellite (in orbit from 26/07/2001 to 05/12/2005), for the first time observed the solar corona in the 175 Å (Fe IX, X and XI lines) and 304 Å (He II and Si XI lines) bands in the coronagraphic mode at the distance of 1.1-5 R_{sun}. This intermediate region between the fields of view of ordinary extreme-ultraviolet (EUV) telescopes and most of white-light (WL) coronagraphs is very important for forming the streamer belt, acceleration of ejected matter and emergence of slow and fast solar wind.

The results of continuous coronagraphic EUV observations in June and December 2002 has shown that in the 175 Å band (Fe IX-XI lines) the corona contained a diffuse quasi-symmetric part and a structure of bright rays (radial or non-radial, features 1 and 2 in Fig.8) started from the solar surface. Some very bright rays were evidently originated from the active regions and possibly revealed the solar wind streams (feature 4 in Fig.8). Several big rising loops (e.g. feature 3 in Fig.8) were associated with the CME in the LASCO catalogue.

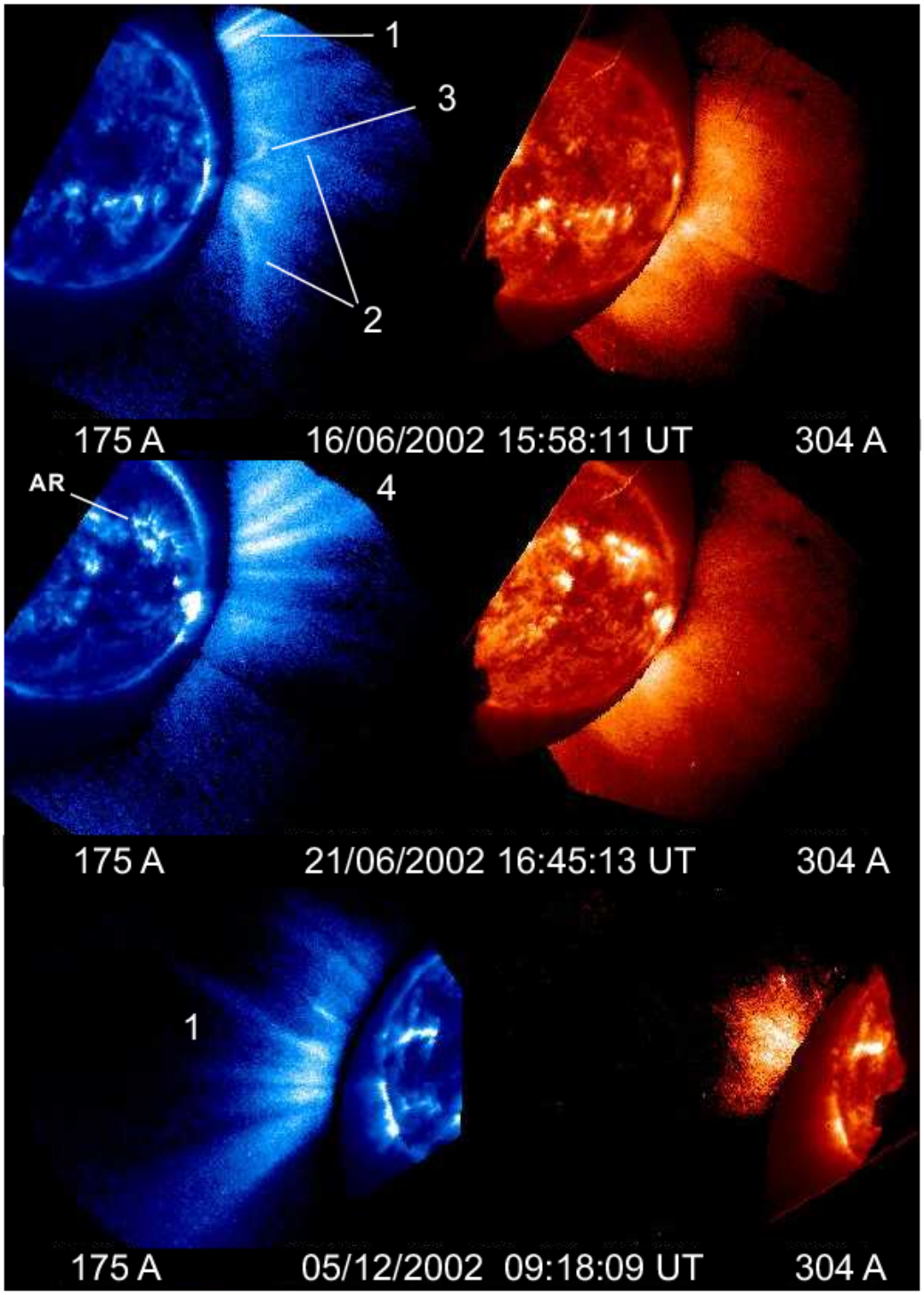

Fig.8.Specific coronal features observed by the SPIRIT EUV coronagraph in the 175 and 304 Å bands: 1 – radial rays, 2 – non-radial rays, 3 – a rising loop, 4 – a fan of rays linked with the active region at the disk (solar wind streams).

In 304 Å the corona is more diffuse and inhomogeneous. Only traces of the coronal rays seen in 175 Å are faintly visible. The analysis of radial distribution of the He II coronal brightness has shown that up to distances of 1.34-1.5 R_{sun} this radiation is excited by collisions (as for the coronal lines), but at greater distances the resonance scattering becomes dominant.

Reference

V.Slemzin, O.Bougaenko, A.Ignatiev, S.Kuzin, A.Mitrofanov, A.Pertsov, I.Zhitnik. Off-limb EUV observations of the solar corona and transients with the CORONAS-F/SPIRIT telescope-coronagraph. Ann. Geophys., 26, 1–10, 2008.

Dynamics of solar flares hard X-ray emission spectra according to the data IRIS/CORONAS-F

The data obtained with the IRIS/CORONAS-F instrument have been used to study the dynamics of the energy spectra of the hard X-ray emission from solar flares of different importance. As a result, time variations have been revealed in the shape of the spectra, which reflect variations in the distribution function of the flare-accelerated electrons. The high-sensitivity flare X-ray spectrometer IRIS allowed a detailed study of the spectral and time characteristics of soft X-rays (2-15 keV) from major and minor solar flares, as well as from the quiet Sun, when the emission intensity did not exceed ~10^{-5} erg $sm^{-2}{\cdot}s^{-1}$ (~10 nW/m^2). The evolution of the X-ray energy spectra was studied using the 64-channel instrumental spectra (2-150 keV) obtained with a time resolution of 1 s. Shown below are the results of the analysis of the X-ray spectrum dynamics for four solar flares of importance C and M recorded with the IRIS spectrometer during 2001-2002.

The time profile of the hard X-ray emission generated in the most intensive flare of importance M1.2 on April 15, 2002 (commencement at 2305 UT) was obtained with a second resolution in five energy ranges (fig.9a). On the profile, one can clearly see the emission pulses of the order of 10–20 s. The spectral analysis of this emission in the energy range of 15-24 keV corroborates the existence of a periodic component with a period of 22 s.

Fig.9 represents the background spectrum before the flare (b) and the hard X-ray spectra measured at one-second intervals at the flare maximum (c) and decline (d). As seen from the figure, the spectrum of the flare emission at all stages of the flare evolution can be approximated with a high accuracy (except for the high-energy background) by a power-law function with the power index changing in time. Thus, the background spectrum before the flare can be described by the power-law function with index $\gamma \approx -2.7$ (Fig.9b), which decreases in the impulsive phase reaching the value $\gamma \approx -3.6$ at the peak of the flare (Fig.9c) and, then, increases in the flare decline phase (Fig.9d).

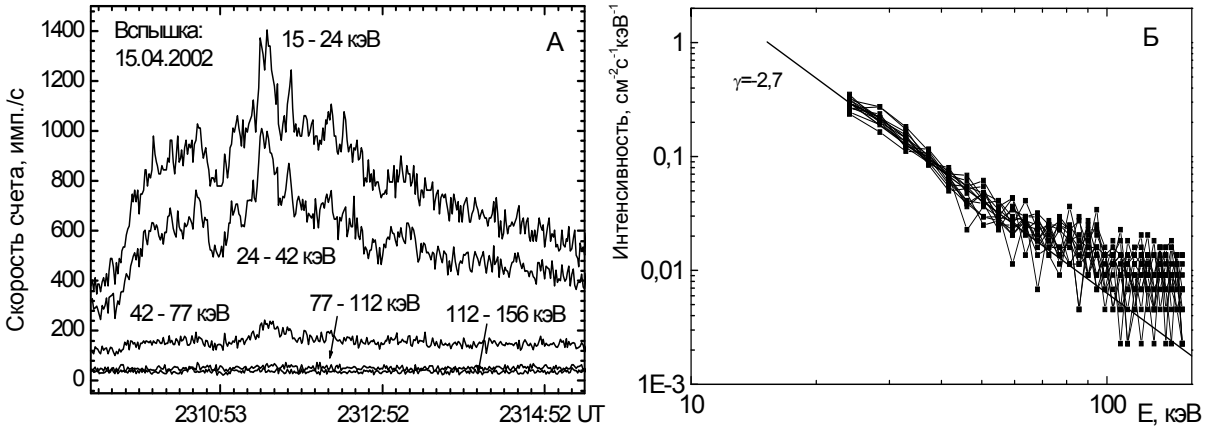

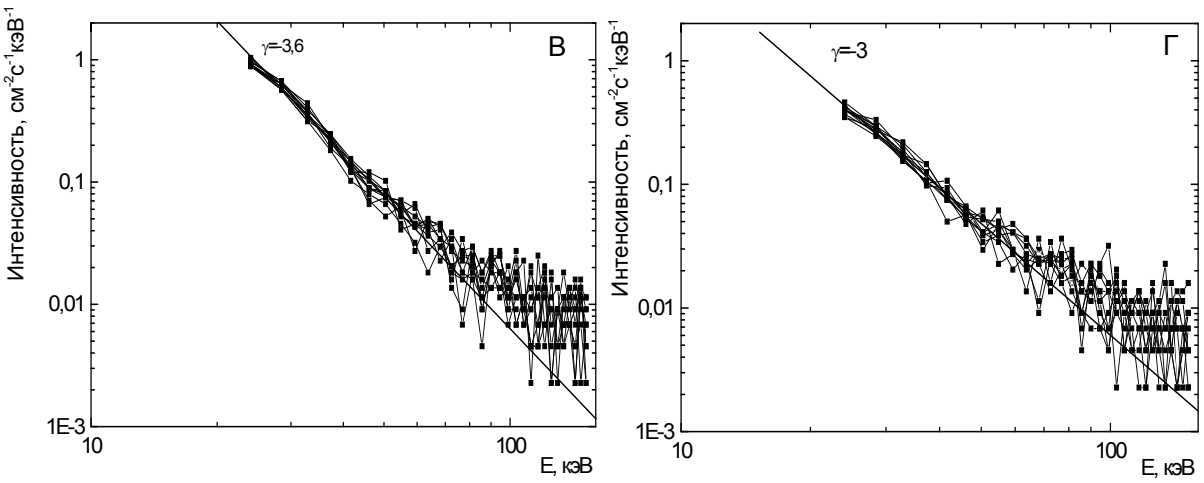

Fig.9.The emission time profile (a) and energy spectra at the maximum (c) and decline (d) of the X-ray flare on April 15, 2002, and the background spectrum before the flare (b).

The hard X-ray emission spectrum from the minor flare of July 26, 2002 (commencement at 09:20:31 UT) differs from the spectrum of the previous flare by its shape changing during the flare evolution. At the flare onset (stage I in Fig.10), the shape of the spectrum is unstable, being described alternately by power-law or linear dependence. In the impulsive phase (stage II in Fig.10), the spectrum becomes stable and is pronouncedly linear (Fig.11a) owing to a large number of quanta with the energy less than 40 keV. The linear shape persists at the maximum and, partly, in the decline phase, after which (stage III in Fig.10) the shape of the spectrum changes and can again be described by a power-law function (Fig.11b). Such behavior of the flare spectrum, obviously, manifests the evolution of the distribution function of the emitting electrons.

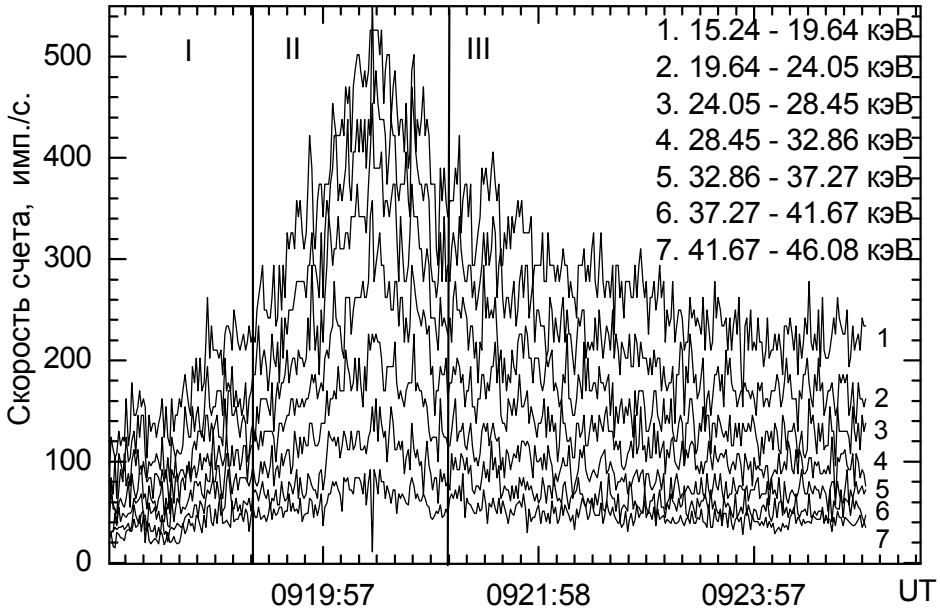

Fig.10.Time profile of the hard X-ray emission from the flare of July 26, 2002.

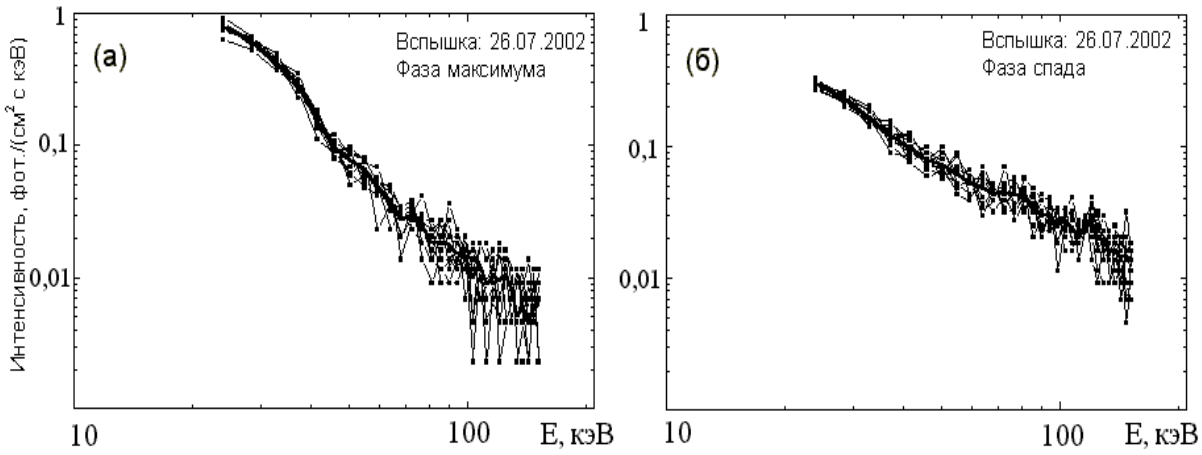

Fig.11.Energy spectra of the hard X-ray emission from the flare of July 26, 2002 at the maximum (a) and decline (b) of the event.

For the flare of December 19, 2001, which belonged to the X-ray class C4.9 (commencement at 0230:40 UT), the X-ray energy spectrum had a linear shape in the impulsive, maximum, and decline phases (Fig.12). The quantum counting rate at the energies above 110 keV for that flare did not exceed the background value. This spectrum can be described by both the thermal and nonthermal models, so that the choice between the models is difficult. The sole argument in favor of the nonthermal model is that the other one would require the heating of plasma to extremely high temperatures (above 10^8 K), which are hardly realistic in the events of this X-ray class.

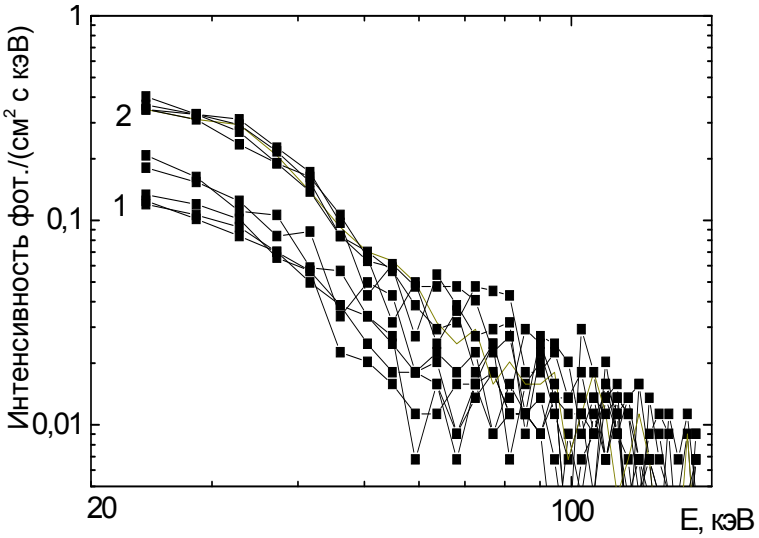

Fig.12.Hard X-ray energy spectra measured with a resolution of 1 s in the impulsive phase (1) and at the peak (2) of the flare of December 19, 2001.

The time profile for the flare of October 29, 2002 (commencement at 2147:02 UT) in the energy range of 24-160 keV summarized from four energy channels of the instrument is represented in Fig.13a. The total duration of the flare-generated X-ray emission was about one minute. The flare importance was C1.8. The emission time profile consists of a slowly changing component with the distinct fine structure of multiple pulses. The pulsed structure was best pronounced at the maximum and decline of the flare emission. This flare differs from those described above by a “bend” in the

energy spectrum in the range of ≈45 keV. Fig.13b shows the spectra measured at one-second intervals in the impulsive, maximum, and decline phases, averaged over 10 s. As seen from the figure, the spectrum formed in the impulsive and maximum phases of the flare has a complex shape, which can be conventionally divided into two components with a "bend" at ≈45 keV. The low-energy part of the spectrum before the bending point is, probably, due to the thermal emission of hot plasma, and the high-energy spectrum after the bend is accounted for by the bremsstrahlung emission of fast electrons. The spectrum keeps this shape in the declining phase, too. Another typical feature of the spectrum of the October 29, 2002 flare is its steepness that increases with the increase of the energy. This behavior can be explained if the distribution function of fast electrons generating the bremsstrahlung emission has a discontinuity at some maximum velocity corresponding to the energy of ≈160 keV.

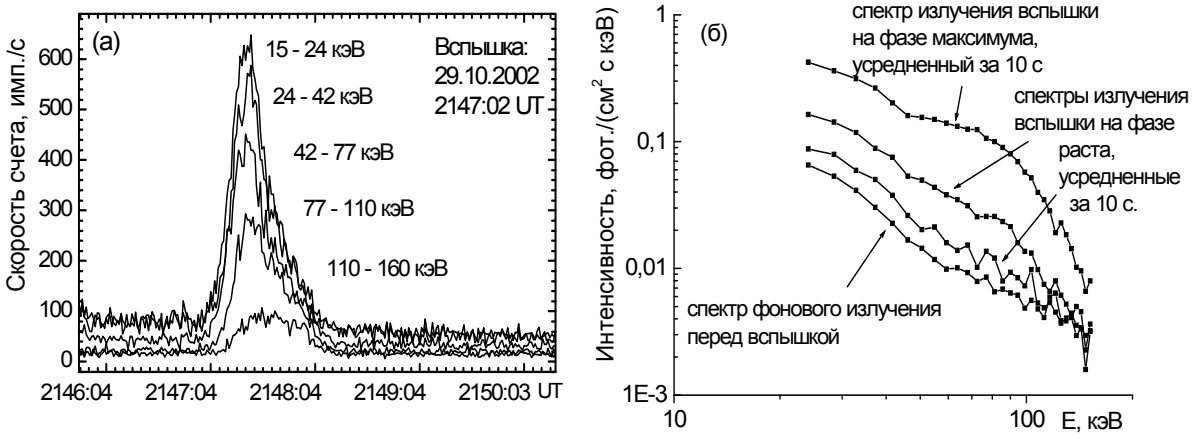

Fig.13.Time profile (a) and spectra (b) of the X-ray emission from the flare of October 29, 2002.

Thus, the analysis has shown that the energy spectrum of hard X-ray emission from the major X-ray flare of importance *M* was power law all over the flare duration. For the weaker flares of importance *C*, the spectrum was linear, possibly, with a bend in the energy range of ≈45 keV. Variations in the flare emission energy spectra reflect the evolution of the distribution function of the flare-accelerated electrons.

Spectrometry of the solar X-ray emission and X-ray nightglow of the Earth atmosphere according to the data of RPS-1/CORONAS-F

The data obtained with the CORONAS-F/RPS-1 device have been used to analyze the energy spectra of some minor solar flares at different stages of their evolution, as well as the spectra of the pre-flare X-ray background. The X-ray nightglow of the Earth atmosphere has been studied, and the Earth contour maps have been plotted to visualize the global pattern of the glows in the energy ranges of 3-5; 5-8; 8-16, and 16-31.5 keV averaged over the time interval selected.

Spectrometry of the solar X-ray emission

The solar X-ray flares are classified on the basis of patrol observations of the Sun in the soft X-ray emission range (1.5-24.8 keV) carried out onboard the GOES satellite (Geostationary Operational Environmental Satellite). The class of the flare is determined by the emission flux at the peak of its evolution. This classification does not provide information on the energy spectra and detailed time characteristics of the flares. The CORONAS-F/RPS spectrometer was measuring solar X-rays in the energy range of 3-31.5 keV and provided vast experimental data on the spectra of soft X-ray emission of solar flares.

Fig.14 shows the spectra of the background emission of the Sun recorded in October 2003 as the satellite was passing over the Earth equator. The date of observation, Wolf number (W), and GOES background class in the same units as the flare emission are specified for each spectrum. One can see that, according both to GOES and to RPS-1 devices, the background flux and rigidity of the solar radiation grow with the increase of solar activity.

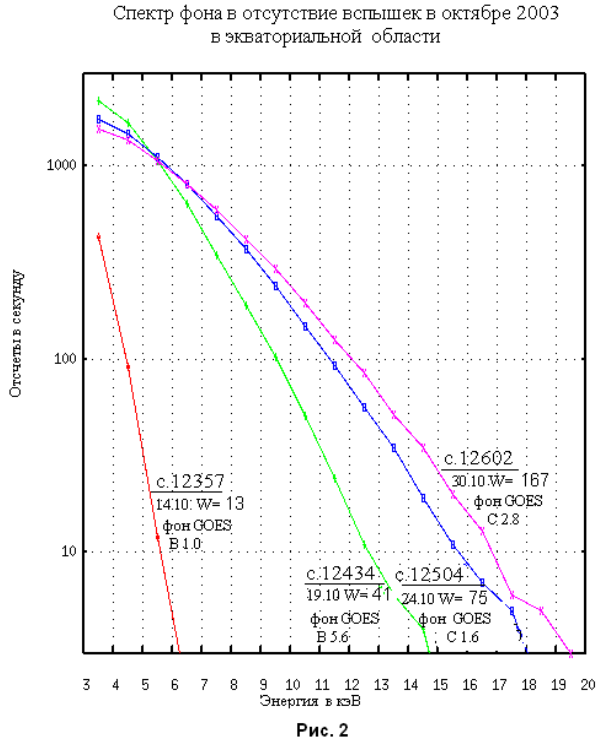

Fig.14.Background X-ray spectra in October 2003 in the absence of flare. The date of observation, Wolf number (**W**), and GOES class are shown alongside.

Fig.15 illustrates the time profiles of three flares and their spectra at points 1-5. The flares were recorded on October 13, 2004 against a low background level (point 1). The first increase was identified as a minor flare of class B1.0 according to the GOES classification. The following two increases were not included in the catalog. Since the signal counting rates at the maximum of the first and third flares (channels 3-5 and 5-8 keV) are virtually equal and their spectra are identical (points 2, 5), the third flare may be also classified as B1.0. The second, much weaker, flare with the maximum flux $<10^{-7}$ W/m^2 can be assigned to class A. The source temperature for all three flares was determined (Fig.16) by comparing the measured spectra with those calculated with the CHIANTI 5.2 model. These three flares are likely to display fast and appreciable changes of temperature (from 9 to10 MK) in one source.

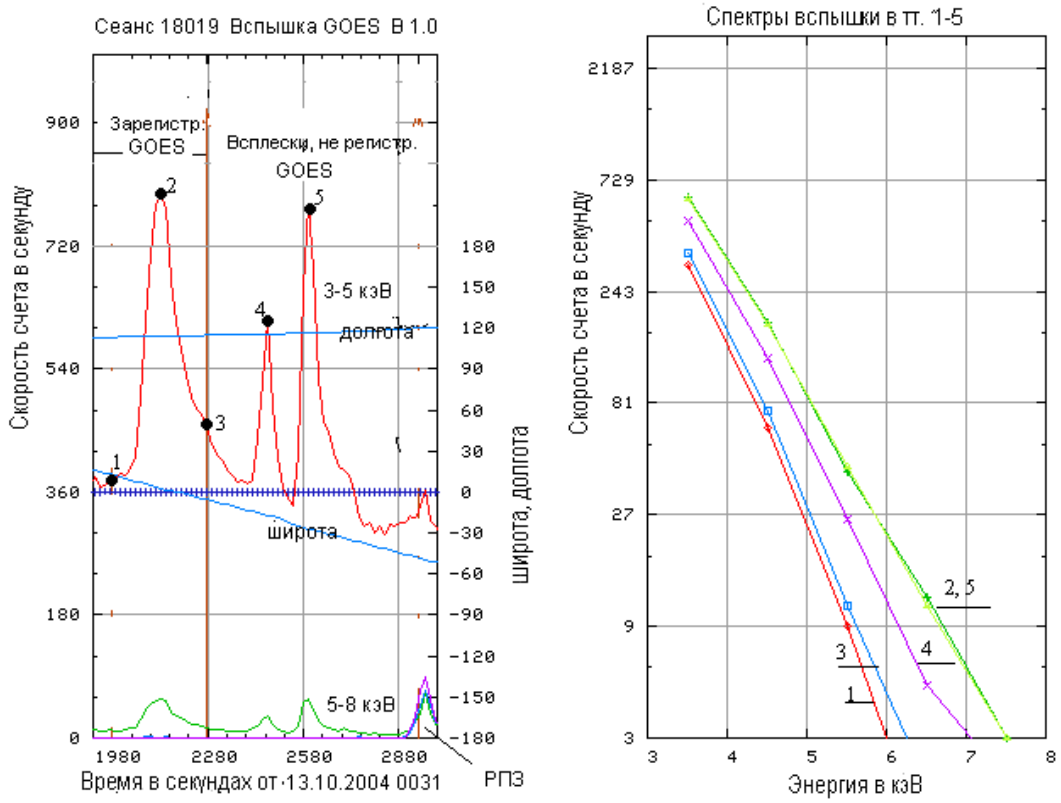

Рис. 3

Fig.15.Time profiles in the energy ranges of 3-5 and 5-8 keV (GOES) and spectra at points 1-5 for three flares recorded on 13.10.2004 (RPS-1/CORONAS-F).

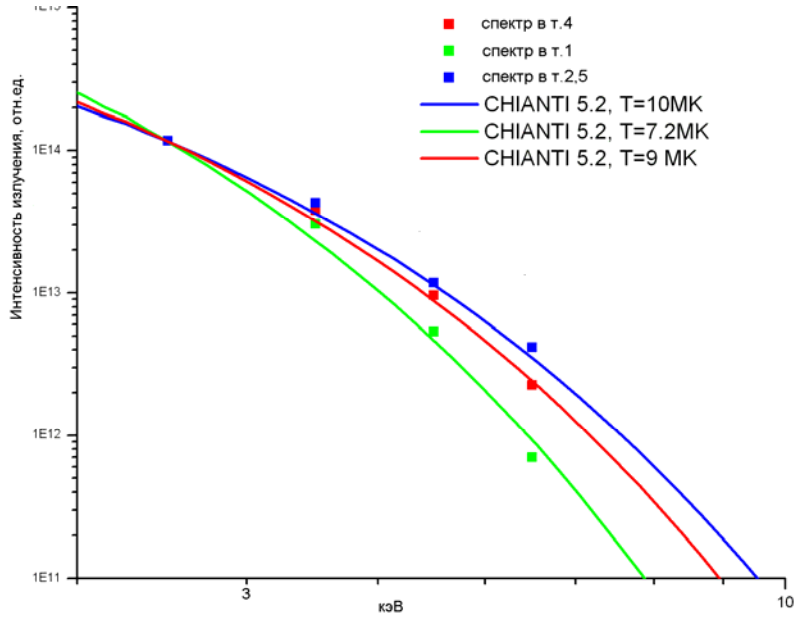

Fig.16.Comparison of the spectra in Fig.15 with the CHIANTI 5.2 model.

The time profiles and spectra at points 1-3 for a more intensive flare of class B7.6 recorded on 21.08.2003 are presented in Fig.17. This event occurred against a more intensive and harder pre-flare X-ray background (point 1) than the one illustrated in Fig.15. The flare was characterized by a typical long ("stepwise") decay; the spectrum at the maximum (point 2) was much harder than the spectrum of the B.1.0 flare (Fig.15, point 2).

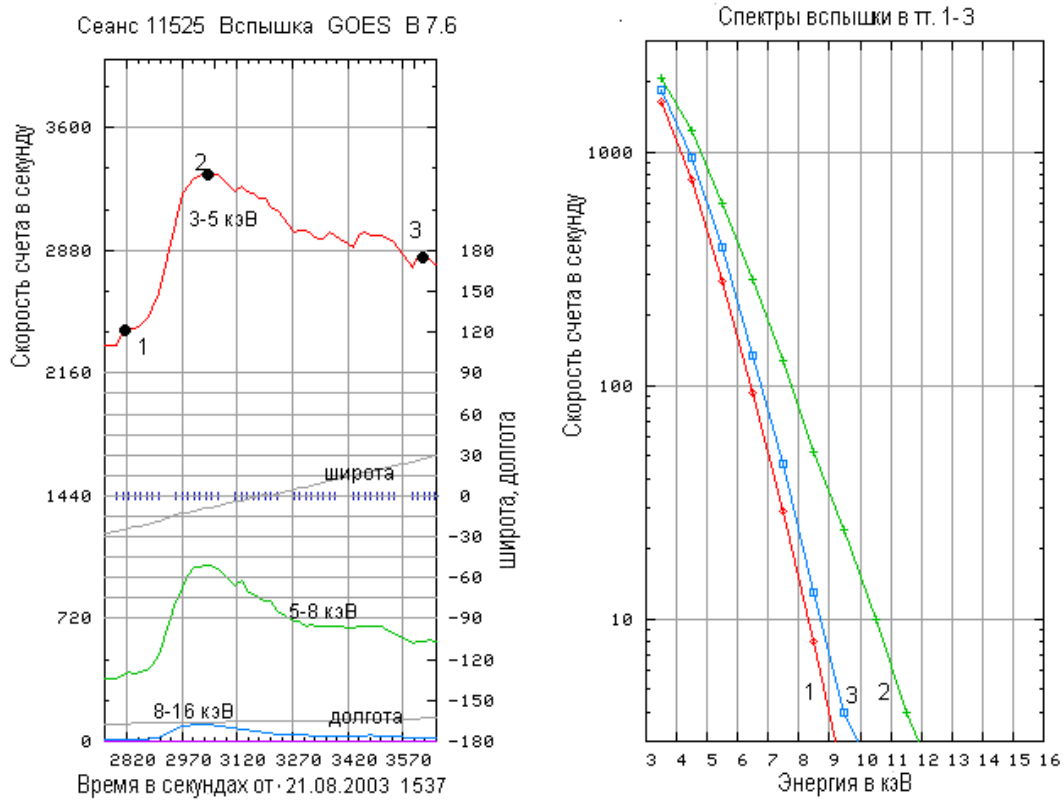

Рис. 4

Fig.17.Time profiles in the energy ranges of 3-5, 5-8, and 8-6 keV (GOES) and spectra at points 1–3 for the flare of class B7.6 recorded on 21.08.2003 (RPS-1/COEONAS-F).

As the activity in cycle 23 was decreasing, the flares were observed at a lower background level. Fig.18 shows the time profiles and spectra of the class B9.5 flare recorded on 02.05.2005. The commencement, maximum, and ending of the flare (points 1, 3, 4) are marked according to GOES. RPS-1 did not register the end of the flare, because the satellite entered the Earth's shadow. The maximum quantum energy recorded in that flare (spectrum at point 3) exceeded the upper energy limit of the GOES instrument.

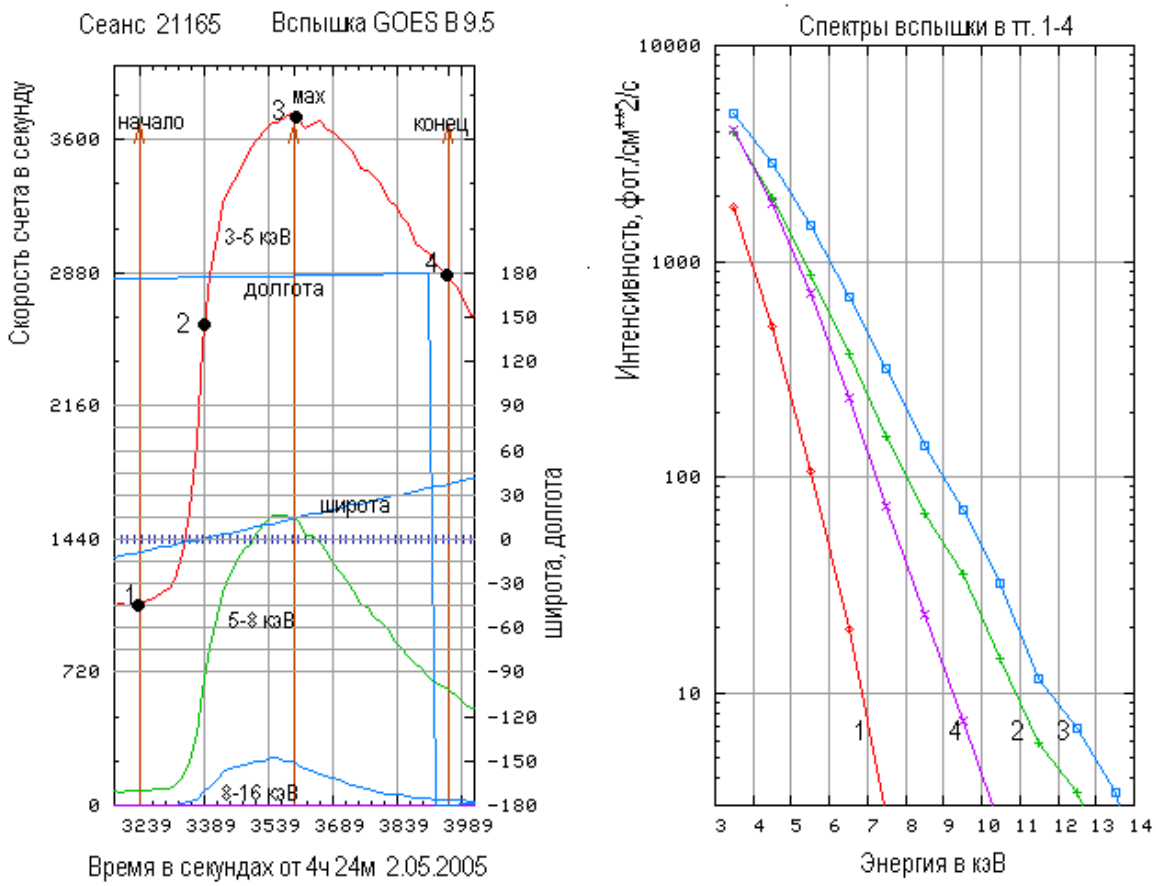

Рис. 5

Fig.18.Time profiles in the energy ranges of 3-5, 5-8, and 8-16 keV (GOES) and spectra at points 1–4 for the flare of class B9.5 recorded on 02.05.2005 (RPS-1/CORONAS-F).

Fig.19 demonstrates a still more intensive flare C1.2 ($1.2 \cdot 10^{-6} W/m^2$), which occurred on 08.11.2005 also against a relatively low background. The commencement, maximum, and ending of the flare are marked according to GOES. RPS-1 could not register the end of the flare because of entering the Earth's shadow. The flare had two maxima, the spectrum of the second maximum being more rigid than the spectrum of the first one. The increase in the highest energy range (8-16 keV) started approximately a minute after the flare began. The second increase is characterized by simultaneous arrival of soft and hard X-rays.

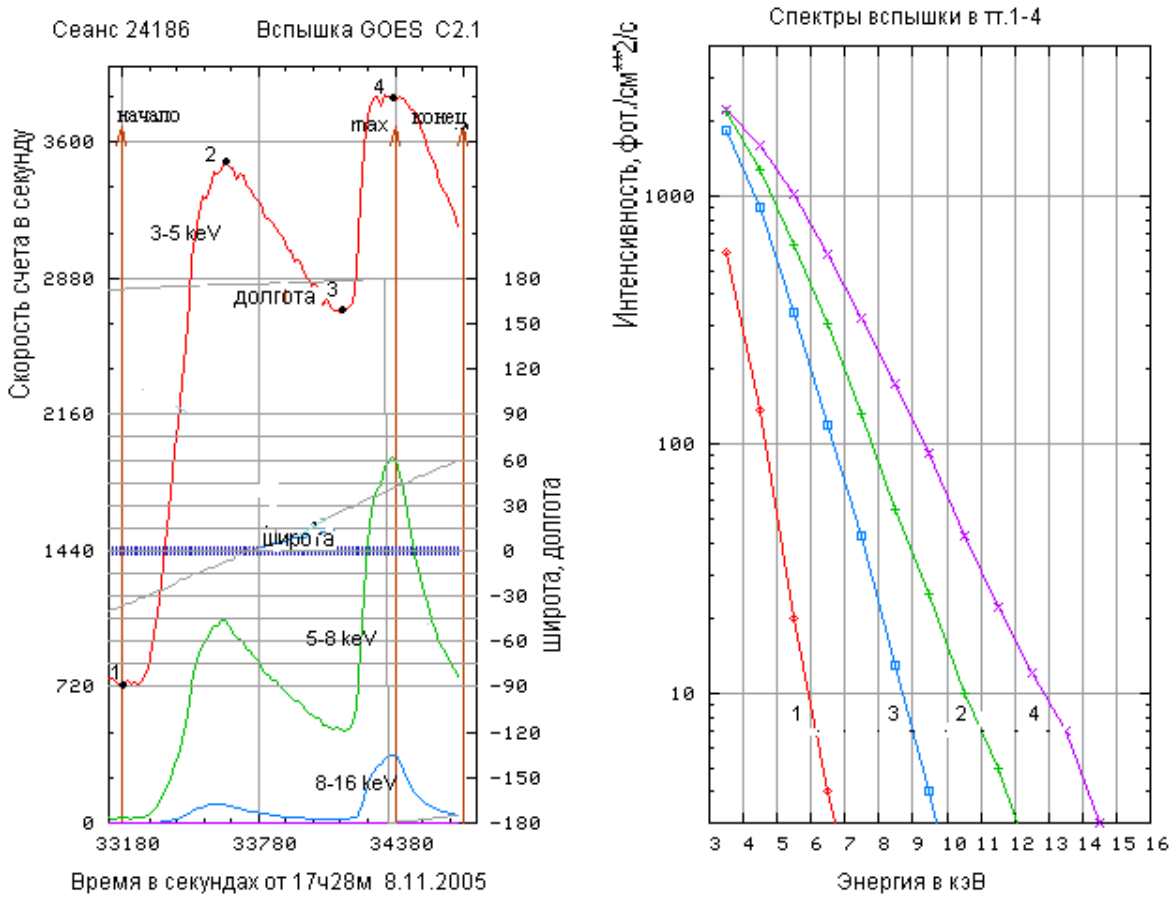

Рис. 6

Fig.19.Time profiles in the energy ranges of 3-5, 5-8, and 8-16 KeV (GOES) and spectra at points 1–4 for the flare of class C1.2 recorded on 08.11.2005 (RPS-1/CORONAS-F).

Upper atmosphere nightglow.

While the CORONAS-F mission was in the Earth's shadow, the RPS-1 instrument was recording the soft X-ray emission of the upper nighttime atmosphere, as well as the signals from charged, high-energy particles of the Earth's radiation belts that were detected when passing the high-latitude regions and the zone of the Brazilian magnetic anomaly (BMA). The X-ray emission in the Earth's upper atmosphere is secondary by its nature. In the energy range under consideration, it is mainly due to the bremsstrahlung radiation of the precipitating magnetospheric electrons. Long-term (07.2001-12.2005) high-sensitivity observations of the nighttime atmosphere with RPS-1 provided us with a global radiation pattern in the form of the X-ray maps of the Earth and revealed its seasonal dependence.

Fig.20 represents the maps of nighttime emission of the atmosphere for the period from 23.03.2002 to 23.03.2003 in the energy ranges of 3-5; 5-8; 8-16, and 16-31.5 keV and for the periods of northern summer (23.03.2002-23.09.2002, Fig.21) and winter (23.09.2002-23.03.2003, Fig.22).

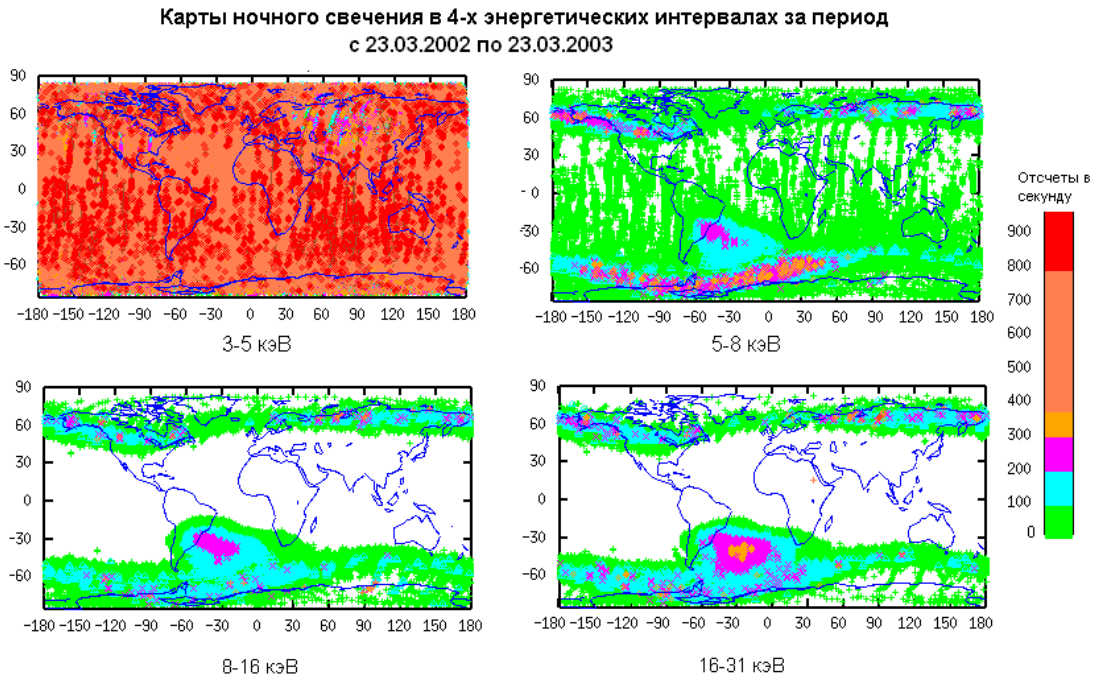

Рис. 7

Fig.20.Maps of the nighttime atmospheric emission in the energy ranges of 3-5, 5-8, 8-16, and 16-3 keV based on the CORONAS-F/RPS-1 data for 23.03.2002-23.03.2003.

Fig.20 shows that the intensity of the nighttime atmospheric emission decreases with the increase of the quantum energy. In the energy range of 3-5 keV, the nighttime glow is observed all over the atmosphere, being the brightest in the southern hemisphere over the Pacific and Indian Oceans. In the northern hemisphere, the brightest glow is observed at high latitudes. At lower latitudes, it fades, vanishing completely in some regions on the map in the range of 5-8 keV. At >8 keV, the instrument detects signals only in the Earth's radiation belts, whose boundaries are clearly seen on the maps for 8-16 and 16-31 keV.

The nightglow intensity changes during the year in various atmospheric regions. The maps for 3-5 keV display the limits of the polar day in summer (Fig.21) and in winter (Fig.22). In summer, the atmospheric nighttime emission at 3-5 keV in the latitude range of 30°-60° north is much weaker than in the other regions.

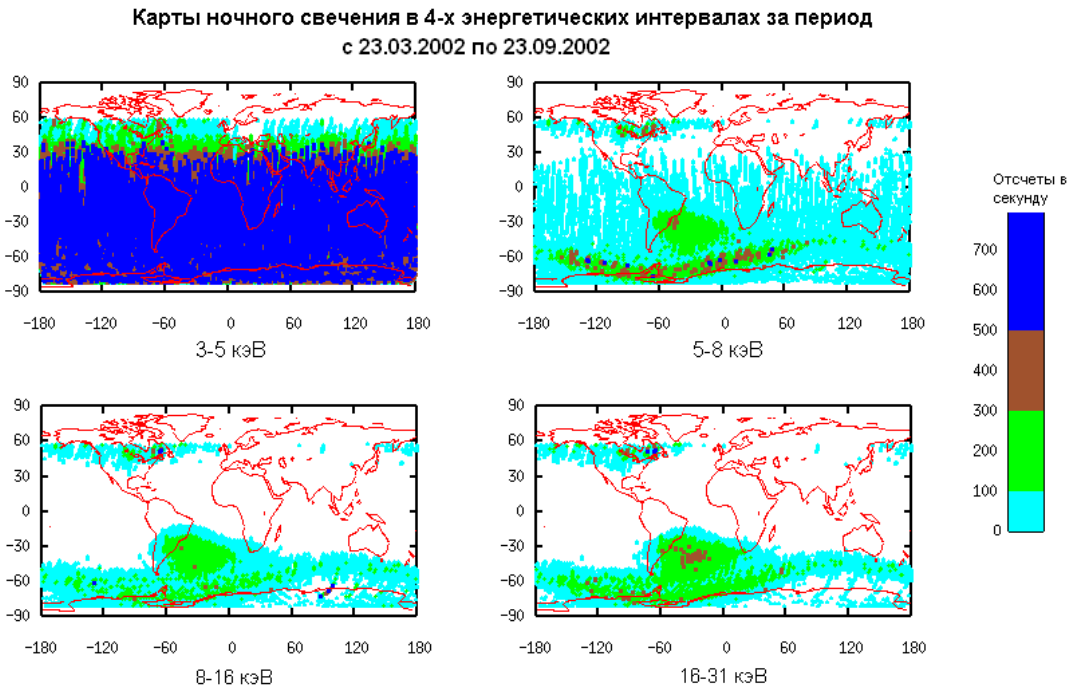

Рис. 8

Fig.21.Maps of the Earth's atmospheric nighttime emission in the energy ranges of 3-5, 5-8, 8-16, and 16-31 keV based on the CORONAS-F/RPS-1 data for 23.03.2002-23.09.2002 (north summer).

On the maps for 5-8; 8-16, and 16-31 keV in Fig.21 (northern hemisphere, summer 2002), the decrease of the emission intensity from the Earth's radiation belt in the northern hemisphere from the Atlantics to Chukotka is seen as a "break" in ERB. In summer, the ERB maximum at the height of 500 km at these latitudes is in the polar day zone and, therefore, is invisible on the map. However, areas of lower intensity might be observable. The "break" (Fig.22) is not observed in winter, and, in the vicinity of the cycle minimum, it is absent even in summer (2004). In the southern hemisphere, no break is revealed at the change of season. The effects observed may be due to the high level of solar activity, when the density of the upper atmosphere increases leading, together with the seasonal warming, to reduction of the ERB particle fluxes at those altitudes. A weak glow at the energy <5 keV in the "break" zone (Fig.21) is, most likely, caused by the galactic cosmic rays.

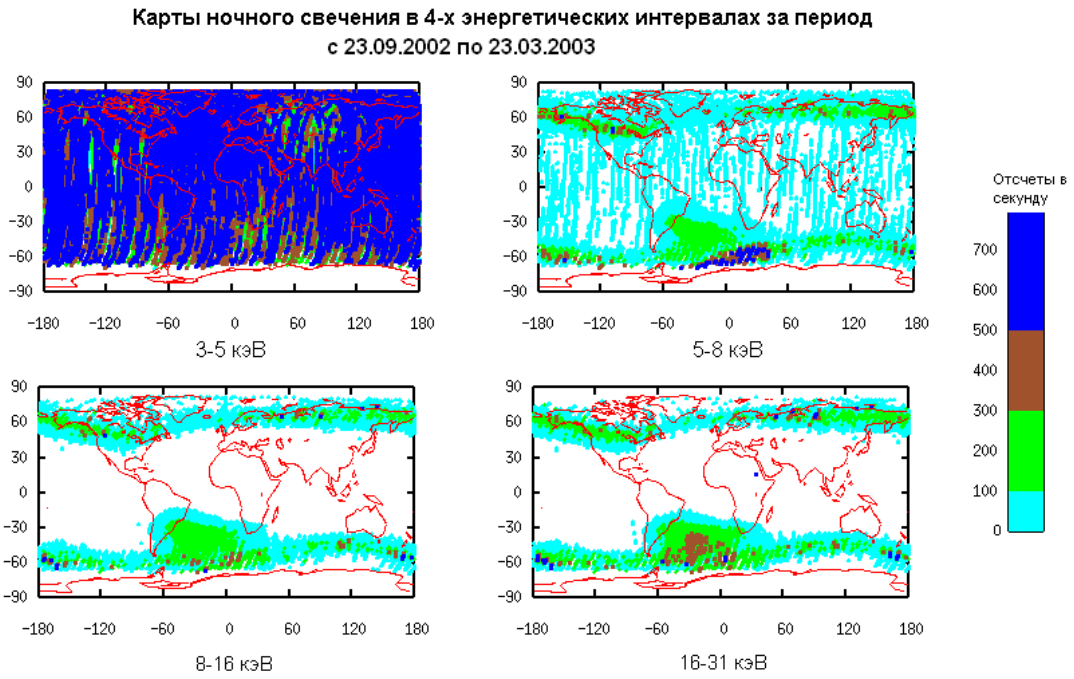

Рис. 9

Fig.22.Maps of the Earth's atmospheric nighttime emission in the energy ranges of 3-5, 5-8, 8-16, and 16-31 keV based on the CORONAS0-F/RPS-1 data for 23.09.2002-23.03.2003 (northern hemisphere, winter).

Conclusion.

Thus, detailed spectral and time characteristics of minor solar X-ray flares were obtained for the first time during the CORONAS-F/RPS-1 experiment. This allowed the precise source temperature to be determined by comparing the measured spectra with those calculated by up-to-date models, such as CHIANTI 5.2. Quantitative estimates were obtained to characterize the increase of the X-ray background spectrum rigidity with the increase of solar activity.

It is shown by observations that, in the energy range of 3-5 keV, the nightglow is observed all over the atmosphere; in the range of 5-8 keV, there are regions where the nightglow is absent; and at >8 keV, it is only present in the zones of the Earth's radiation belts. In summer 2002, in the northern hemisphere (from the Atlantics to Chukotka), the glow in the ERB zone was observed to decrease.

2.1.2.2. CORONAS-PHOTON: Solar and Solar-Terrestrial Physics

Helioseismic monitoring of the Sun in the SOKOL/CORONAS-PHOTON experiment

The CORONAS-PHOTON mission (was launched in 30.01.2009) continue helioseismic studies with the multichannel photometer SOKOL (Solar Oscillations). The instrument was designed at IZMIRAN (Fig.1). It will be used to conduct continuous, high-stability measurements of the solar emission intensity aimed at the study of global oscillations of the Sun. The proposed instrument is a modified and updated version of the DIFOS photometer, which carried out similar observations on board the CORONAS-I (1994-2001) and CORONAS-F (2001-2005) missions. By its observation method and technical characteristics, this instrument closely resembles the SOHO/SPM solar photometer. Observations with the SOKOL photometer will cover a broad emission spectrum from the near UV to infrared wavelengths (280 nm - 1500 nm) (see Table 1). The photometer will observe the Sun as a star, which will enable registration of solar oscillations of low order ($l < 3$).

Tables 2 and 3 provide, respectively, comparative characteristics of the helioseismic devices SOKOL/CORONAS-PHOTON, DIFOS/CORONAS-F, and SOHO, as well as the mutual position of their spectral bands.

The main technical characteristics of the multichannel photometer SOKOL are as follows:

The photometer was designed for measuring the intensity fluctuations of the solar optical radiation in order to obtain the spectrum of global oscillations of the Sun;

The intensity measurements will be taken simultaneously in 7 optical spectral channels: 280, 350, 500, 650, 850, 1100, and 1500 nm with the bandwidth equal to 10% of the central frequency (Table 1);

The relative resolution in intensity is 10^{-6} of the total solar irradiance in the 30 s time interval;

The time interval between the intensity counts is 1s;

The spatial resolution is absent;

The field of view of the photometer is 2^{o};

The resolution of the position detector of the photometer is 5 arc sec.

Table 1. Spectral bands of the photometer SOKOL and their widths.

Band number	**Central wavelength of the spectral band, nm**	**Width of the spectral band, nm**
1	280	30
2	350	35
3	500	50
4	650	65
5	850	85
6	1100	110
7	1500	150

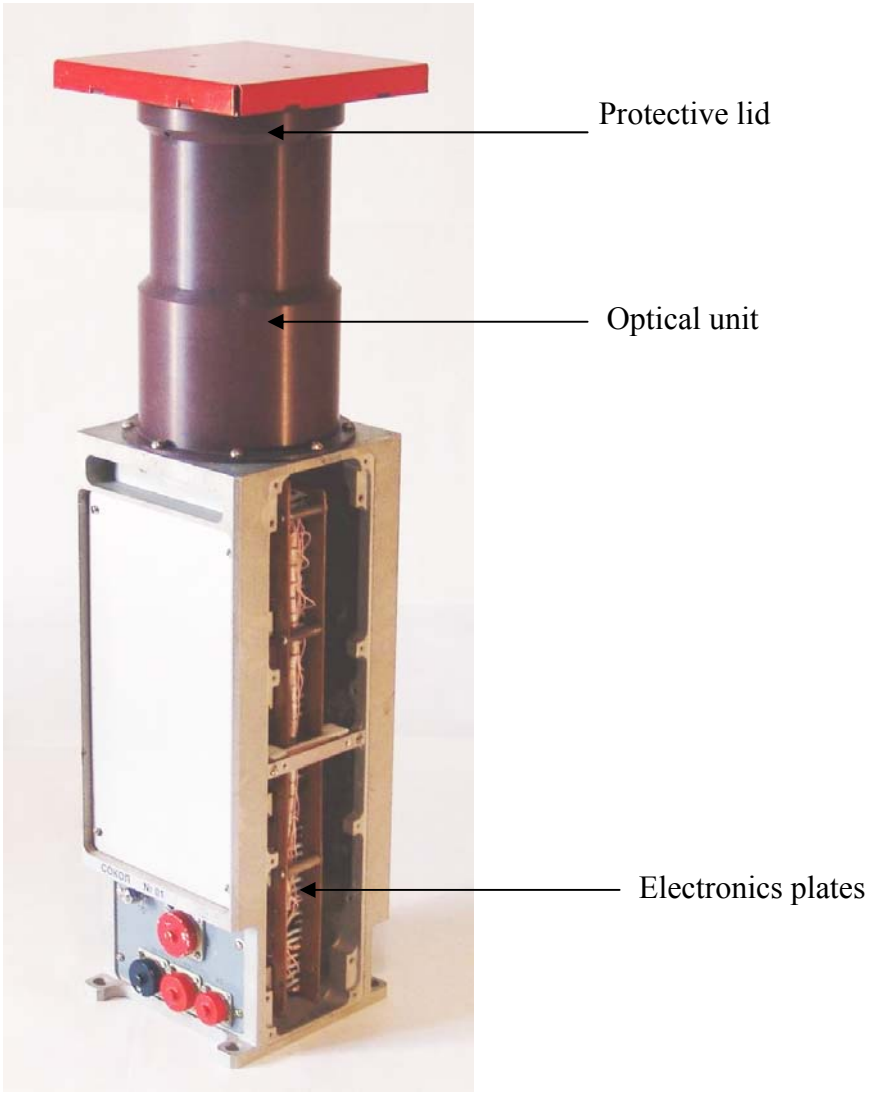

Fig.1. Multichannel photometer SOKOL/CORONAS-PHOTON.

Table 2.Comparative characteristics of the SOKOL-DIFOS-SOHO helioseismic instruments

Mission	Device	Method	Observational spectral band	Spatial resolution
SOHO	MDI	Fourier tachometer, velocity oscillations	676.8 nm	CCD martix 1024x1024 pixel, l = 0 - 4500
	GOLF	Resonance cell with sodium vapor, velocity oscillations	589,0 nm	Absent, l = 0 - 3
	LOI (VIRGO)	Emission intensity oscillations	500 nm	12-element photodiode, l = 0 - 7
	SPM (VIRGO)	Emission intensity oscillations	402 nm 500 nm 862 nm	Absent, l = 0 - 3
CORONAS-F	DIFOS	Emission intensity oscillations	350 nm 500 nm 650 nm 850 nm 1100 nm 1500 nm	Absent, l = 0 - 3
CORONAS-PHOTON	SOKOL	Emission intensity oscillations	280 nm 350 nm 500 nm 650 nm 850 nm 1100 nm 1500 nm	Absent, l = 0 - 3

Table 3. MUTUAL POSITION OF THE SPECTRAL BANDS

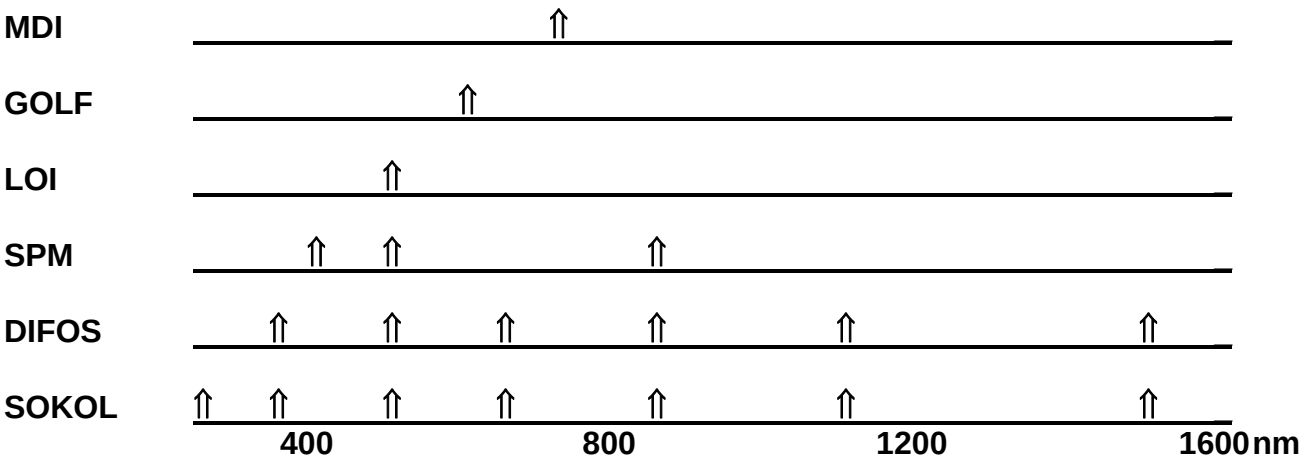

2.1.3. V.I. Vernadskiy Institute of Geochemistry and Analytical Chemistry of the RAS

2.1.3.1. Magellan: Mission of USA (1990-1994)

1.1. Study of volcanic-tectonic structure Lakshmi on planet Venus based on results of photogeologic analysis of radar images taken by the Magellan spacecraft. Formation of this structure, first imaged with high resolution by the Venera 15 and 16 spacecraft, for several decades remained enigmatic. As a result of photogeologic analysis of images taken by the Magellan spacecraft there were identified major episodes of formation of this structure and suggested a model of its formation due to lateral stress and underplating of the volcanic northern plains under the ancient tessera craton. The latter is now almost completely flooded by lavas. Results of this work have been published in international journal Planetary and Space Science.

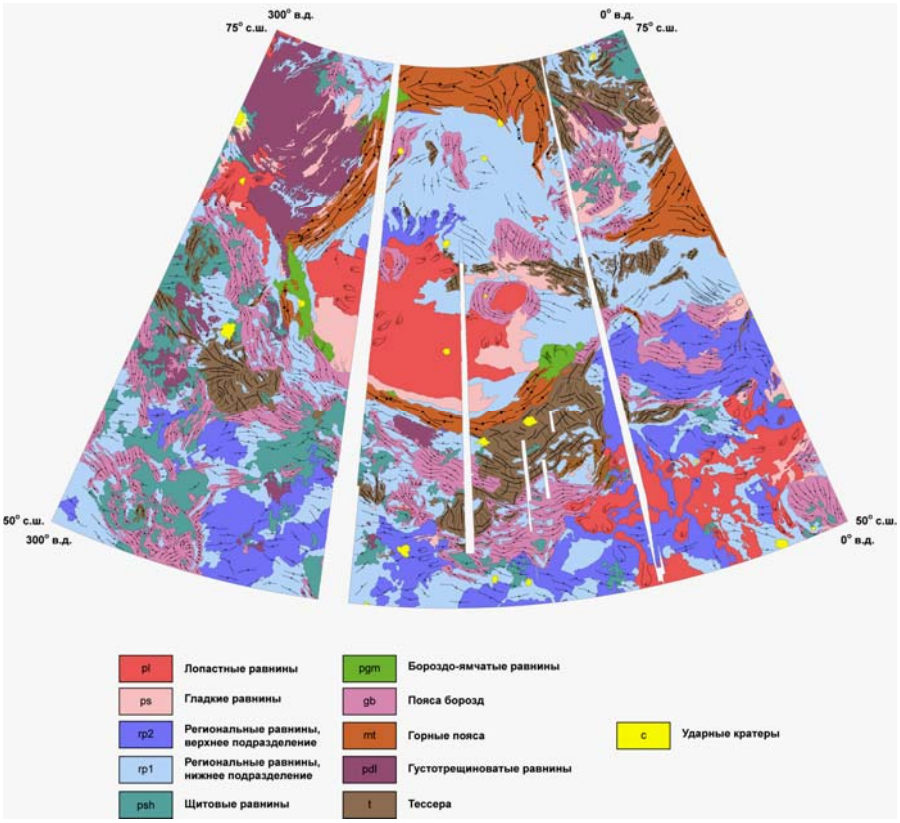

Geologic map of volcanic-tectonic structure Lakshmi.

The work has been done jointly with Brown University, Providence, Rhode Island, USA.

1.2. Investigation of radial volcanic-tectonic structures of Venus: Analysis of duration of their activity based on photogeologic study of radar images taken by the Magellan spacecraft. There was studied a duration of volcanic and tectonic activity of the astrum type radial structures of Venus. Under analysis were age relations between the composing astra faults, regional volcanic plains and impact craters. Based on density of the superposed impact craters, age of regional plains was earlier estimated as ~750 million years, while ages of concrete impact craters near the studied astra were estimated based on the degree of preservation of their ejecta. There has been done analysis of images of all (78) astra identified on Venus and 163 impact craters having the estimated age. For the majority of studied astra it was found that their formation started before the time when

regional plains were emplaced, and for 7 astra it was found that their faults cut craters younger than 100-300 million years. This allowed to conclude that tectonic activity of these seven (and probably most of other) astra lasted for hundreds of million years. Results of this work have been published in the international journal Icarus.

The work has been done jointly with Brown University, Providence, Rhode Island, USA, and University of Oulu, Finland.

2.1.3.2. Mars Global Surveyor and Mars Odyssey, missions of USA, and Mars Express, mission of European Space Agency

2.1. Mapping of contents of ice and bounded water in near-surface soil of Mars in different seasons using data gained by the IR spectrometers TES and Omega. It has been done analysis of results of mapping by TES (Mars Global Surveyor) and Omega (Mars Express) spectrometers of contents of ice and bounded water in surface layer of soil of Mars in the winter and spring seasons. It was shown that areas of the highest hydration of Martian soil tend to be within a periphery of zone of appearance of seasonal water ice in the soil. This is due to saturation state of water vapor in the areas where water ice is present in the soil and because of this an intensive hydration of salt component of the soils occurs. The farther from this icy zone the lower is relative moisture of the near-surface air and the smaller is a degree of hydration of salts. These results are important for understanding of specifics of modern circulation of water on Mars and suggest that the surface layer of soil in winter is a significant reservoir for removing water from the atmosphere. Six abstracts have been published and two papers submitted to Geophysical Research Letters and Kosmicheskie Issledovaniya (Space Research).

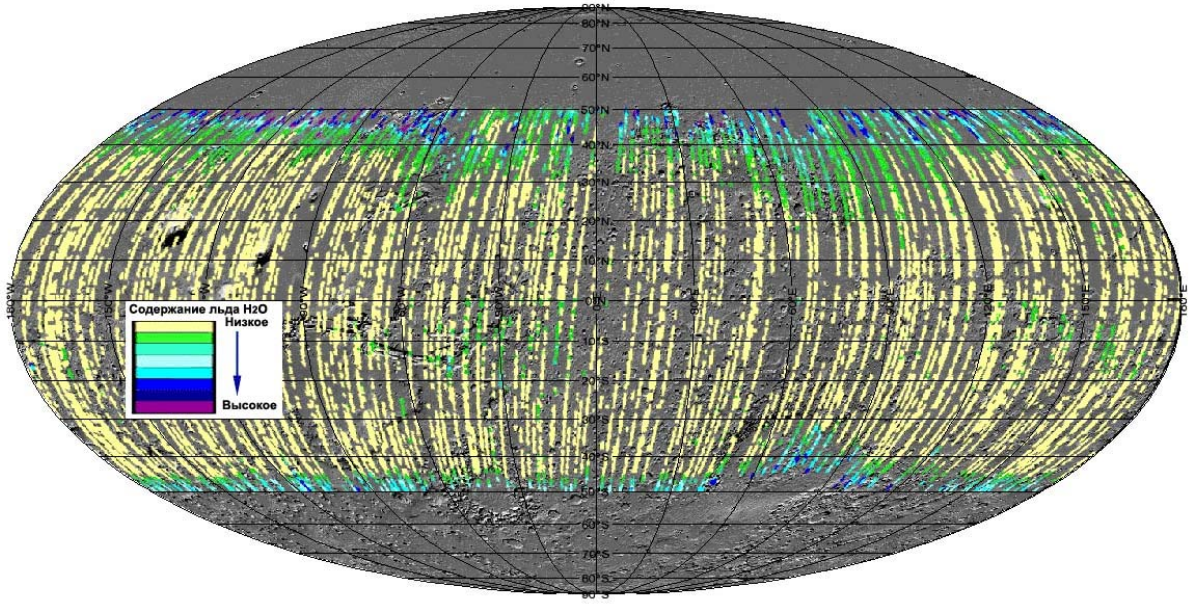

Water ice contents in near-surface (2-10 cm) layer of soil within the ± 50^{o} latitudinal belt. The map was made for winter seasons in the northern and southern hemispheres of Mars.

The work has been done jointly with Space Research Institute, Moscow, Russia, and Arizona State University, Tempe, Arizona, USA.

2.2. Photogeologic analysis of images on the volcanic province Terrena-Mallea on Mars. Geologic-morphologic analysis of images taken by HRSC camera onboard of Mars Express spacecraft and analysis of MOLA topography, Mars Global Surveyor, have been done for the

southwestern part of the Hesperian volcanic plateau at the east of Terrena-Mallea province. Results of this study show that in this region a volcanic activity was alternating with deposition of atmospheric precipitations during all the Hesperian period of history of Mars. Ice-containing deposits formed thick lenses in the layered volcanic sequence. The lenses were then a source of water for formation of large outflow channels (Dao, Niger, Harmakis) connecting Hesperian plateau and Hellas basin. In this region are seen numerous features interpreted to be the head parts of magmatic dikes. The latter probably had been formed at the terminal stage of volcanic activity in the southwestern part of Hesperian plateau? And probably namely they caused melting the buried ice lenses and formation of outflow channels. The work was submitted for publication in international journal Earth and Planetary Science Letters.

The work has been done jointly with University of Oulu, Finland.

2.3. Photogeologic analysis and geologic-morphologic mapping of areas ancient valleys of Mangala Valles. Mangala Valles are extended (50-100 x 900 km) system of flood channels in Marian highlands west of Tharsis uplift. Geologic analysis of image 0286 taken by HRSC camera onboard of Mars Express spacecraft showed that there were several sources of flood water. The main source was the Mangala Fossa graben which formation was probably caused by emplacement of large magmatic dike. Besides there were additional sources: 1) at the places of outcropping of the head parts of other magmatic dikes, 2) in the beginning parts of two clusters of small sinuous channels, 3) in several small local chaos-like features. Crater counts on various elements of the valleys showed that the first episode of the Mangala Valles formation took place ~3.5 billion years ago. It was followed by three others: ~1 billion years, ~ 500 million years, and ~200 million years ago. East of the mapped area are seen fields of extended lava flows having large thickness whose source seemed to be the eastern continuation of the Mangala Fossa graben which supposedly was the main source of water formed Mangala Valles. Crater counts on these lava flows showed that they correlated in time with the elements of Mangala Valles. This supports the suggestion that graben, the major source of the flood water, was formed due to emplacement of magmatic dike. It was found that at the latest stage of the last flood episode, in the initial segment of the valley a formation of meandering channels having characteristics typical of terrestrial river meanders occurred. It this analogy is correct this may mean that at that time there was an episode of global warming on Mars and the related thickening of the atmosphere. The work published in the international journal Planetary and Space Science.

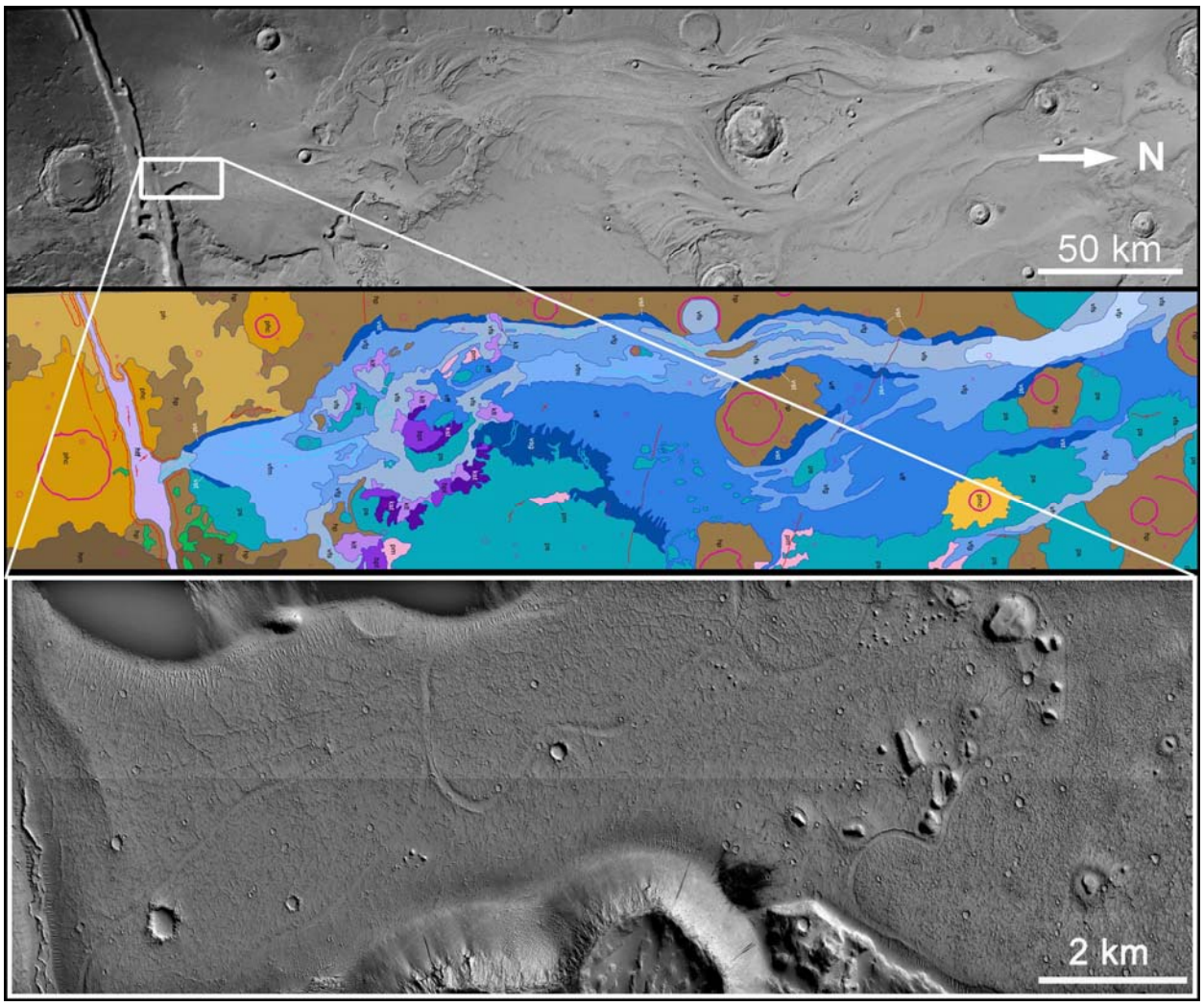

Top and bottom are fragments of the HRSC image 0286, in the middle is geologic-morphologic map of the study area. The bottom image shows meanders in the floor of the initial part of the Mangala Valles. The meander presence may suggest an episode of global warming on Mars ~200 million years ago.

The work has been done jointly with Free University of Berlin, Germany, Geological Survey of USA, Flagstaff, Arizona, Brown University, Providence, Rhode Island, USA, and Arizona State University, Tempe, Arizona, USA.

2.4. Study of geometry of craters on the surface of Martian satellite Phobos based on analysis of images taken by HRSC camera, Mars Express. Geometry of craters (shape of topographic profile and the depth/diameter ratio) have been determined by two techniques: by making profiles from the digital terrain model of part of the Phobos surface and by analysis of distribution of shadows in craters located in the zones with different solar elevations above the horizon. Identification of such zones and preparation of the digital terrain model have been done in the DLR Institute of Planetary Studies, Berlin, Germany. It was found that craters of Phobos with diameters from 200 m to 5 km in their geometry are not distinguishable from lunar craters of the same sizes. These results are important for understanding of mechanics of impact cater formation on the bodies with very small gravity and for preparation of engineering models of Phobos surface which are used for planning of Russian mission Phobos-Grunt. Results of this work have been published as an abstract of the 39th Lunar and Planetary Science Conference, Houston, March 2008.

The work has been done jointly with DLR Institute of Planetary Studies, Berlin, and Free University of Berlin, Germany,

2.5. Study of Phobos surface based on analysis of new images taken by HRSC camera, Mars Express. As a result of synthesis of various data on characteristics of global and regional relief of Phobos as well as microrelief of ancient parts of lunar surface there were made models of surface roughness of Phobos, which are being used for testing hardware and software systems of Phobos Grunt spacecraft to approach this celestial body and land on it. There were made digital models of surface roughness of several levels of detailness (DM-1, DM-2 and DM-3). Depending on resolution of the used images the detail of relief was represented by three overlapping ranges of linear sizes: 1) from 30–90 м to 400 м and more; 2) from 20 м to 50 м; 3) from 2 м to 20–30 м. The work results have been published as an abstract of the 40th Lunar and Planetary Science Conference, Houston, March 2009.

The work has been done jointly with Lavochkin Association, Khimki, Moscow province.

2.1.3.3. Geochemical Constraints on the Internal Structure of the Moon

In spite of the fact that a lot of works are concerned with the internal structure of the Moon, its composition, thermal history and sizes of the core are uncertain. The temperature of the Moon's interior remains one of the most speculative and uncertain physical parameters. According to the data of the Apollo-15 and Apollo-17 lunar missions, the estimates of the heat flux are known only at two points of the Moon's surface, which at the present time are being revised. Seismic data, augmented by such parameters as the mass and the moment of inertia of the Moon, make it possible to find the constraints on the distribution of density and temperature in the interior of the planetary body, and also to estimate its chemical composition and core sizes. Chemical models of the Moon, which are model-dependent, are shown in Fig. 1.

The internal structure of the Moon depends strongly on its composition and thermal regime. However, geochemical studies of returned lunar samples do not give direct information about the composition and physical properties of the mantle. Seismic models and surface heat flow measurements provide only indirect information about the composition and temperature of the mantle. In the studies of GEOKHI RAS, we have proposed new approaches to the solution of the problem of modeling the constitution of the Moon, based on the data on the composition of terrestrial and lunar rocks available in the literature. The approaches consist of retrieving the chemical composition of the mantle and core sizes, and assessing the internal temperature and density distribution from the geophysical constraints including the seismic data, the moment of inertia and mass of the Moon (inverse modeling). The adjustment of the geochemical and geophysical models of the Moon is carried out with the help of the methods of physicochemical modeling. These methods make it possible to transfer the models of the bulk composition into the equilibrium phase associations and the seismic-density characteristics matched with them (the direct problem), and to convert the velocity profiles in the models of the composition and/or temperature distribution (the inverse problem). The procedure of the solution of the direct and inverse problems is realized with the help of the minimization of the Gibbs free energy and the equations of state of the mantle's substance, taking into account the phase transformations, anharmonicity, and the effects of inelasticity. The solution of the direct and inverse problems was carried out on the basis of the THERMOSEISM software and database in the Na_2O-TiO_2-CaO-FeO-MgO-Al_2O_3-SiO_2 system with solid solutions. The database contains the internally consistent thermodynamic parameters on the enthalpy, entropy, heat capacity, the Grueneisen parameter, the thermal expansion, the compression and shear moduli of minerals, and also the mixing parameters of solid solutions. The calculation of the equation of state of minerals is carried out in the quasi-harmonic

approximation of Mie–Grueneisen–Debye, on the basis of the model of elastic continuum with the use of the Born–Mayer potential for the approximation of the potential part of the equation of state and the Debye approximation for its thermal part.

The results of calculations of the content of major oxides are shown in Figs. 1 and 2. Figure 3 and Table 1 show the allowed radii of a Fe–FeS-core that will agree with both the mass and moment of inertia requirements.

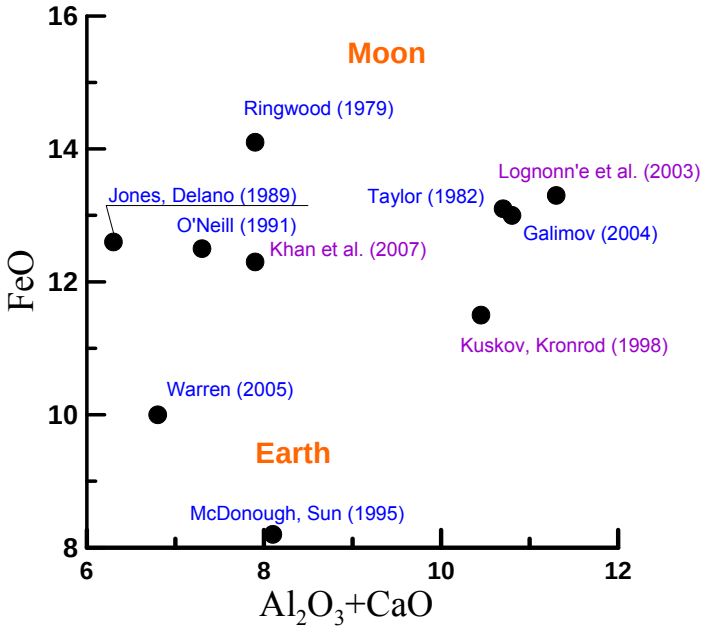

Fig. 1. Bulk composition models of the silicate Earth and Moon

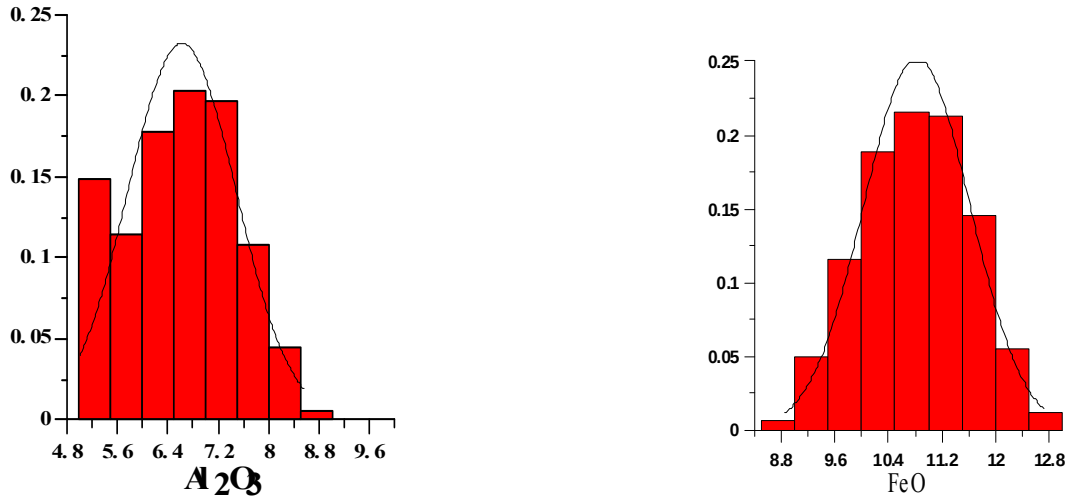

Fig. 2. Probability estimates of the Al_2O_3 and FeO content in the lunar mantle calculated by Monte-Carlo method

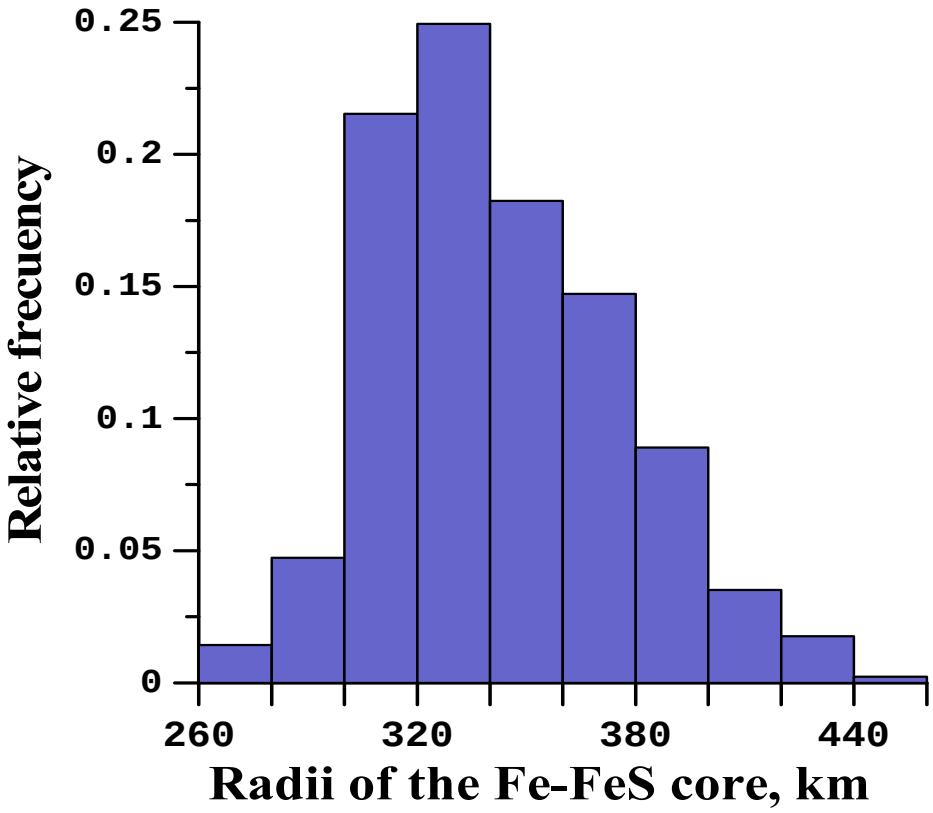

Fig. 3. Probability estimates of the radius of the Fe-10 wt %S-core [Kuskov et al. The systems of Jupiter and Saturn: Formation, composition and internal structure of large satellites, Moscow, 2009] based on the mass, moment of inertia and seismic constraints from [Gagnepain-Beyneix et al., Phys. Earth Planet. Inter., 2006].

Table 1. Maximal radii of the lunar Fe-S core at various thickness of the crust

Core composition	Core density, g/cm^3	H_{cr} = 60 km, ρ_{cr} = 3 g/cm^3		H_{cr} = 30 km, ρ_{cr} = g/cm^3	H_{cr} = 80 km, ρ_{cr} = g/cm^3
		$R_{макс.}$, km	M_{core}/M(Moon), %	R_{max}, km	R_{max}, km
γ-Fe(Ni)	8.1	350	2	380	330
Fe-10%S	5.7	445	2.9	480	420
Eutectic Fe-FeS	5.15	490	3.4	525	460
Troilitic (FeS) core	4.7	530	4.1	-	-

In summary, it is evident that new heat-flow experiments and geophysical networks are required for determining the fine seismic structure of the Moon. Knowledge of chemical composition, thermal regime and core sizes is essential for the understanding the internal structure of the Moon and its origin.

2.1.4. The RAS Institute for Bio-Medical Problems

In 2008-2009 under the realization of long-term Program of the Scientific and Applied Research on the Russian Segment of the International Space Station (ISS) 2 biomedical experiments in the field of Space Medicine and Physiology "Cardio-ODNT" and "Profilaktika" and 1 experiment in the field of Space Biology - "Regeneratsiya" have been completed.

In the experiment **"Cardio-ODNT"** (PI of experiment – Doctor of Medical Sciences V.V. Bogomolov, Research Manager – Candidate of Medical Sciences I.V.Alferova) results from complex research on dynamics of the heart activity basic parameters, central and regional blood circulation at rest and during LBNP were evaluated.

In the research conducted in flight it was revealed that under the relative rest conditions sphygmic blood filling of the forearm vessels was increasing and calf did not change. The tonus of large vessels in the forearm and shin practically has not changed. The tonus of small vessels in the forearm was considerably reduced and in the calf it only had a slight tendency to decrease. Sphygmic blood filling of lung vessels was considerably rising; the tonus of large and small vessels was increasing. The duration was changed for separate temporary phases in systolic blood flow to the pulmonary artery system in the form of increase in fraction of slow and maximum blood filling. Speed of the maximum and medium blood filling in lung vessels was rising. All the mentioned changes in hemodynamic parameters for the lung area in flight had indicated the hypervolemia and hypertension of pulmonary circulation vessels.

At effect of LBNP the level of decrease in sphygmic blood filling for calf vessels and manifestation of difficulty in blood outflow did not differ significantly from preflight results. Reduction in parameters for the sphygmic blood filling and a tonus of small vessels in the lung area was noted; speed of maximum and medium blood filling was reduced. In flight during deposition of part of the blood in a decompression zone, changes of the listed parameters were much more evident than in tests before flight. As a result, their values came close to the numbers received at corresponding decompression modes during preflight test.

In long duration space flights in comparison with terrestrial conditions there are changes in the functional equilibrium between vascular areas of systemic and pulmonary circulation as development of the changed functional load on blood circulation system under the impact of flight conditions.

The effect of LBNP during flight led to a normalization of hemodynamic situation in the lung area.

Quantitative characteristics of parameters for sphygmic blood filling and the tonus of calf and lung vessels at decompression were close or equal to their values received in preflight tests.

Experiment "**Profilaktika**" **(**PI of experiment – Doctor of Medical Sciences I.B.Kozlovskaya) was devoted to the study of action mechanisms and efficiency of various countermeasures intended to prevent disorders of the musculoskeletal system in weightlessness. For the first time in space flights history the energy cost and physiological response of an astronaut's organism to the locomotor, bicycle ergometry and power loads at different stages of flight were measured. At the same time, based on the received results, distinctions in executed loads cost changes in microgravity are noted and the statement that efficiency of 1st month training under space flight conditions is lower than during the next months of the flight is confirmed.

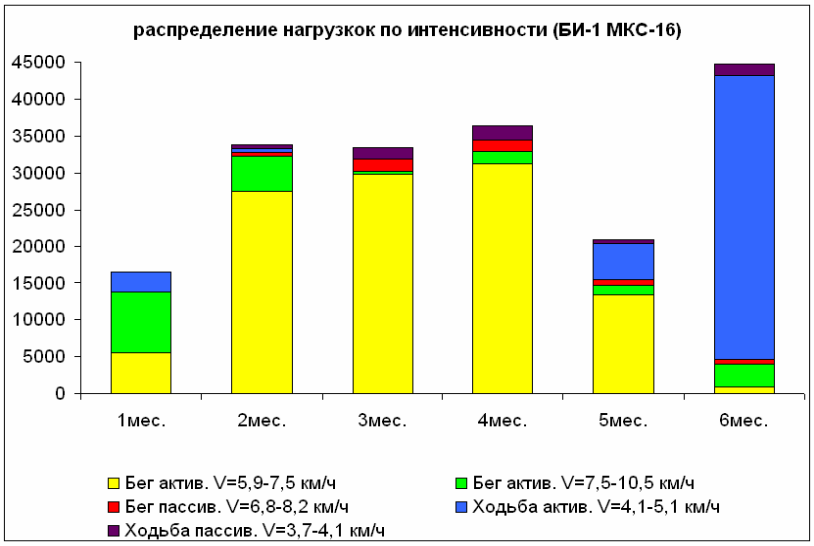

Fig 1. Y. I.Malenchenko at carrying out the bicycle ergometry test of "Profilaktika" experiment.
Fig. 2 Distribution of intensity for locomotor loads

Finding the significance of gravity in various vital processes at terrestrial organisms is a paradigm of Space Biology. One of such problems is studying of regeneration of organs and tissues after their damage or full loss under the space flight conditions. Experiment **"Regeneratsiya"** that has been focused on this problem, studied the impact of microgravity on regeneration processes at bio objects using electrophysiological and morphological parameters (PI of experiment - Doctor of Biological SciencesG.I.Gorgiladze)

Fig. 3. Regeneration of the snail shell in 109 days SE.

Fig. 4. Regeneration of a snail leg in 163 days SE.
1 – intact leg, 2 – dissected away distal part of the leg, 3 – snail before flight, 4 – regenerated part of a snail leg postflight

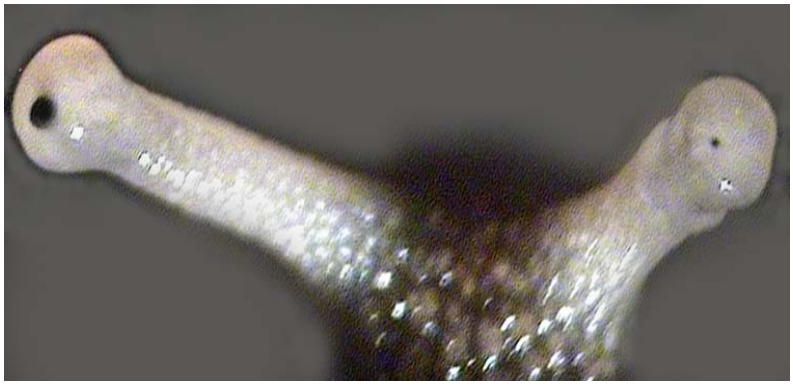

Fig. 5. Regeneration of eye tentacles of a snail in 163 days SE. - left intact, right regenerated tentacle

Fig. 6. Regeneration of planaria after a medial body dissection. 1 – Planaria in intact condition, 2 and 3 – Right after its medial dissection in two halves, 14 hrs prior to manned spacecraft "Soyuz" launch, 4 – Planaria regenerated from the right half. Photo made 8 hrs after the completion of 11 days OF

The received results testify that absence of gravity is not the limiting factor for the realization of regeneration mechanisms. They have shown a preservation of high regeneration ability at the chosen experimental objects under microgravity conditions. In experiments on snails during OF from 3 to 5,5 month in duration instead of dissected away eye tentacles new ones with functioning eyes were developed, the leg had partially grew and the shell had completely regenerated. Species which are not considerably different from control terrestrial objects had regenerated from laterally cut fragments of planaria during 10-12 days OF. At the same time an abnormal character of regeneration was found in experiments with planaria which regenerated from the fragments received at their medial dissection.

2.1.5. D.V. Skobeltsyn Scientific-Research Institute Nucleus Physics of M.V. Lomonosov Moscow State University

The objective of the scientific research of the Institute's team is to obtain breakthrough knowledge and quantitative information about the fundamental laws which control interrelated dynamics of space radiation and electromagnetic processes on the Sun, in the heliosphere and in the Earth's magnetosphere. Experimental and theoretical studies are aimed at the development of the practically important physical basis for monitoring of the near-Earth space conditions and for the clarification of the mechanisms of the influence of space radiation factors on space and ground-based systems under the conditions of changing solar activity. Space experiments and intensive theoretical studies accompanied by mathematical simulation and development of the modern storage systems for space monitoring data are conducted. The main subjects of the studies in 2008-2009 included the following directions of the solar-terrestrial physics: studies of radiation conditions both in the interplanetary and near-Earth space during the solar activity cycle including 2008 and 2009 – the period of prolonged solar activity minimum.

1. Development of scientific equipment for radiation measurements onboard satellites.

- Experimental studies of the radiation fields of the Earth's magnetosphere are carried out on the basis of the data of the dose radiometer onboard GLONASS series satellites (circular orbit at the altitude of 20,000 km) and of the radiation control system onboard International Space Station (device R-16 and system of semiconductor dosimeters DB-8). Mass volume of experimental space-physics information was obtained.

In 2008-2009 the following satellites were successfully launched:

- six satellites of GLONASS series with dose radiometer (RD) in order of the near-Earth space monitoring;
- «CORONAS-Photon» (circular polar orbit): the purpose of this experiment is to study the composition, flux and energy spectra dynamics of the charged solar energetic particles (SEP) in the near-Earth space and to study the electron components of the Earth's radiation belts.
- «Universitetskij-Tatiana» micro-satellite (polar orbit at the altitude of ~800 km): the experiment is aimed at the studies of luminous phenomena in the Earth's atmosphere, caused by galactic and solar cosmic rays and energetic particles in the auroral and equatorial regions, along with monitoring of solar activity and studies of ionosphere's and upper atmosphere's dynamics.
- «Meteor-3» solar-synchronous satellite (polar orbit at the altitude of ~800 km) with experimental equipment developed by SINP scientists onboard: MSGI-MKA and SKL-M for registration of electron and proton flux with energy from 50 eV up to several hundreds MeV.

2. The dynamical processes on the Sun and in the heliosphere.

– Influence of the active regions (AR) located inside or on the border of the coronal holes (CH) on the parameters of high-speed solar wind flow (HS SW F) was analyzed according to the data of the spacecrafts STEREO-A, STEREO-B, SOHO/EIT and ACE situated near the Earth's orbit at different longitudes and latitudes. A complex consisting of ARs and CHs was observed during the studied period of solar activity minimum (September, 2007 – April, 2008). This complex did not produce any observable sporadic solar activity. Presence of sufficiently large close-ended

magnetic structures inside the CHs and fast, one day long variations of the CH's shape lead to the changes of HS SW F which can noticeably vary for different spacecrafts. ARs situated behind the CH along the Sun's rotation do not affect the HS SW F forming.

– The possibility of the prediction of high-speed solar wind flows was analyzed basing on the coronal holes' dynamics. Using a simple empiric models sufficiently good prediction results for the period around the minimum of the 23rd solar cycle were obtained. For the independent data set correlation coefficient was increased from 0.66 up to 0.8.

– The turbulence properties of the solar wind plasma, in particular, the alternation of fluctuation of the solar wind ion flux in the previously unstudied region of the relatively high frequency (0.01-1 Hz) was studied. It is determined that the solar wind observation intervals with sharp jumps of the flux are essentially more alternated than the quiet solar wind intervals.

– Comparing the distributions of the shock waves fronts in 1991 and 2004 lead to new elements of similarity and difference. In both cases the best approximation in front of the wave is made by lognormal distribution, behind the front – by Gauss distribution. Probably, it means majority of multiplicative and additive processes in each case.

– The response of the proton flux in the interplanetary space for the quiet Sun and MgII solar activity index was analyzed. Best of all the minimum values of solar activity are described with the values of MgII index comparing with other indices (Rz, radio 10 cm) which do not follow small variations.

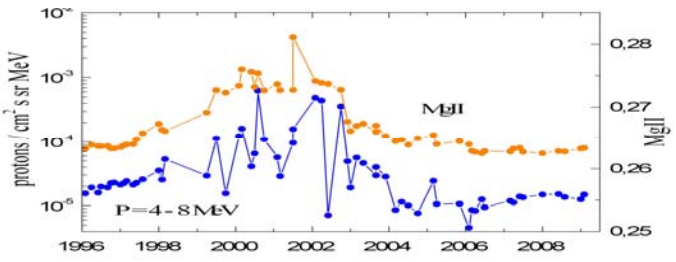

Fig. The proton flux and MgII index as a function of time.

3. The studies of physical processes connected with solar cosmic rays generation and propagation.

– Photon spectra up to the energy of 300 MeV were retrieved and the component of the spectrum associated with neutral pion decay was separated according to the data of the experiment onboard CORONAS-F satellite during four powerful solar flares. It allowed to determine the time of generation of the protons accelerated up to the energy over 3000 MeV on the Sun and to calculate absolute values of gamma-radiation of such energy and the number of the protons accelerated during this event. Comparing the time of the beginning of high-energy protons acceleration with the time of registration of the particles at the distance of 1 a.u. it was shown that practically the protons escape into the interplanetary space in the point of acceleration.

– The increases of the counting rate at the separate stations of the global network of neutron monitors introducing the main increase of solar cosmic rays was discovered. Occurrence of such advanced increases proves that the high-energy (over 500 MeV) protons begin to escape from the solar atmosphere into the interplanetary space directly after their acceleration, moreover for a part of protons the path is shorter than the specific length of the interplanetary magnetic field's lines.

– For the first time the flare of 20.01.2005 was analyzed in a complex multi-wave way. It is shown that Hα and UV radiation and the source of hard X-ray and gamma radiation are concentrated within a compact region which is located in the shade of large spot.

Acceleration of the protons up to the energy of several hundreds MeV begins simultaneously with the main flare energy release.

- The full energy of the accelerated electrons and the thermal energy of the radiating plasma were compared. It is shown that in the beginning of the pulse phase of the flare the full energy of the accelerated electrons is 1.5-2 times greater than the thermal energy of plasma, then these two energies grade up to each other and became equal to (4-5)×10^{30} erg for electrons on the assumption that the coefficient of the flare loops filling with hot plasma is 0.5-0.6.
- Data analysis for the flux profiles in the SEP events according to the different spacecrafts has shown that for a half of the events there is a kind of declining phase for the flux of the electrons with energy of Ee >> 1 MeV and protons with energy of Ep >> 10 MeV and congruence of the characteristic time of declining for electrons and protons. Non-trivial feature of this fact consists of by two orders of magnitude difference between the magnetic rigidities R of the electrons and protons of the mentioned energies. Therefore time profiles for electrons and protons should differ greatly. It leads to the following conclusion: in the interplanetary space the diffusion processes do not have a dominant role in the energetic charged particles propagation, it's also necessary to take into account their convectional carrying-out, adiabatic cooling and capture of the particles in separate magnetic structures.
- The vast data base containing about 40000 X-ray solar flare events compiled and visualized as histograms and movies presented on the site (http://dec1.sinp.msu.ru/~pavrus/) for different flare classes according to their intensities. Spacecraft measurements were analyzed during 21nd-23rd solar cycles with a time resolution of 1 min. New result obtained is that the rising time and total duration distributions follow the lognormal laws with parameters depending on the class and the solar cycle. One-modal distributions cover both 'impulsive' flares (~20-30 min duration) as well as 'long-duration' events (> 30 min and up to many hours) at the level of 1-3 sigma.

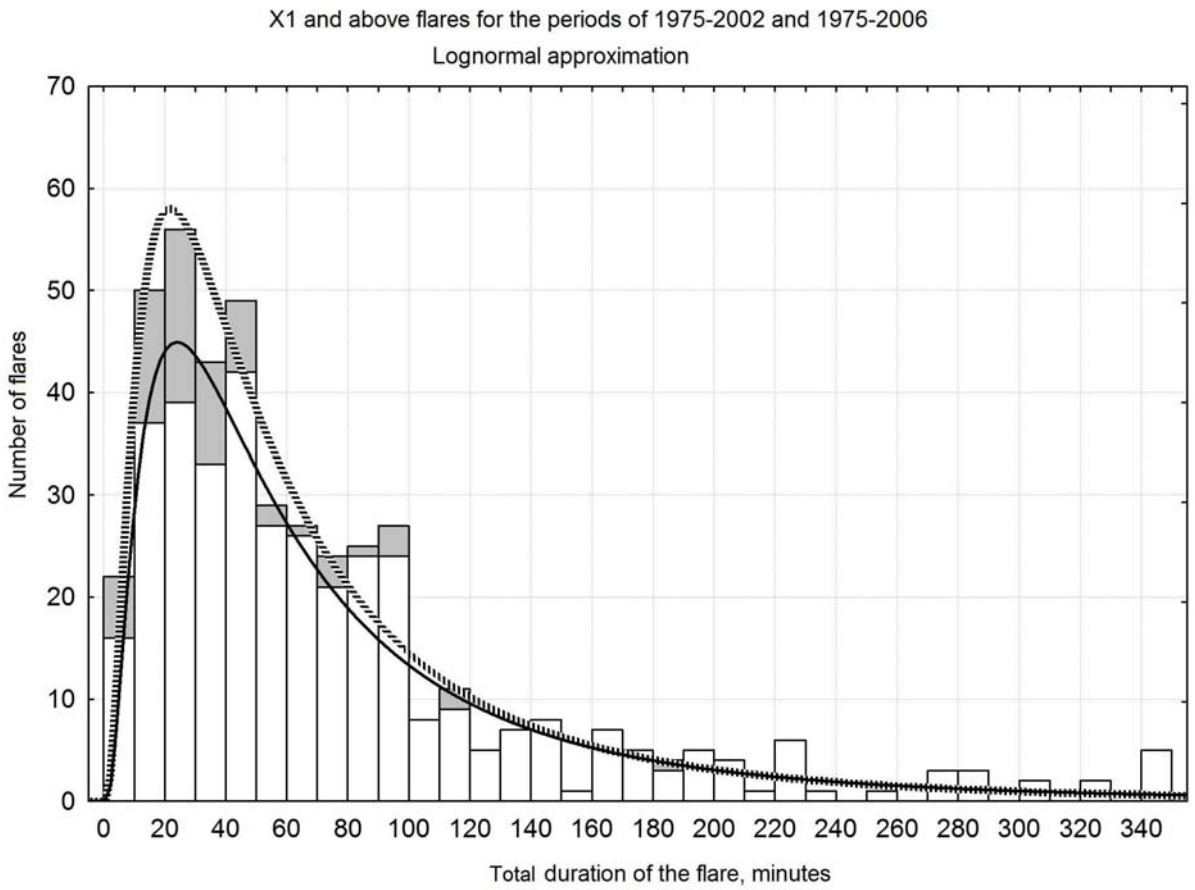

Fig. The number of flares versus their total duration (min) for the X-ray flares of the X1 class and higher during 1975-2002 and 1975-2006 together with their lognormal approximations. Excesses and fluctuations of histograms are shown in gray.

- A catalog of ground-level enhancements (GLE) during the period of 21-23 solar cycles is developed. The main features and time distribution of these events are studied, along with their interrelation with the solar sources and proton increases observed by the satellite equipment.
- The analysis of a number of SEP events for which annual fluences during 450 years were determined from the samples of Greenland ice has shown that the values of SEP events are distributed as power functions with cutting of the set at large fluence by exponential function.

4. The studies of the characteristic features of the processes of solar cosmic rays propagation and influence on the Earth's magnetosphere.

During the recovery phase protons in the belt are captured and accelerated by 1-3 orders, and it results in the appearance of maximums at L=2 and 3. Deep penetration makes it possible to capture solar protons on the close shells. The capture is possible after each leap of the solar wind pressure during the temporal return to the dipole structure of the magnetosphere. Such capture is mostly fragile, the next expansion of the quazi-capture region towards the Earth wash the formed belt off. Only at the recovery phase the final, essential for the long-term history of the proton belt capture of the solar protons of MeV energies will happen at L=2. In the medium storms the solar protons are also captured, but at more distant shells.

Most effective acceleration took place during the magnetic storms combined by 2 or 3 separate storms.

Aceleration results in the increasing of the proton flux in the belt within the wide range of latitudes, but due to fast ejection of the particles into the loss cone a new belt structurizes with appearance of maxima at L=3 and 3. Fast ejection is explaned by generation of ion-cyclotronic waves. During the following slow ejectrion the intensity of the proton flux of 1 MeV energy kept increases for 1 year at L=3 and for 4 years – at L=2.

Extrapolation onto the other solar cycles shows that about half of the time influence of the magnetic storm on proton belt intensity and it must be taken into consideration in the proton belt models.

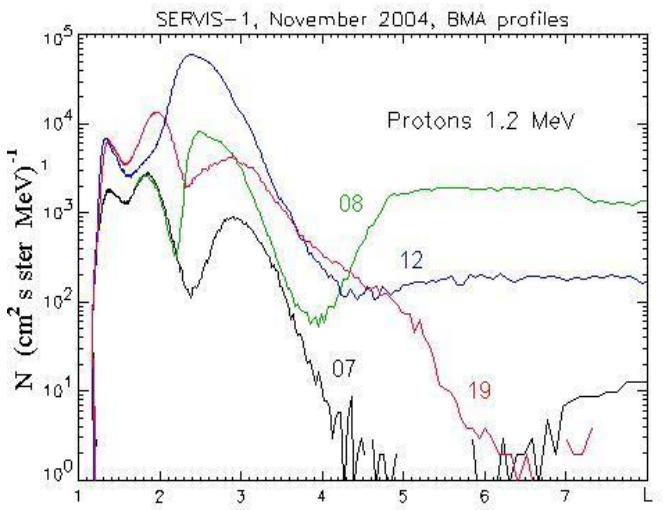

Fig. Latitudinal profiles of the proton belt measured on November 07, 08, 12, and 19, 2004 by SERVIS-1:
07 – before the magnetic storm, regular belt maximum at L=3 and additional one at L=1.8 remains after the July 2004 magnetic storm,
08 — new maximum appeared after the recovery phase of the 7-8.11.04 storm by capture and acceleration of the solar cosmic rays,
12 — additional acceleration of this belt after 11.11.04 storm,
19 — division onto two maxima as a result of the proton diffusion into the loss cone.

– The maximum solar cosmic rays flux within the energy ranges from ~ 1 MeV up to ~ 100 MeV during three solar cosmic rays increases in December 2006 was analyzed basing of the experimental data of ACE spacecraft in the interplanetary space, "Universitetskij-Tatiana" and POES satellites in the polar caps region of the Earth's magnetosphere and GOES-11 satellite at the geostationary orbit. It is shown that basically there are three factors principal for the observed changes of the maximum flux of the increasing of the solar cosmic rays with energy > 10 MeV and 30 MeV inside the Earth's magnetosphere comparing with the interplanetary space. They are the level of anisotropy of the solar cosmic rays flux, conditions of the interplanetary magnetic field and the level of geomagnetic activity.

– Solar cosmic rays penetration into the polar regions during the long solar proton events in December 2006 are investigated basing on the data from five NOAA/POES satellites. Along with already known effect of the penetration region increasing due to geomagnetic activity several new phenomena were discovered. In particular diurnal variation of the position of the center of the energetic solar cosmic rays penetration region associated with the inclination angle of geodipole (tilt-angle). It is shown that the region of the solar cosmic rays penetration moves towards night hours due to increasing geomagnetic activity, and at the main phase of the geomagnetic storm it moves towards the evening, which caused by intensification of the geomagnetic tail current and asymmetric ring current, respectively. An empiric model for the solar cosmic rays penetration into the north and south polar caps is developed for the protons with energy from 240 keV up to > 300 MeV and electrons with energy of > 300 keV. This model allows to determine the latitude of cutting for each sort of particles depending on local time, tilt-angle and geomagnetic indices: Dst, Kp and AE.

– A simple method for calculating of the effective vertical cutoff rigidity of charged particles was developed, taking into account the Kp-index and the local time, on the basis of synthesis of the results of the extensive trajectory calculations for trial particles moving in the geomagnetic field. According to the Tsyganenko-89 model the vertical cutoff rigidities were calculated by an

International Standard Geomagnetic Reference Field (IGRF) model and thereafter corrected in accordance with the geomagnetic disturbance and local time conditions. The fits from the proposed method agree with the results of cutoff rigidity measurements carried out by satellites. The method is intended for applications using cutoff calculations, such as evaluating particle penetration of spatial boundaries, calculating magnetospheric transmissions for low-orbital spacecrafts flights and interpreting the results of orbital experiments.

– The most steady quasi-periodic variations both for the cosmic rays flux and the solar activity and the interplanetary space parameters are separated basing on the data during five solar activity cycles. It is shown that the period of about 1.7 years is clearly seen in the variations of the general solar magnetic field and the angle of heliospheric current sheet's inclination. Relations of the quasi-biennial variations of the cosmic rays and of the general magnetic field of the Sun is discovered.

5. The investigations (analysis of the experimental data, theoretical studies and comparison of theoretical results with experimental data) of the dynamics of the processes in the space plasma, including the magnetospheric plasma, and solving of space weather problem.

– The increases of the relativistic electrons out of the borders of the outer electrons' radiation belt is studied on the basis of the experimental data from the satellites “CORONAS-F” and “CORONAS-PHOTON”. It is discovered that the studied increases are localized at the latitudes of the auroral zone. An event with the increasing of the particle flux was observed at high latitudes during the sub-storm. The observed increases were compared with the geomagnetic micropulsation. The first simulation results have demonstrated the possibility for the appearance of the local traps which are living during the several hours and in which the drift trajectories of the energetic particles do not ring around the Earth.

– For the first time basing on “Meteor” data it was shown that during the collapse of the trapped radiation region at the main phase of the super-storm the night boundary of the trapped radiation, the equatorial boundary of the precipitating auroral electrons and the center of the western electrojet coincided within the limits of ~1° of invariant latitude, moving to L ~ 3. Under the conditions of the fast developing main phase of the powerful magnetic storm (with the rate of amplitude's rise of Dst > 100 nT/hour) the known empirical dependences for the position of the night boundary of the auroral zone, western electrojet boundary from the amplitude of Dst variation derive greatly from the experimental data. At the same time the dependence of the position of the maximum of the relativistic electrons injected during the magnetic storms from the storm's amplitude $|Dst|_{\max}$ are in good compliance for all the studied structures and can be usefull for the prediction of their extreme latitudinal position during the storm.

– The dynamics of the external radiation belt of the Earth is studied during the periods of maximum, decrease and minimum of the solar activity cycle and at different levels of the geomagnetic activity according to the data of the protons and electrons flux measurements by the satellites “CORONAS-F” and “CORONAS-PHOTON”. During 2001-2003 significant increase of the relativistic electrons flux of the external radiation belt of the Earth was observed, electron flux variations at L-shells from 3 up to 5 were sufficiently close and this can be associated with the increasing mean speed of the solar wind during this period. It is shown that even the weak geomagnetic disturbances accompanied by wave activity can significantly influence on the radiation conditions in the near-Earth space.

– The bursts of the electron flux near the geomagnetic equator (L<1.2) are investigated. Analysis of the data from the satellite “Universitetskij-Tatiana” and other spacecrafts has shown a knee of the electron spectrum near the energy of 1 MeV. Up to 1 MeV the spectrum is

approximated by thermal (Maxwell) function, at high energies it becomes a power function. It can give an evidence of two sources of the electrons in the mentioned area.

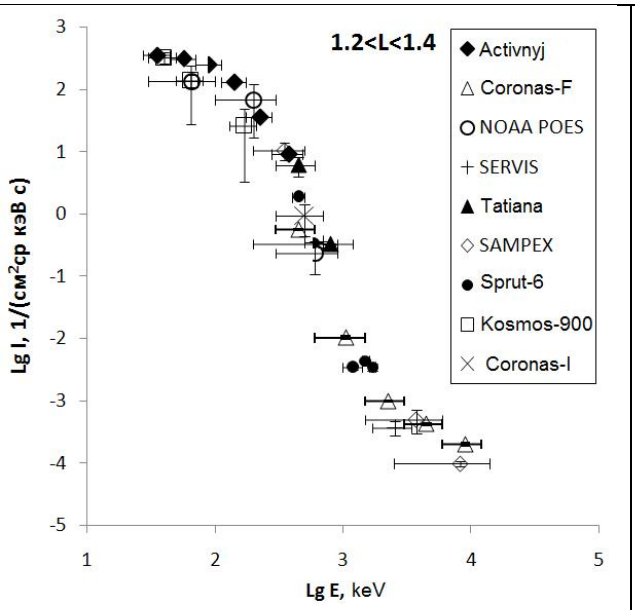

Fig. Differential spectra of the electrons at 1.2<L<1.4. The region of the South-Atlantic Anomaly was cut out from the experimental data array.

- Long-term variation of the proton flux at the energy of 800-2500 keV in the region of the South-Atlantic Anomaly (SAA) was studied. The presence of the anomaly's drift towards the north-west direction is proved. The method of "center of mass" was developed in order to determine the position of the anomaly's center. Being applied to the experimental data obtained in 1992-2008 on the NOAA series satellites this method has shown that the anomaly drift speed towards the western direction is about 0.3 deg/year, and towards the northern direction is less than 0.1 deg/year. The anomaly center position according to the data on the particles flux and to the geomagnetic field intensity do not coincide. Model calculations are proposed in order to explain this phenomena.

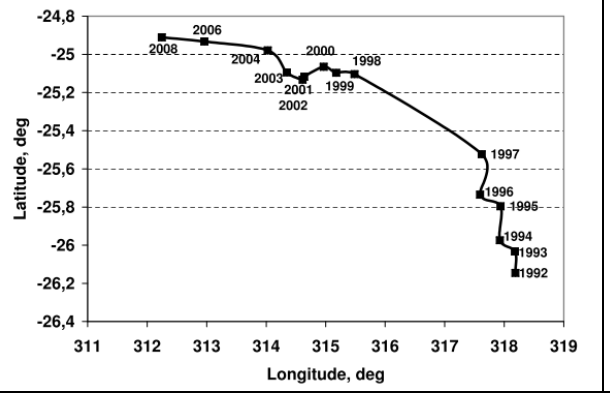

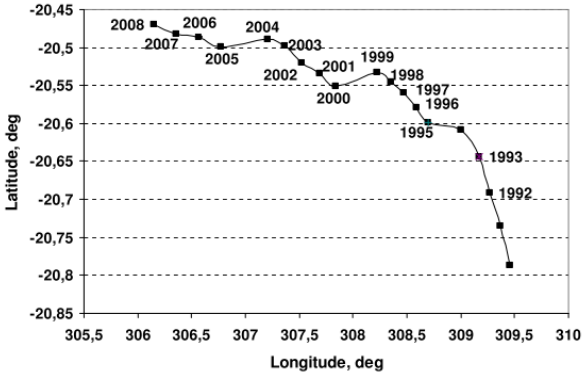

SAA drift in 1992-2008: position of the SAA center

According to the data of the NOAA/POES series satellites Ep=800-2500 keV	According to the model of the Earth's magnetic field IGRF

– The studies of the bursts of the proton flux at the energy from dozens keV up to several MeV near the geomagnetic equator (L<1.15) are studied on the basis of the data of the NOAA

series satellites (altitude of 900 km). It is shown that the particles are injected into the near-equator region starting from the moment of the beginning of the storm's main phase (extremely powerful storm 12.05.1992 with Dst=-300 nT and medium storm 23.03.2007 with Dst=-70 nTesla), proving the theory of double charge-exchange of the ring current protons. By the example of 70 geomagnetic storms during the period of 1992-2008 it is shown that the coefficient of the flux increasing is proportional to the storm's power (the value of Dst index). The studies of the long-term variations of the quasi-trapped electron flux within the energy ranges from several dozens of keV up to 1 MeV at L<2 has shown the presence of the seasonal variation: the flux is maximum in summer and in winter, while the flux of the precipitating particles increases in spring and in autumn. The steady seasonal variation of the anisotropy of the electron flux under the radiation belts is observed in the 23rd solar cycle.

– The long-term variations of the flux of the Earth's radiation belts trapped protons are discovered. Processing and analysis of the data of the low-orbit satellites (NPOES, CORONAS-F, Universitetskij-Tatiana) have shown that without solar events and geomagnetic disturbances:

- the experimental flux of the trapped protons with the energy of less than 10 MeV exceeds the model calculations of AP8 and SALAMMBO at the drift-shells L<1.6 (in the region of SAA), but corresponds to the model LOWPRO,
- satisfactory agreement of the experimental flux of the trapped protons with the energy >10 MeV and the model calculations of AP8 at the drift-shells L<2 (in the region of SAA).

The studies of the variations of the trapped proton flux during the 23rd cycle of the solar activity at the drift shells L = 1.14-1.20 and their comparison with the data of the previous cycles have shown that:

- the time delay of the proton flux variation in relation to the solar activity change depends on the evenness of the solar activity cycle and increases with the increasing of the altitude of the drift shell;
- the proton flux variation is caused by the variation of the atmosphere's density due to the solar activity changes;
- time variations of the mentioned proton flux correlate with the solar activity changes taking into account the time delay;
- the time delay differs for the different L-shells, for L>1.14 it also depends on the evenness of the solar activity cycle: for the even 22nd cycle it is lower, than for the odd 21st and 23rd cycles.

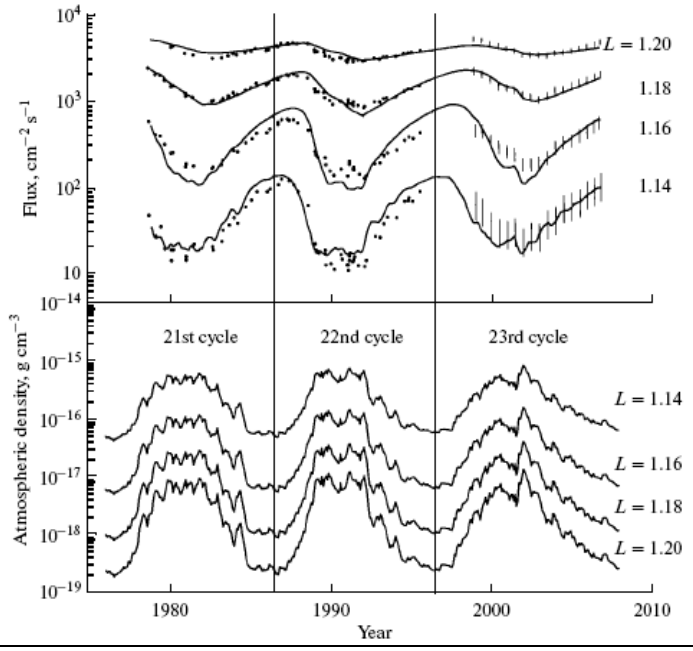

Fig. The flux of trapped protons with the energy above 70 MeV (points and curves show the experimental data and calculation results, respectively) for the 21st–23rd SA cycles (top panel) and calculated values of the averaged atmospheric density on the geomagnetic equator $\rho_{atm}(t)$ as a function of time.

– The relations between the inputs of the ring current and magnetotail current into Dst value were studied by means of paraboloid model of the magnetosphere basing on the statistic processing of 70 magnetic strorms happened during 1998-2003. Calculations of the magnetic fields variations on the Earth's surface during the studied disturbances and in the corresponding magnetic quiet day of the month took into account the effect of the telluric currents inside the Earth. According to the developed in the Kioto WDC procedure Dst and magnetospheric current systems inputs into Dst were calculated for each storm. The relations of the ring current's input and tail current sheet input into the storm's maximum depending on the Dst value "corrected" according to the solar wind pressure were calculated. The calculations resulted in the description of the amplitude of the plasma injection from the magnetotail depending on the storm's power.

– The supposed methods for estimation of the fractional ring current value are based on the variations of ASY-H geomagnetic index. The effect of the ring current asymmetry is studied for the magnetic storm November 20-22, 2003. The values of the fractional ring current value for the maximum of the storm and its input into Dst value are calculated basing on the developed model. Time characteristics of the development and dissipation of the fragmentary ring current during the magnetic storm are studied.

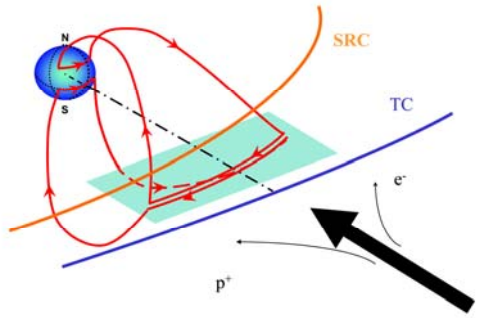

Fig. Schematic drawing of the elementary circuit of the fragmentary ring current system in the night part of the Earth. Big black arrow shows the direction of the large-scale magnetospheric convection. SRC and TC are the elements of the large-scale current systems (symmetric ring current and tail current), which are linked up with the equatorial fragment of the fragmentary ring current.

– Basing on the experimental data obtained by the satellites near the equatorial plane during 12 magnetic storms with amplitude from -61 to -422 nT it is shown that the effect of the significant increase of the slope of the ring current external edging at the pass from the main phase to the recovery phase of the typical storms can be associated with the difference in the ring current asymmetry.

– The density of the magnetostatically-balanced transversal current in the day-side part of the magnetosphere is estimated. Since the integral current on the day-side field lines corresponds to the integral current on the night-side field lines at the same geocentric distances the traditional ring current continues at high latitudes up to geocentric distances of ~10 R. It was experimentally proved that isolated magnetospheric sub-storm begins at the geocentric distances of ~7-8 R in the ring current region. The model of high-latitude continuation of the ring current is developed. It allows to evaluate the magnetic disturbance value produced by the current during the magnetic storm.

– The studies of the pressure balance at the magnetopause basing on the results of the international project TEMIS have shown that the level of fluctuations in the magnetosheath is extremely high even for the periods of the exclusively quiet geomagnetic conditions at the quiet solar wind. Herewith the accuracy of the pressure balance for the magnetopause can be up to 3%.

– The key role of the kinetic thin current sheets in the magnetotail fast transformations is revealed: the current sheet formation is in close relation with the magnetotail mesoscale turbulent dynamics. The disturbance initiated by the localized splash of the magnetic reconnection which appears in the magnetotail at the smaller time scale produces disequilibrium at the parts of plasmasheet which have intermediate spatial scale. Theoretical concepts and numerical simulation show that the relaxation process which later happen at the larger time scale causes the appearance of the utmost thin embedded current sheaths with complicated anisotropy of the ion distributions and to the generation of the fast plasma flux. This process provides an effective mechanism of transformation of the magnetic energy accumulated in the magnetotail into the kinetic energy of plasma flows.

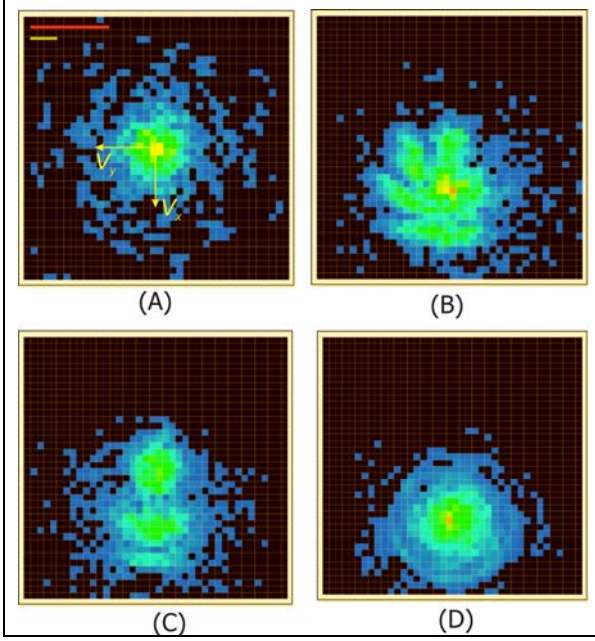

Fig. Examples of the ion distribution functions: phase space densities at v_z=0; v_x=v_y=0 at the cenetr of each plot. (A) Initial state, (B), (C), (D) – later moments at different values of the task options. The red bar is the value of the hot ions thermal velocity, the green one – that of the cold ions. Density decrease is denoted by the color sequence from red to blue, black denotes negligible density.

- Magnetospheric models of the Solar System magnetized planets (Mercury, Earth, Jupiter, and Saturn) were developed. Paraboloid model of the Earth's magnetosphere was chosen as the basis for the International Standard (ISO 22009) which was accepted by ISO members in 2009. The observational evidence of coincidence of the polar boundary of the Saturn auroral ovals with the open field lines bundle has been demonstrated. Last years (2008-2009) Cassini magnetometer data and Hubble UV images of the Saturn polar regions were used. A new paraboloid model of the Mercury magnetosphere was constructed. This model gave us a possibility to estimate the interior dipole parameters by fitting of the Mariner 10 and MESSENGER measurements in the Mercury environment. The model gave closed approach to all Mercury magnetic field data which have been received till now. The dipole and magnetospheric current systems parameters were determined by using the model calculations.

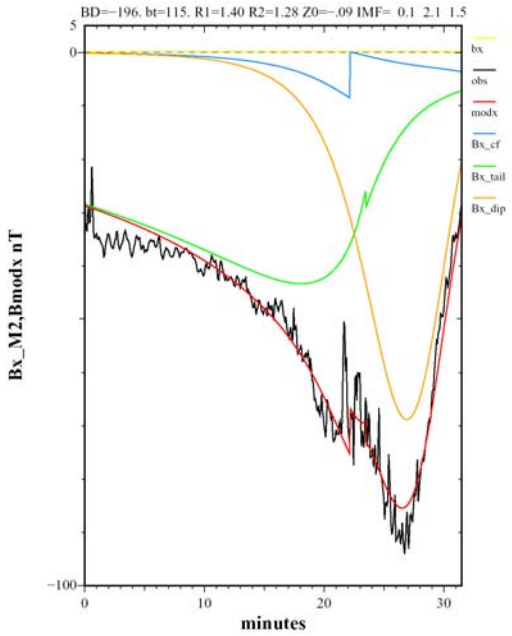

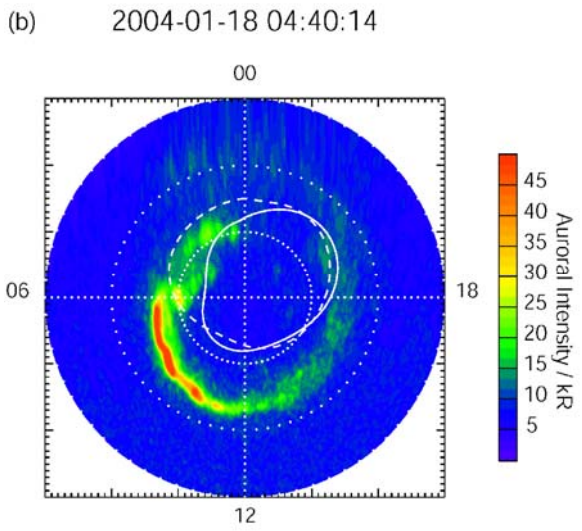

Mercury. MESSENGER 2 flyby on 6 October 2008, σ =8.8 nT

Saturn. Sothern polar oval (Hubble) and open field line ionospheric level boundary (model).

6. The investigations of the galactic and extragalactic cosmic rays.

– The difference of cosmic ray proton and helium nuclei energy spectra was found out by the ATIC experiment. All primary nuclei should follow the same power-law predominated. The balloon experiment ATIC has obtained new accurate data in the energy region from 30 GeV to 30 TeV and have shown that:

- the spectra of protons and helium nuclei are different,
- the spectra of protons and helium nuclei are significantly nonpower-law.

It means that some items of the existing conception should be improved in order to describe the new experimental data. Recently the ATIC results were completely confirmed in the CREAM experiment.

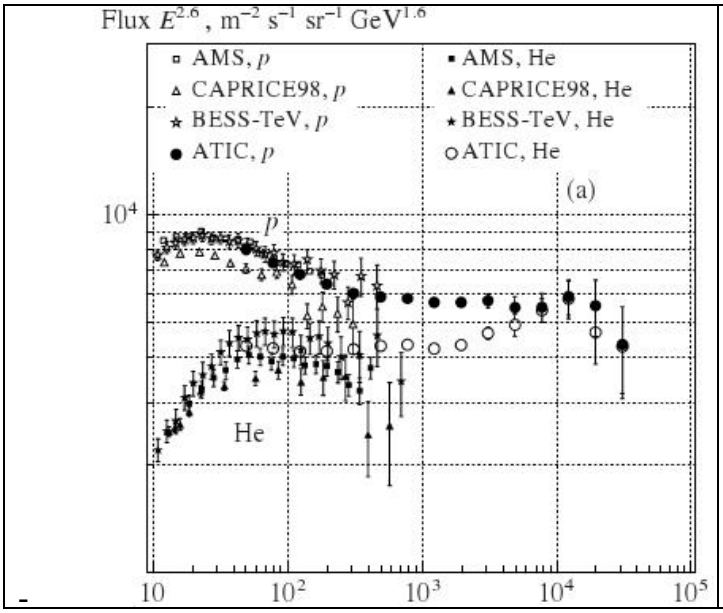

Fig. Energy spectra of protons and helium nuclei measured in the ATIC experiment along with other experimental data.

-

-

- The analysis of the experimental data on the extensive air shower size spectrum confirms the existence of the additional component in primary cosmic rays at energies above 10^{17} eV that differs from the bulk of Galactic cosmic rays generated by shocks in supernova remnants.

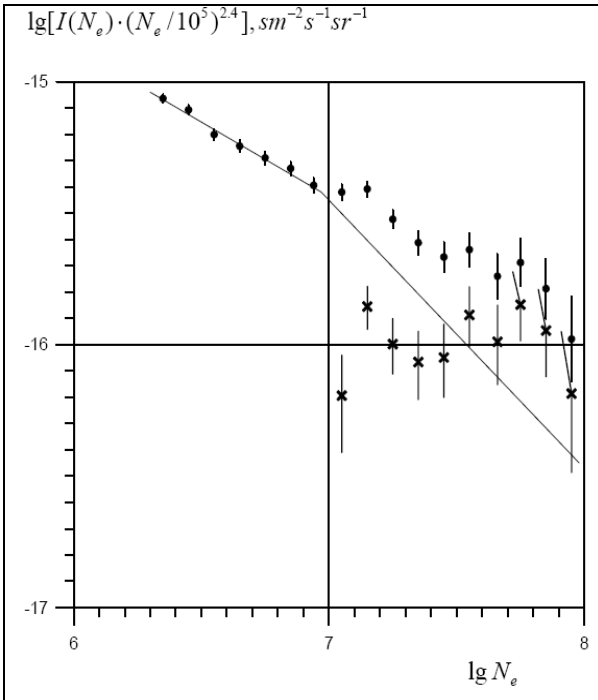

Fig. Number of particles spectrum. Full circles – experimental data of EAS MSU array, curve - the calculated spectrum, crosses – the additional component EAS spectrum.

- Basing on a series of works devoted to the analysis of medium-scale anisotropy (or: arrival directions) of extensive air showers (EAS) generated by cosmic rays (CRs) with energies around PeV and registered with the EAS MSU and the EAS-1000 Prototype it is concluded that isolated pulsars can probably give a more noticeable contribution to the flux of PeV cosmic rays than it is usually assumed.

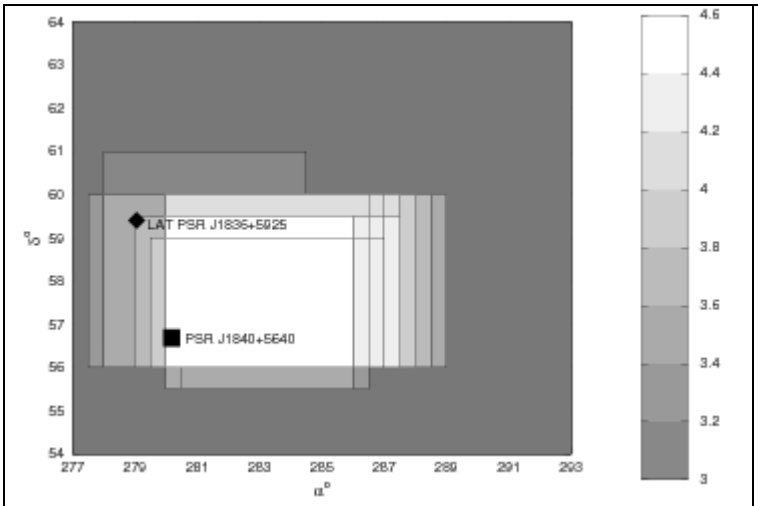

Fig. The region of the cosmic rays excessive flux in the EAS MSU data set and pulsars J1836+5925 and J1840+5640.

7. Studies of UV-radiation in the upper atmosphere.

- New relations between the parameters of the atmosphere, ionosphere and magnetosphere under the stable conditions (time scale is time of orbiting) were discovered basing on the experimental data on UV luminescence of the atmosphere at different latitudes and longitudes of the shadowed (night) side of the Earth obtained onboard the satellite "Universitetskij-Tatiana-1".

Established correlation between the electron flux bursts in the polar region and UV radiation intensity was discovered basing on the simultaneous measurements of UV-radiation and the flux of the electrons with energy above 70 keV onboard "Universitetskij-Tatiana-1". It is shown that latitudinal section of the intensity of the UV radiation of the night atmosphere measured from the satellite towards nadir direction repeats the section of the electron flux intensity at the orbit of the satellite. Experimental data obtained by "Universitetskij-Tatiana-1" satellite denote to the existence of the UV luminescence with intensity an order of magnitude lower than aurora borealis intensity at the medium and low latitudes. Latitudinal shift (about 10 degrees) of the UV intensity peak appearance (wavelength of 300-400 nm) as against electrons intensity peak (from 70 keV up to 1 MeV) is explained by different altitude of the measurements of the electron flow at the satellite's orbit (950 km) and the altitude of UV-radiation (~200 km) where intensive energy losses of the electrons happen. Electrons which produce UV in the atmosphere move along the magnetic field line and come to the altitudes where they lose energy at the higher latitudes.

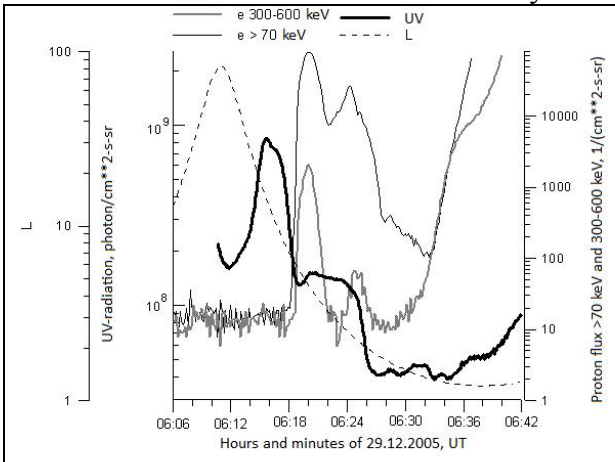

UV radiation intensity (thick curve) and the flux of the electrons with energy of above 70 keV (thin black curve), 300-600 keV (thin

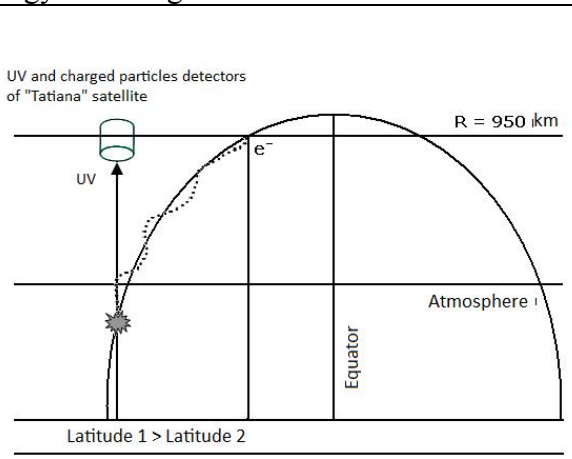

Illustration of the time difference between the registration of UV-radiation and the electron

grey curve), L-shell (dashed line) as measured onboard “Universitetskij-Tatiana-1” satellite 29.12.2005.	flux by the experimental equipment onboard the satellite with the orbit altitude 950 km (UV sensor is directed towards nadir).

8. Space dosimetry investigations.

– Diurnal dose rate is separated into the components of the GCR and RB origin basing on the analysis of the dose rate data measured by the system of radiation control (SRK) of the Russian segment of ISS during 2005-2009. For the period from July to October 2008 relation between the dose rate and the altitude of the station's passing across the SAA region is discovered.

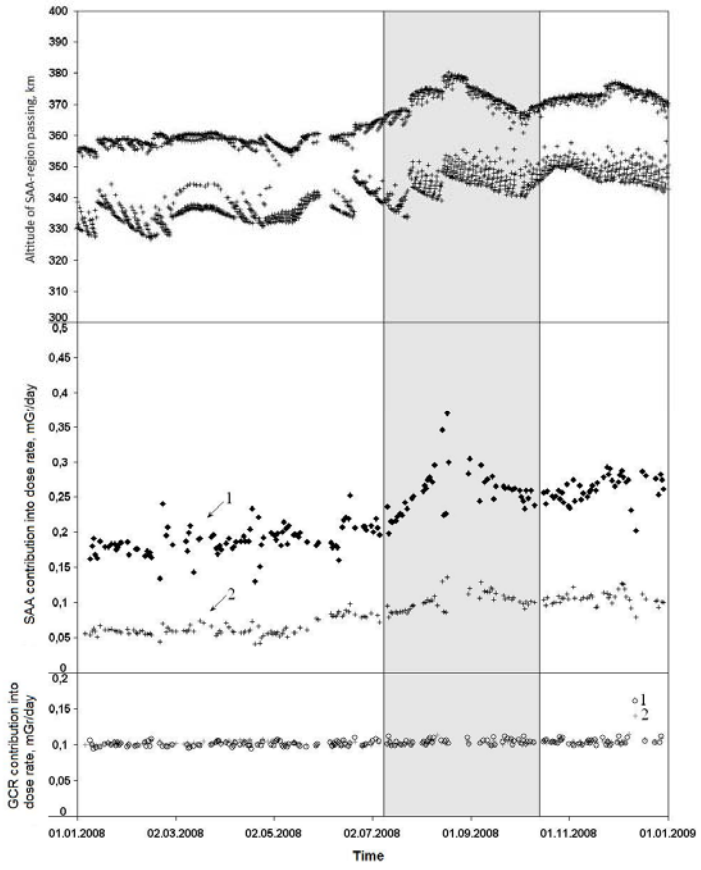

Fig. The upper panel presents the altitude of the ISS passing across the SAA region as a function of time. Two branches of a curve are explained by different altitude of the station's passing at the ascent and descent parts of the trajectory.

The middle and the low panels present the values of the contributions of the radiation belts (RB) and galactic cosmic rays (GCR) into the diurnal dose rate, respectively. Curve 1 corresponds to the measurements of the worst protected detector, curve 2 – the most protected one.

9. Space monitoring data center.

One of the key points of the scientific space research is data storage, support and availability. Therefore the development of information and calculation systems including the arrangement for data storage and intellectual data access is the necessary element for any space experiment. Such systems are of particular importance for the applied studies related to the radiation conditions prediction, because the energetic charged particles along with other space factors influence on the materials and equipment of spacecrafts, ground-based systems and sometimes on the health and survival of the crewmembers.

– The ground-based data acquisition, telecommand and tracking station was organized in SINP MSU for scientific information reception from small satellites, in particular, from “Universitetskij-Tatiana” and from the remote sensing satellites. Take-up speed is 9600 bps in the

range of 70 cm and transmission speed is 2400 bps in the range of 2 m. The antenna station includes two “wave duct with circlar polarization” antennas, turning unit and low-noise antenna amplifiers. Controlling software makes ballistic calculations of the spacecraft's trajectorty, controls the transciever taking into acount Doppler flequency shift, transmits flight task, receives and stores scientific and service telemetry and displays the current position of the spacecraft.

– A prototype of the topical information-analytical center for data storage, processing, displaying and analysis for the information about the penetrating radiation obtained onboard spacecrafts. A number of data bases of space-physics information about the space radiation conditions are developed running data base management system Oracle. They include information obtained during the last 15 years by Russian space experiments onboard spacecrafts Coronas-I, Coronas-F, Meteor-3M, Universitetskij-Tatiana, MIR station, CORONAS-Photon, Universitetskij-Tatiana-2, etc. (http://smdc.sinp.msu.ru) Informational services for data approach and presentation, both tabular and graphic, are developed. On the front page of the site there are the elements of space weather monitoring. The first element real-time builds and displays the current distances to the subsolar point of the Earth's magnetosphere calculated on the basis of the magnetopause position model developed in SINP and the solar wind data obtained by the ACE satellite. The second element is a projection of NOAA N3KL monitor, which detects the magnetospheric conditions and the solar activity.

– A unique fully-automatic system of data processing and storage for the measurements of the charged particles flows carried out onboard CORONAS-PHOTON satellite and atmospheric luminescence registered by “Universitetskij-Tatiana” satellite is developed. The obtained information is on open access via Internet-site of the Space Monitoring Data Center of the Institute http://smdc.sinp.msu.ru.

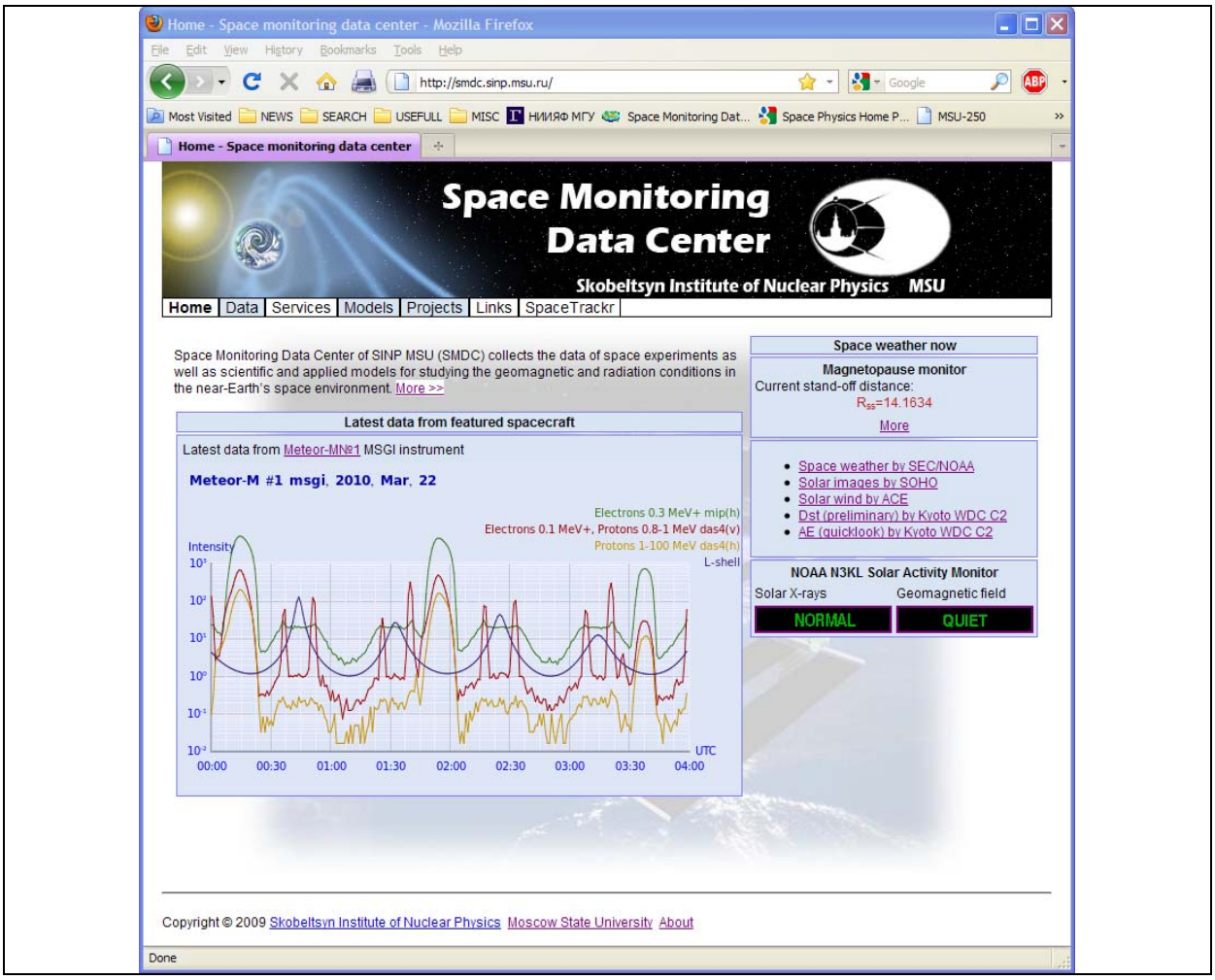

Fig. The front page of the site includes real-time images of the current space data.

– The refined data base on the interplanetary energetic proton flux is offered to be used in order to simulate the radiation conditions. It is shown that the experimental data on cosmic rays proton flux from different space experiments are fairly heterogeneous and have different errors. It is offered to refine the data base on the interplanetary proton flux by means of statistical analysis of proton fluence calculated for different long time intervals – from half a year up to 10 years. Basing on the analysis of different data bases on cosmic rays protons including, in particular, criteria of the solar proton event (SPE) the specific objective method for separation of SPE flux from background ones (GCR) is offered. It is shown that the character of the contribution of different sources into the flux of cosmic rays protons with energy < 4 Mev differs from that for higher energy protons.

– New engineering versions of the models and prototypes of calculating Internet-services necessary for the operative space analysis were developed basing on the system of data management and theoretical models of the magnetosphere and the radiation conditions in the near-Earth space. Web-versions of the space radiation model COSRAD (http://cosrad.sinp.msu.ru) and model of the magnetosphere are developed for the Internet-portal. They provide interface for model access, user guides and physical descriptions of the models, a possibility for experimental and simulation results comparing and the methods for radiation dose calculation within the model of the "cubic" sensitive layer.

– Software complex for space data analysis is developed. It includes four-step algorithm based on neural networks in order for predicting and search of the precursors in the multivariate time series. It allows to improve the prediction's efficiency and to separate the precursor. This algorithm was used for the prediction of Dst-index by the values of the Interplanetary magnetic filed (IMF) in two different coordinate systems Bx, By_GSE, By_GSM, Bz_GSE, Bz_GSM, absolute value of IMF B_magn, protons density in the solar wind n, solar wind speed v and temperature T along with a number of parameters for timing, total of 15 parameters. As a result it was found out that prediction of Dst-index worst depends on Bz_GSM with time delay of 2, 3, 6, 9, 11 and 15 hours before the predicting moment; B_magn with time delay of 2, 8 and 14 hours; n with time delay of 1 hour, v with time delay of 14 hours. Generally the selected parameters correspond with the physical idea of the task.

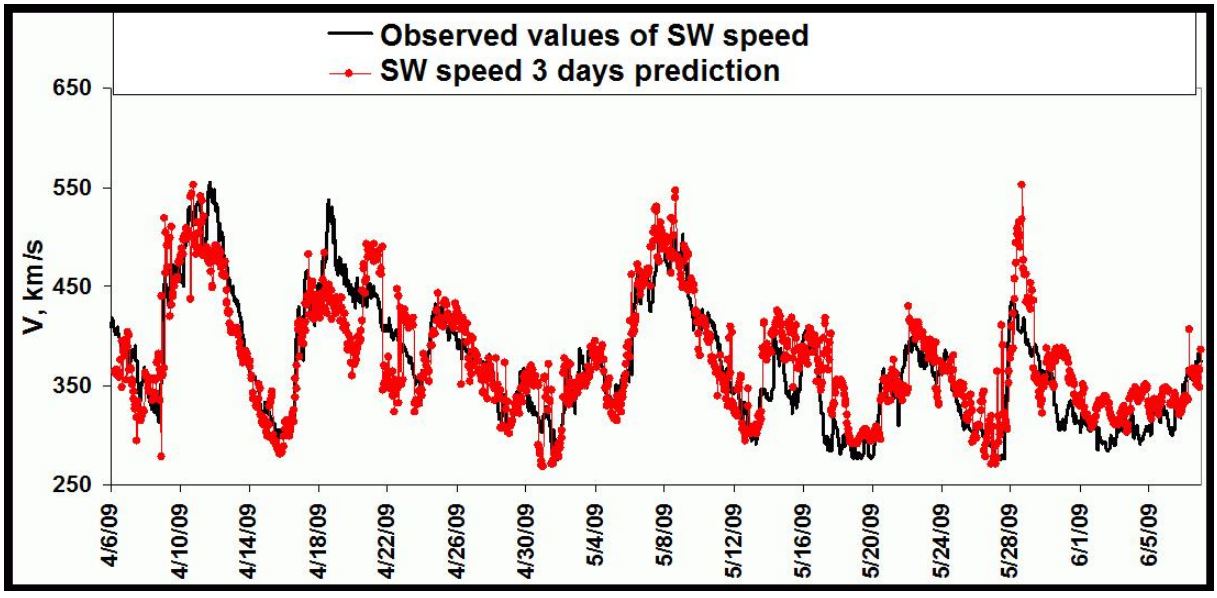

- Software for the analysis of the solar images obtained by the SOHO satellite is developed. Its results were used for the studies of the coronal holes' dynamics and for the prediction of the parameters of the solar wind quasi-stationary flux for the period of solar activity minimum.

10. Educational activity.

The students, postgraduates and young scientists actively participated in the theoretica and experimental scientific research along with development of the computational infrastructure of the Space Monitoring Data Center. Scientific equipment for space experiments is developed with the direct participation of the students and postgraduates of the MSU Physics Faculty. They are also engaged into space data processing and scientific analysis. Outreach program for space physics and occupational guidence of the pupils includes the development of the popular materials and carrying out of specific measures. An educational multimedia slide-film “And what's up in space?” («About the cosmic rays and the galaxies, about the stars and the planets, about the Sun and the Earth») is being distributed among the schoolchildren and the students of the first years of the non-core Universities since 2008. All people who are interested in space science are also in the targeted audience. In 2009 the second version of this slide film with popular explanation of space phenomena and ways of their investigation was published.

The third revised version of the electronic multimedia course “Life of the Earth in the solar atmosphere” is being developed. The first two versions (2005 and 2008) were first of all oriented at school and University teachers. The new version appeared as a result of the need of such a course for individual studies of the students and pupils. The course includes about 1500 slides from three sections: the Sun, the Earth and the solar-terrestrial relationship accompanied with a small glossary.

“Space laboratory course” was developed for the students of the 4-5 courses of the classical and technical Universities. Its objective is to appeal the students to the modern space research and implementation of the information about space into the University education. All tasks of the course are based on real space data including that obtained by the experiments onboard “Universitetskij-Tatiana” and “Universitetskij-Tatiana-2” satellites. There were already two versions of this course, and some tasks were included into the electronic space laboratory course “Space physics” intended for distant education, which was developed in cooperation with the Ulianovsk State University and distributed to a number of Universities.

Beginning with 2004 conferences-schools for young scientists are organized in cooperation with different Russian Universities. Their purpose is not only to introduce the participants with the last achievements in the field of modern space physics, space physics practice and possibilities, but also to demonstrate the availability of serious space research for the modern Russian Universities. Every year about 100 students and teachers from different Universities participate in these conferences, and none of them previously had any experience in space research. One of the main results of these conferences became the practical realization of the possibility for the students of Russian Universities to develop and defend their diploma thesis under the supervision of the leading MSU scientists using the scientific data from the University scientific-educational satellites. About 30 diplomas on space research were defended as a result of the formed University collaboration.

SINP MSU regularly participates in a number of popular events and exhibitions. A site of the MSU Space Scientific-Educational Project space.msu.ru is developed and maintained. It contains actual information about the MSU space projects and educational materials. The students of different Russian Universities come to the Institute for their practical and predegree training.

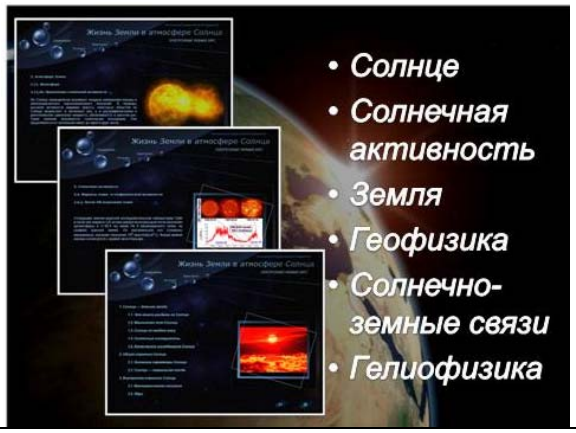	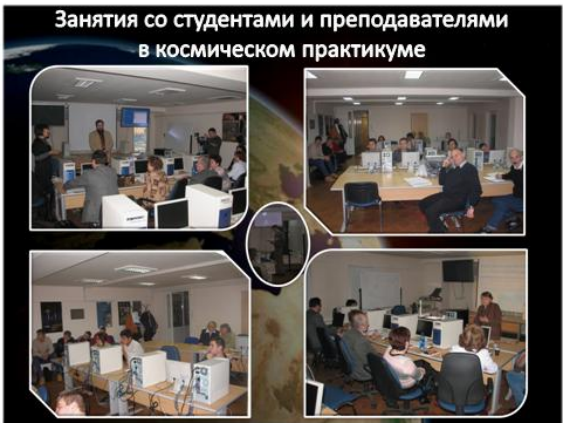
Multimedia course “Life of the Earth in the solar atmosphere”	Space laboratory course in SINP MSU

2.1.6. MOSCOW ENGINEERING PHYSICS INSTITUTE (STATE UNIVERSITY). ASTROPHYSICS INSTITUTE

2.1.6.1. Project “CORONAS-PHOTON”

SCIENTIFIC PROGRAM AND OBJECTIVES OF THE PROJECT “CORONAS-PHOTON”

CORONAS (**C**omplex **OR**bital **N**ear-Earth of **A**ctivity of the **S**un) – Russian program for study of the Sun and solar-terrestrial connections physics by series of spacecrafts, which provides launching of three solar-oriented satellites onto the near-Earth orbit.

“CORONAS-PHOTON” is the third satellite in this series. Two previous missions of the project are “CORONAS-I” (launched on March 2, 1994) and “CORONAS-F” (launched on July 31, 2001).

Satellite “CORONAS-PHOTON” was launched on 30 January 2009 from cosmodrome “Plesetsk”.

MEPhI – Moscow Engineering Physics Institute (State University) is the main organization responsible for the scientific payload complex of the “CORONAS-PHOTON” mission.

NIIEM – Research Institute for Electromechanics (Moscow region, Istra) is the main organization responsible for the spacecraft “CORONAS-PHOTON”.

Principal Investigator of the project

Director of Astrophysics Institute at MEPhI (IAF MEPhI) **Dr. Yuri D. Kotov**

Technical director and chief designer of the spacecraft

Deputy Chief Designer of NIIEM **Dr. Rashid S. Salikhov**

Technical director and chief designer of the scientific payload complex

Deputy Director of Astrophysics Institute at MEPhI **Dr. Vitaly N. Yurov**

Contacts:

Dr. Yu.D. Kotov

- Astrophysics Institute at MEPhI, 31, Kashirskoe shosse, Moscow, 115409,
- Phone: (+007-095) 323-9193, (+007-095) 323-9077
- Phone/Fax: (+007-095) 324-0616
- E-mail: kotov@mephi.ru

WWW: http://iaf.mephi.ru/photon/

Main goal of the project: The investigation of energy accumulation and its transformation into energy of accelerated particles processes during solar flares; the study of the acceleration mechanisms, propagation and interaction of fast particles in the solar atmosphere; the study of correlation between the solar activity and physical-chemical processes in the Earth upper atmosphere.

Objectives of the mission:

Physics of the Sun and solar-earth connection

- Systematic study of processes responsible for solar flares development, periodicity and intensity to refine the models of short-term and long-term solar activity forecast;
- Receiving of observational data on energy and temporal distribution functions of solar radiation during quite time and flares in different wave length bands from EUV to high energy gamma-rays.
- Observation of CME and solar eruptive prominence and diagnostic of plasma physical parameters in these processes: temperature, electron and ion densities, emission measure. These parameters are important for calculation of energy balance in that active coronal processes;
- Study of propagation of accelerated particles in solar atmosphere, theirs escape in outer space (thin or thick interaction model) and angular distribution in the target;
- Determination of composition of accelerated ions and ambient solar medium by gamma-spectroscopy observations;
- Study of linear polarization of hard X-ray radiation in intense flares;
- Definition of input of heated and direct accelerated electron in soft and hard X-ray radiation.
- Study of peculiarity electron-dominated flares.
- Gamma-spectroscopy observation of rear elements production (D, ^{3}He, Li, Be) by accelerated ions.
- Monitoring of the Earth upper atmosphere by absorption of extreme ultraviolet of the quiet Sun;

Astriophysics

- Study of hard X-ray and gamma radiation from gamma-ray bursts;

- Study of X-ray radiation from the bright local sources along Ecliptic plane.

Cosmic rays

- Study of dynamic of particle trapped in radiation belts during quite and perturbation periods;
- Research of element composition of nuclei accelerated in flare on the Earth orbit, and also energy and temporal parameters of flare electrons and protons;
- Study of hard X-ray and gamma radiation from gamma-ray bursts;
- Study of X-ray radiation from the bright local sources along Ecliptic plane.

SPACECRAFT "CORONAS-PHOTON"

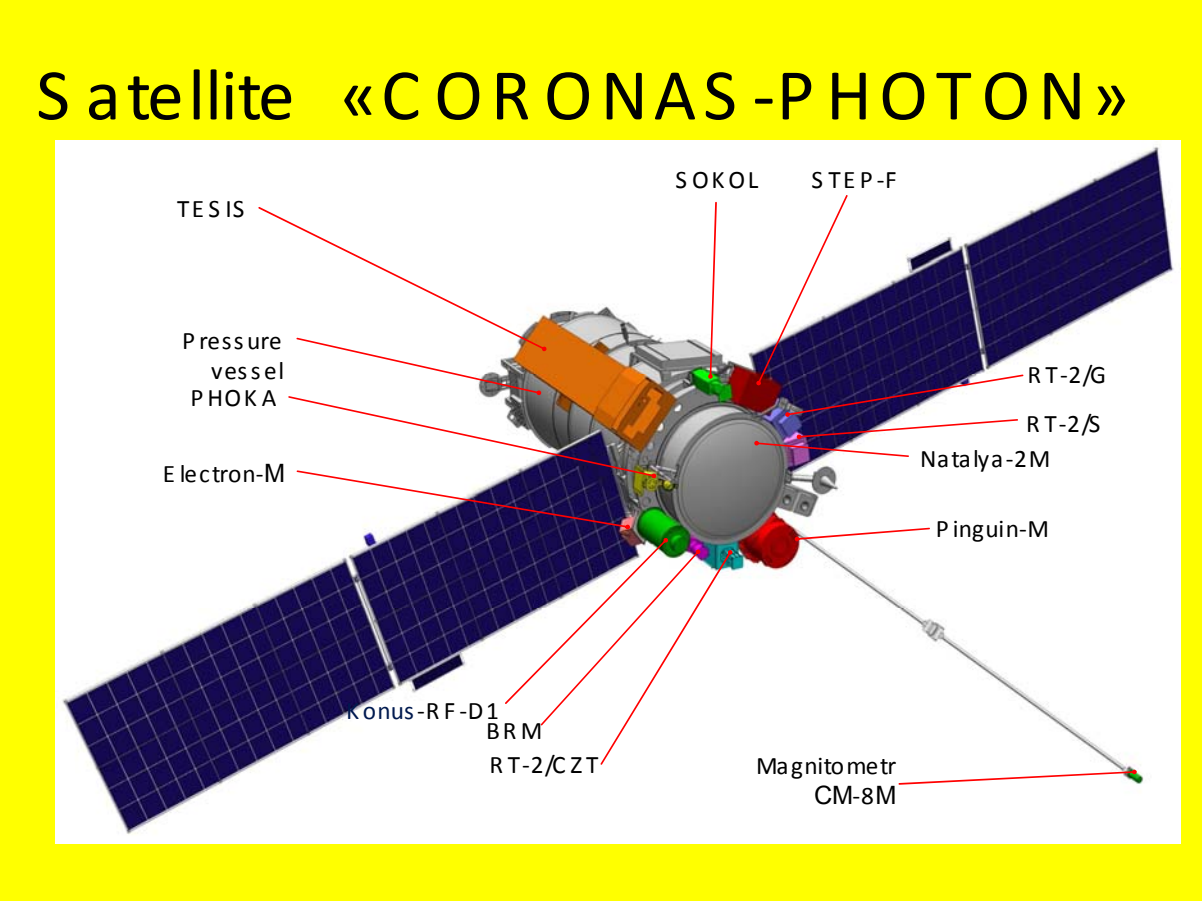

Fig. 1. General view of the spacecraft "CORONAS-PHOTON"

MAIN CHARACTERISTICS OF THE SPACECRAFT

Satellite "CORONAS – PHOTON" (METEOR type)

Spacecraft weight, kg …….. 1860

Scientific payload weight, kg ……..…….…….……. 600

Orbit:

- type ……. near circular
- height, km ……..… 557-574
- inclination, deg …….. 82.5

Accuracy of the spacecraft longitudinal axis orientation to the Sun, arc min ……....….±2'

Angular velocity destabilization of the spacecraft, deg/s ……..……..≤0.002

Accuracy of the satellite position measurement:

- along the orbit, m …….. ±1000
- by height and in transverse directions, m …… ±500

Volume of scientific information stored per day, Gbit ……..…… 8.2

SCIENTIFIC PAYLOAD COMPLEX

Instrument	Parameters, registered radiation	Developing organization
Electromagnetic radiation and neutron monitors		
High energy spectrometer **NATALYA-2M**	- Gamma-ray spectroscopy 0.2 - 2000 MeV - solar neutrons 20 - 300 MeV	*MEPhI, Moscow, Russia* Eugene E. Lupar [EELupar@mephi.ru]
Low energy gamma-ray telescope **RT-2**	- Hard X-ray spectroscopy 15 - 150 keV in phoswich mode - Spectrometric mode 0.10 - 1MeV - Hard X-ray solar flares image	*TIFR, Mumbai,, India* A. Raghu Rao [arrao@mailhost.tifr.res.in] *Indian Centre for Space Physics, Kolkata, India (ICSP)* Sandip K. Chakrabarti [chakraba@bose.res.in] *MEPhI, Moscow, Russia* Andrew I. Arkhangelsky [angel1966@list.ru]
Hard X-ray polarimeter-spectrometer **PENGUIN-M**	- Hard X-ray polarization 20 - 150 keV - Soft X-ray monitoring 2-20 keV - X-ray & gamma-ray spectroscopy 0.015 - 5 MeV	*MEPhI, Moscow, Russia* Alexander S. Glyanenko [asgl2005@rambler.ru] *Ioffe PhTI, St-Petersburg Russia* Mikhail V. Savchenko [mikhail.savchenko@pop.ioffe.rssi.ru]
X-ray and gamma-ray spectrometer **KONUS-RF**	Solar flares and gamma-ray bursts hard X-ray & gamma-ray spectroscopy in the energy range of 10 keV - 12 MeV with high time resolution	*Ioffe PhTI, St-Petersburg, Russia* Rafail L. Aptekar [aptekar@mail.ioffe.ru] Evgeny P. Mazets [mazets@mail.ioffe.ru]
X-rays		
Fast X-ray monitor **BRM**	Hard X-ray monitoring 20 - 600 keV in six channels with time resolution 2 - 3 ms	*MEPhI, Moscow, Russia* Yury A. Trofimov [yutrofimov@gmail.com]
Fast Solar Photometer in X-rays **SphinX**	Measurements with high time resolution (0.01 s) of the solar spectra of quiet and active corona in the range 0.5-15 KeV	*SRC, Wroclaw, Poland* Janusz Sylwester [js@cbk.pan.wroc.pl]
EUV/XUV photometer **PHOKA**	- Full disk EUV/XUV radiation in three pair spectral bands 0,5 - 11 nm, 27 - 37 nm, 121,6 nm - occultation measurements of EUV/XUV absorption in Earth atmosphere 150 - 500 km	*MEPhI, Moscow, Russia* Aleksey V. Kochemasov [kochemasov@rambler.ru]
Solar telescope/imaging spectrometer **TESIS**	Solar images in narrow spectral regions and monochromatic radiation	*Lebedev FIAN, Moscow Russia* Sergey V. Kuzin

	lines of transition zone and corona: - telescope 130 - 136 A, - telescope-coronograph 290 - 320A, corona (0,2 - 4) Rsol - spectroheliometer (8,418 - 8,423) A, 285 - 335 A - photometer-spectra-heliometers 1 - 12 A, resolution 0.05 A Angle of view up to 2 angular degrees	[kuzin@lebedev.ru] Sergey A. Bogachev [bogachev@sci.lebedev.ru]
Helioseismology		
Multichannel solar photometer **SOKOL**	Continuous observations of solar optical radiation variations in seven spectral channels at wavelength range of 280 - 1500 nm, view range - 2°	*IZMIRAN, Troitsk, Russia* Vladimir D. Kuznetsov [kvd@izmiran.rssi.ru] Nikolai Lebedev [lebedev@izmiran.rssi.ru]
Cosmic rays		
Charged particle analyzer **ELECTRON-M-PESCA**	Flux and energy spectra registration: protons 4 - 80 MeV electrons 0.2 - 4 MeV nuclei (C, N, O) 6-15 MeV/nucleon	Mikhail I. Panasyuk [panasyuk@sinp.msu.ru] Vladimir V. Kalegaev [klg@dec1.sinp.msu.ru]
Satellite telescope of electrons and protons **STEP-F**	Flux and energy spectra registration: protons 9.8 - 61.0MeV electrons 0.2 - 15 MeV ***a*-** particles 15,9 - 246.0 MeV with accuracy of particle direction (8 - 10)°	*Karazin KNU, Kharkov, Ukraine* Olekiy V. Dudnik [Oleksiy.V.Dudnik@univer.kharkov.ua]
Scientific supply system		
Magnetometer **SM-8M**	Measurements of three components of constant magnetic field on satellite orbit in the range of -55 $\mu.T$ +55 $\mu.T$	*MEPhI, Moscow, Russia* Vitaliy N. Yurov [VNYurov@mephi.ru] *Geologorazvedka, St-Petersburg, Russia*

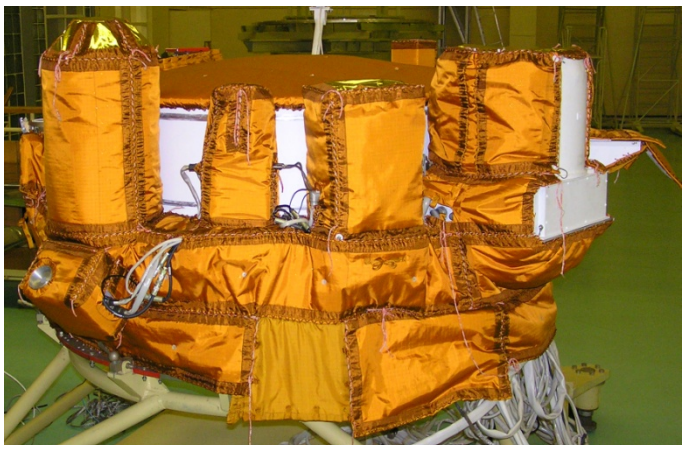

Fig.2.
Set of scientific instrument detectors during thermo-vacuum tests in NIIEM.

High energy radiation spectrometer «NATALYA-2M»

Yu.D. Kotov[1], V.N. Yurov[1], V.T. Samoilenko[1], A.S. Glyanenko[1], A.I. Arkhangelsky[1], E.E. Lupar[1], I.V.Rubtsov[1], V.G.Tyshkevich[1], V.V.Kadilin[1], K.F.Vlasik[1], P.Yu.Tchistyakov[2]

[1] Moscow Engineering Physics Institute (State University), Russia
[2] OOO "Skiner", Moscow, Russia

Scientific tasks of the experiment:

- Determination of mechanisms and requirements of electrons and protons acceleration at different flare phases, and parameters of trap and propagation region of accelerated particles in solar atmosphere.

Goals of the experiment:

- Study of the temporal dynamics of hard electromagnetic radiation in a wide energy range from 0.2 to 2 GeV;
- Registrations of solar neutrons in the energy range of 20 – 300 MeV.

Main parameters and configuration of the instrument:

Channel	Energy range, MeV	Effective area, cm^2	Energy resolution, ΔE/E	Time resolution
R (X-rays)	0.3 – 2	920	10% (662 keV) measured	1 ms
L (low gamma)	2 – 10	900	5% (2,5 MeV) measured	1 s
M (medium gamma)	7 – 200	800	6% (10 MeV) calculated	1 s
H (high gamma)	50 – 2000	750	32% (500 MeV) calculated	1 s
N (neutrons)	20 – 300	37 – 120	–	32 s

"NATALYA-2M" includes registration block, data handling and output systems and high voltage supply block.

There are two spectrometers of eight scintillation modules with CsI(Tl) crystals each and polystyrene anticoincidence detectors in the registration block of "NATALYA-2M" (Fig. 3). The upper spectrometer is surrounded by the anticoincidence protection which consists of the 2 cm thick scintillation dome and 1.5cm plane detector. All scintillation modules are identical, they are CsI(Tl) crystals 4.5×8×36 cm in size. Modules form two layers (4 modules in each); the nearby layers are rotated relative to each other by 90°.

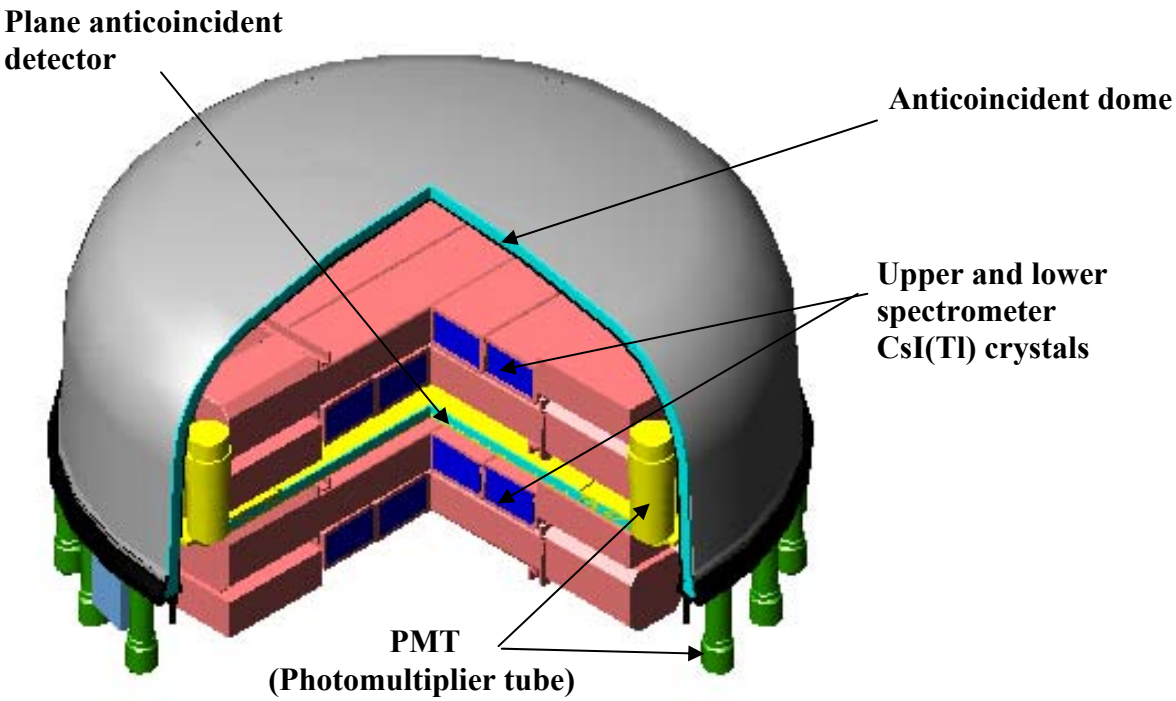

Fig.3. High energy radiation spectrometer "NATALYA-2M" registration block

Each block is viewed by two photomultiplier tubes from opposite sides. All spectrometer channels are stabilized by reference light source signals through optical fibers during operation. α and γ nuclear radioactive sources are used for absolute energy calibration. Output signals from the opposite preamplifiers of each module are summed. Laboratory tests confirmed that the stabilization system provides maintenance of the specified amplification of PMT+electronics channel not worse than 1.5% in wide ranges of temperature, magnetic field and spectrometer loading.

Non-uniformity of the signal value for different radioactive source positions is about 2%. Energy resolution for a wide parallel gamma beam measured for radioactive sources and estimated by numerical simulation is about 10.0% (at E = 0.662 MeV), 6.0% (10 MeV) and 32% (500 MeV).

Separation of "gamma" and "neutron" events is based on the scintillation signal shape analysis in the upper spectrometer. Coefficient of the neutron/gamma separation is about 10^3.

"NATALYA-2M" works in three modes: background, «burst» and «flare».

Total weight of the instrument is about 260 kg.

Low energy gamma-ray telescope RT-2

A.R. RAO[1], S.K. CHAKRABARTI[4], J.P. MALKAR[1], S. SHRICUMAR[2], M.K. HINGAR[1], A. NANDI[4], YU.D. KOTOV[5], A.I. ARKHANGELSKI[5], V.N .YUROV[5], R.A.ZYATKOV[5]

[1]Tata Institute of Fundamental Research, Mumbai, India (TIFR)
[2]Indian Space Research Organization, Bangalore, India
[3]Indian Centre for Space Physics, Kolkata, India (ICSP)
[4]S.P.Bose National center of fundamental physics, India

Scientific tasks of the experiment:

- Research of X-ray and gamma-ray space sources (Sun, galactic and extragalactic X-ray sources, active galaxies nuclei, gamma-ray bursts, hard X-ray diffuse background).

Goals of the experiment:

- Registration of the temporal profiles of solar and galaxy X-ray radiation in the energy range of 15 keV– 1,0 MeV;
- X-ray radiation spectrometry in the energy range of 0.15 – 1 MeV.
- Solar disk imagining in hard X-ray band with using semiconductor detectors CdZnTe and CMOS matrix coved by scintillator GdOS.

Main parameters and configuration of the instrument

Parameter	*Scintillation detector* Mode: Phoswich	*Scintillation detector* Mode: Spectrometric	*Semiconductor solid state detector* CdZnTe	GdOS/CMOS
Energy range	10 – 150 keV	0.10 – 2 MeV	10 – 80 keV	15-200 keV
Effective area, cm^2	150	150	100	4.5
Energy resolution	16.5% (60 keV)	12% (662 keV)	2% (60 keV)	Threshold
Time resolution, ms	1 (0.1)		1 (0.1)	

RT-2 includes three detector blocks RT-2/S, RT-2/G, RT-2/GA and electronics block RT-2/E. Detector blocks are situated outside the satellite hermetic module.

There are two similar composite scintillation detectors (phoswich) 3 mm NaI(Tl)/25 mm CsI(Na) 11.7 cm in diameter in RT-2 instrument. The scheme of scintillation detector block is shown in Fig. 3.

Detectors are identical except collimators angles of sight equal to 6×6 and 10×10 degrees. The scintillators are surrounded by passive shielding and plastic anticoincidence counters (veto).

The third gamma-ray detector is based on a new type of semiconductor Cd-Zn-Te (CZT). Its feature is high energy resolution in the temperature range of –10…+10 ºC. Thickness of the crystal is 2 mm.

Principle of operation

Radiation falls on NaI(Tl) crystal through the collimator and thin beryllium glass and then on CsI(Na) crystal. In scintillators radiation is transformed in a light flash which is registered by a photomultiplier tube. Signals from PMT arrive at the electronic block for further processing.

Scintillation detectors work simultaneously in two modes: phoswich mode (10 – 150 keV) and spectrometric mode (0.27 – 1MeV).

Detectors were calibrated on radioactive source ^{241}Am.

RT-2/CZT payload, a hard X-ray imaging instrument, consists of two different type of imaging detectors, namely CZT and CMOS detectors. Three CZT detector modules and one CMOS detector are arranged in a configuration of 2 x 2 array. It also uses two different type of coders, namely Coded Aperture Mask (CAM) and Fresnel Zone Plate (FZP) for casting the shadow of the sky plane into detector plane. RT-2/CZT payload is the only imaging device onboard the CORONAS-PHOTON satellite to image solar flares in hard X-rays of energy range 20 keV to 150 keV. The CZT detectors have good spectral resolution along with moderate spatial resolution, whereas, the CMOS detector has high resolution imaging capability without any spectral information.

Cadence time by different detectors in flare and monitoring modes			
	Phoswich	CZT	GdOS/CMOS
Cadence (monitoring mode)	1s light curve 100s spectral	1s light curve 100s spectra	100s imaging
Cadence (flare mode)	0.1s light curve 10s spectra	1c light curve 100s spectra	100s imaging
Remarks: 1) Energy spectrum is measured in 512 channels; in the band 0,27–1MeV 256 channels are used. 2) Light curves and images in CZT detector are measured in four channels (<40keV; 40–60keV; 60–100keV; >100keV); band heads can be changed by telecommands.			

The on-board memory storage is 10 Mbit during one or two telemetry transmissions to the Earth.

RT-2 full weight is 44 kg; it includes three detector blocks of 15 kg each and the electronics block of 10 kg.

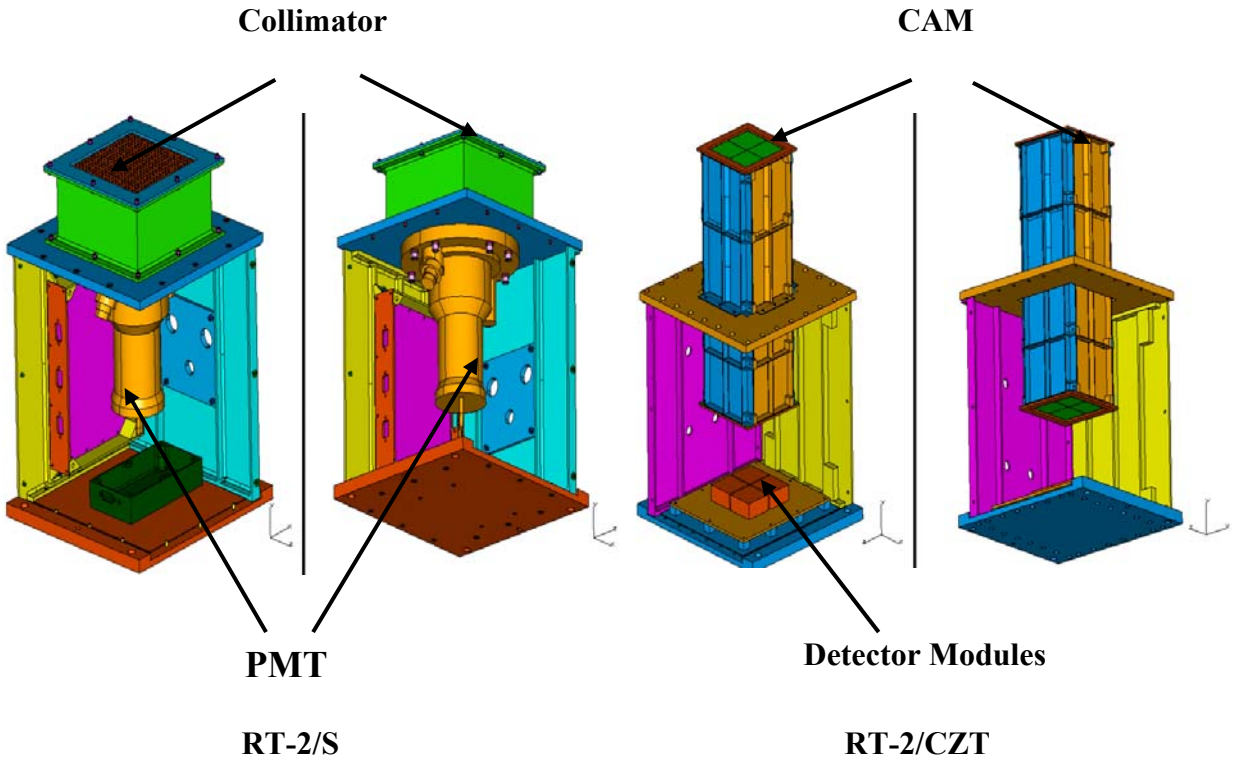

Fig.4. Detector blocks of RT-2 instrument

Hard X-ray polarimeter "PENGUIN-M"

Principal Investigators: Yu.D. Kotov[1], V.A. Dergachev[2]

Designers: V.N. Yurov[1], A.S. Glyanenko[1], A.E. Firsanov[1], E.M. Kruglov[2], V.P. Lazutkov[2], G.A. Matveev[2], G.A. Pyatigorsky[2], M.I. Savchenko[2], D.V. Skorodumov[2], V.V. Khmylko[2], Yu.A. Chichikaljuk[2], I.I. Shishov[2], A.I. Arkhangelski[1]

[1]Moscow Engineering Physics Institute (State University), Russia

[2]Ioffe Physical-Technical Institute of the Russian Academy of Sciences, St-Peterburg, Russia

ST-PETERSBURG, RUSSIA

Scientific tasks of the experiment:

- Investigation of the processes of magnetic energy accumulation and its transformation into accelerated particle energy and radiation during solar flares;
- Study of the energy release processes dynamics in weak flares.

Goals of the experiment:

- Measurement of hard X-ray linear polarization parameters in solar flares in the energy range of 20 – 150 keV;
- X-ray and gamma-ray spectroscopy of solar flares in the energy range of 15keV – 5MeV;
- Monitoring of soft X-ray solar radiation in the energy range of 2 – 10 keV.

Main parameters of the instrument:

The principal scheme, configuration and detectors characteristics of “PENGUIN-M” instrument allow to investigate the following parameters of hard electromagnetic solar flares radiation:

1. Degree of hard X-ray linear polarization in the range of energies 20 – 150 keV;
2. Hard X-ray and gamma-radiation spectra in the energy ranges:
   a) 15 – 500 keV (96 energy channels),
   b) 15 – 150 keV (16 energy channels);
3. Soft X-ray radiation spectra in the energy range of 2 – 20 keV (12 channels), including weak ("thermal") flares and fore-flare stage.

The instrument is working in two modes: “PATROL” and “FLARE”.

Configuration of the instrument

The detector block “PENGUIN-MD” (PMD) together with the electronic block “PENGUIN-ME” (PME) constitutes the scientific equipment “PENGUIN-M”. The PMD block is developed and produced by Ioffe Physical-Technical Institute, RAS; the PME block – by Moscow Engineering Physics Institute (MEPhI).

The PMD block is based on scintillation and proportional counters and is intended for registration of spectral and polarization characteristics of X-ray and gamma-radiation of solar flares. Besides the radiation detectors, the PMD block contains the active shielding from charged particle background, flight calibration and auto stabilization systems of detectors amplification, and also electronic schemes carrying out processing and analysis of registered impulses, intermediate accumulation and storage of the obtained information. The connection of the PMD block with the spacecraft on-board systems and with the data acquisition and registration of scientific information system (SSRNI) is carried out through the PME block.

Principle of operation

Linear polarization.

The degree of linear polarization and polarization plane positional angle of hard X-rays are measured by Compton scattering asymmetry in case of polarization of an incident flux. There are four p-terphenyl detectors-scatterers for Compton scattering electrons registration and there is also an assembly of six spatially oriented detectors from CsI(Na) for registration of scattered radiation in the configuration of “PENGUIN-M”. The method of coincidences is used for Compton scattering registration.

Hard X-ray and gamma-ray spectra.

“PENGUIN-M” registers radiation incident on the upper surfaces of the scattered radiation detectors in the energy range of 15 – 500 keV (96 energy channels) in the absence of coincidences with impulses from the detector-scatterer. The instrument also registers radiation incident on the detector-scatterer in the energy range of 15 – 150 keV (16 energy channels) in the absence of coincidences with impulses from scattered radiation detectors.

Soft X-ray spectra.

Proportional counters with appropriate electronic analyzers are used for research of soft X-ray solar flares radiation. Spectrum of soft X-rays is registered in the interval of energies 2 – 20 keV (12 channels). The width of the channel is about 0.2 keV at the lower energy threshold, it increases with radiation energy up to ~ 2 keV.

Radiation is registered by one of two proportional counters with beryllium entrance windows and pure xenon filling. The counters have four sections located each under other. The upper section is intended for low radiation flux registration. The second section becomes the main one for intense radiation fluxes when it registers radiation weakened by absorption. Calibration and background sections are located below.

One detector operates in a patrol mode while the second detector is in “a cold reserve”.

The upper and lower anticoincidence screen detectors with PMT are used for the detectors protection from charged particles background and for the increase of the detectors operation stability. Each detector of scattered radiation consists of two plates composed together and viewed by one PMT. The inner plate is a scintillation detector made of CsI(Na), and the outer plate is a side protective detector made of scintillation plastic considerably lowering the charged particles background by using an anticoincidence method. The effectiveness of the background registration by all anticoincidence screens is not worse than 0,999.

There are systems of the detectors energy scale stabilization (compared with a signal from the reference device) and those of monitoring of polarimeter symmetry in “PENGUIN-M”, these systems allow to support stability at the level of 1%.

Configuration of the detector block “PENGUIN-MD”

Five basic elements (Fig. 5) constitute the structure of the block detection part.

1) Detector-scatterer of hard X-rays which is in fact the assembly in the form of a disk from four sectors of p-terphenyl (PTF) crystals with photoelectronic multiplier tubes (PMT) pasted below them. Boards of potentiometers, preamplifiers and high-voltage power supply are fixed on the PMT. These elements are not shown on the detector block scheme. The PMT assemblies are identical for all 13 scintillation detectors of the block, and therefore only PMTs will be indicated further.

2) Six detectors of scattered and direct X-ray and gamma-radiation assembled in a regular hexahedron installed around the scatterer. Each detector contains crystal CsI(Na), protection from the background noise of charged particles by the "phoswich" scheme and the PMT assembly.

3) The upper anticoincidence screen detector in the form of a disk from plastic scintillator with PMT attached to it. This detector is located above the detector-scatterer and detectors of scattered radiation.

4) The lower anticoincidence screen detector in the form of a glass from plastic scintillator, enveloping the detector-scatterer from below and on the side surface. Two PMTs are installed on the lower screen detector.

5) Two assemblies of soft X-ray detectors include proportional counters, preamplifiers, a high-voltage power supply and a block of analog-digital processing of signals.

Total weight of “PENGUIN-M” is 43 kg; weight of the detector block is 35 kg.

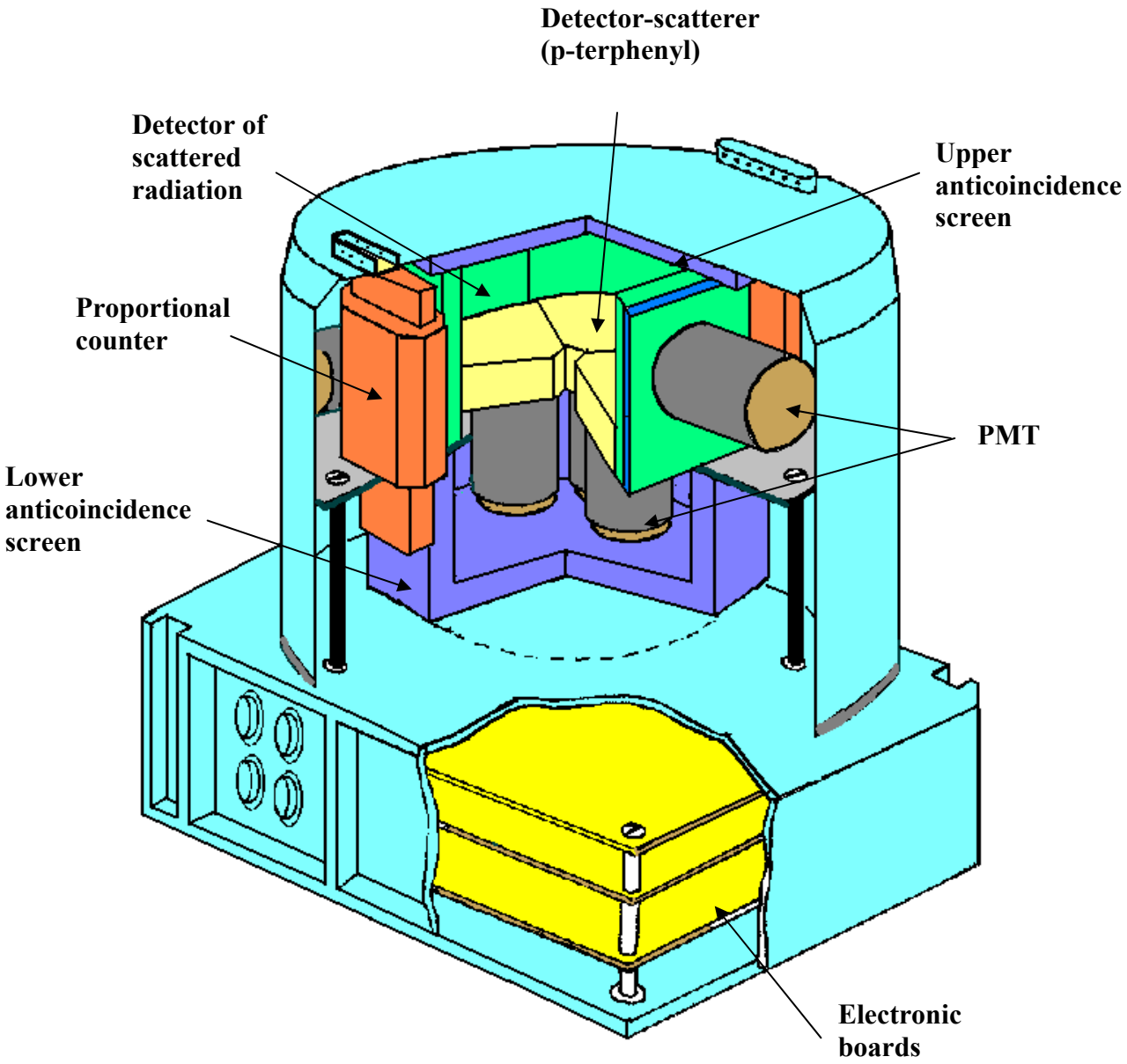

Fig. 5. Construction of the detector block "PENGUIN-MD"

X-ray and gamma-ray spectrometer «KONUS-RF»

E.P. Mazets, R.L. Aptekar, S.V. Golenetskii, V.N. Il'inskii, F.P. Oleinik, D.D. Frederiks, A.A.Kokomov, M.V. Ulanov, V.N. Panov

Ioffe Physical-Technical Institute of the Russian Academy of Sciences, St-Petersburg, Russia

Scientific tasks of the experiment:

- Research of gamma and X-ray solar radiation;
- Study of cosmic gamma-ray bursts.

Goals of the experiment:

- Monitoring of hard X-ray solar radiation, cosmic gamma-ray bursts and search for unusual X-ray and gamma-ray transient events during continuous all sky monitoring;
- Research of temporal history and spectral evolution of solar X-ray flares with high time resolution up to 2 ms;
- Search and study of solar flares gamma-radiation, including emission in nuclei lines;
- Study of gamma-ray bursts temporal structure, energy spectra and mechanisms of fast spectral evolution;
- Detail research of radiation environment on spacecraft orbits and its variations for detection of other cosmic transient and permanent discrete sources during Earth occultation.

It is supposed to include spacecraft "CORONAS-PHOTON" in the international interplanetary network of foreign and domestic spacecrafts IPN (International Planetary Network) for localization of gamma-ray burst sources by a triangulation method.

Main parameters and configuration of the instrument

"KONUS-RF" instrument uses the scintillation method of radiation registration in combination with microprocessor processing of the spectral and temporal information from the detector. Measurements are conducted in a wide energy range from 10 keV up to 12 MeV. Time resolution automatically adapts to a current level of emission energy during measurements depending on the observation task and covered energy range. It may vary from 2 ms up to several minutes which provides sufficient statistical accuracy of the information accumulated during these time intervals.

"KONUS-RF" consists of two detector blocks and a separate electronic block which includes a power supply and the interface with spacecraft service systems.

The field of view axis of the first detector "KONUS-RF-D1" is directed at the Sun. The detector field of view is 2π steradian. The second detector "KONUS-RF-D2" is focused in an anti-solar direction. Crystals of NaI(Tl) 127 mm in diameter and 76.2 mm in height are used in both detectors. The scintillator is placed in the thin-walled aluminium container with an entrance front window from beryllium. The crystal is viewed by the photo multiplier put behind thick lead

glass of high transparency that allows to lower the intensity of the radiation background from the spacecraft. Energy resolution of the detector at 662 keV is 8%.

Response functions for both detectors in the energy range of 10 keV – 10 MeV for incidence angles of 0 – 90° are calculated by the method of numerical simulation with the use of GEANT program and confirmed for several monochromatic lines by laboratory calibrations.

The operation program of the instrument provides for two main modes of observations:

1. Continuous background mode;
2. Flare mode.

Continuous measurements of radiation intensity are made in the background mode in the energy range of 10 keV – 12 MeV broken into a number of energy channels (8 – 12). Time resolution is 1 – 2 seconds. It allows to control though with low spectral resolution the general situation and variations of X-ray and gamma radiations on the earth orbit and to find out the reasons of their occurrence. Measurements of multi-channel energy spectra are carried out also for the detector pointed at the Sun in the range of 200 keV – 8 MeV with accumulation time from one to several minutes.

When a solar flare or gamma-ray burst is detected, "KONUS-RF" instrument goes into the mode of their in-depth study with limited spectral and adapted to the intensity level time resolution. The duration of measurement in such a mode may reach 8 minutes for solar flares and 4 minutes for gammas-ray bursts.

The onboard time code is used in both modes for exact timing of measurements. The received information is collected in the RAM of the device as separate files of 16 Kbytes size and is entered into the SSRNI accompanied by the necessary service information. Two detectors form two independent digital sources. Direct programs of measurements (including the amount and borders of energy channels, the number of channels in spectra, the levels of adaptation) are contained in the read-only memory of the instrument.

The information content of the "KONUS-RF" when its capabilities are fully realized is 10 – 12 Mbytes per day.

Single relay commands and a set of digital commands are used for the control of the instrumentation. The total power consumption is about 10 W.

Weight of "KONUS-RF" is about 32 kg.

Fast X-ray monitor BRM

Research of hard X-ray radiation of solar flares

Principal Investigator: E.V. Fedorovih, Yu.D. Kotov, V.N. Yurov, Yu.A.Trofimov, A.I. Arkhangelski[1], A.S. Glyanenko, M.Yu. Zaporogcev

Moscow Engineering Physics Institute (State University), Russia

Scientific tasks of the experiment:

- Investigation of magnetic energy accumulation and its transformation into accelerated particles energy and radiations during solar flares;
- Research of energy release dynamics in weak flares.

Goals of the experiment:

- Fast monitoring of hard X-ray solar radiation in the energy range of 20 – 600 keV with 2 – 3 ms time resolution;
- Registration of solar flare X-ray radiation temporal profile in six energy sub-bands.

Main parameters and configuration of the instrument

BRM is based on a fast scintillation detector. The scintillation crystal material is $YAlO_3(Ce)$. It has the following parameters: de-excitation time is 28 ns; density is 5.35 g/cm^3; maximum wavelength in emitted spectrum is 347 nm. The crystal has a cylindrical shape with dimensions of 13 mm in height and 68 mm in diameter.

BRM registers radiation in the energy range of 20 – 600 keV, divided into six intervals. Boundaries and effective areas of energy channels are listed in the table below.

Channel number	Energy channels, keV	Effective area, cm^2	Time resolution, ms
1	20 – 30	20	up to 2 – 3
2	30 – 40	20	
3	40 – 50	20	
4	50 – 70	20	
5	70 – 130	20	
6	130 – 600	15	
7	20 – 600	15	
8	> 600	20	

The instrument consists of two blocks: the detector block BRM-D (Fig. 6) outside the hermetic module and the electronics block BRM-EM inside the spacecraft.

Principle of operation

The collimator with 6° field of view is installed in front of the crystal to decrease the background. The measurement channel is stabilized using precise impulses from the light source (light-emitting diode) placed in the collimator in front of the crystal. The system stabilization reaction time is 1 s. This system controls the PMT power supply. This helps one to avoid the influence of output characteristics at high count rate. Signals from PMT separated according to their amplitude into six channels are transmitted to the electronic block BRM-EM for further processing. Two channels for gamma-rays are provided in the BRM-D block too.

Total BRM weight is 19.5 kg, weight of the detector block BRM-D is 5.5 kg.

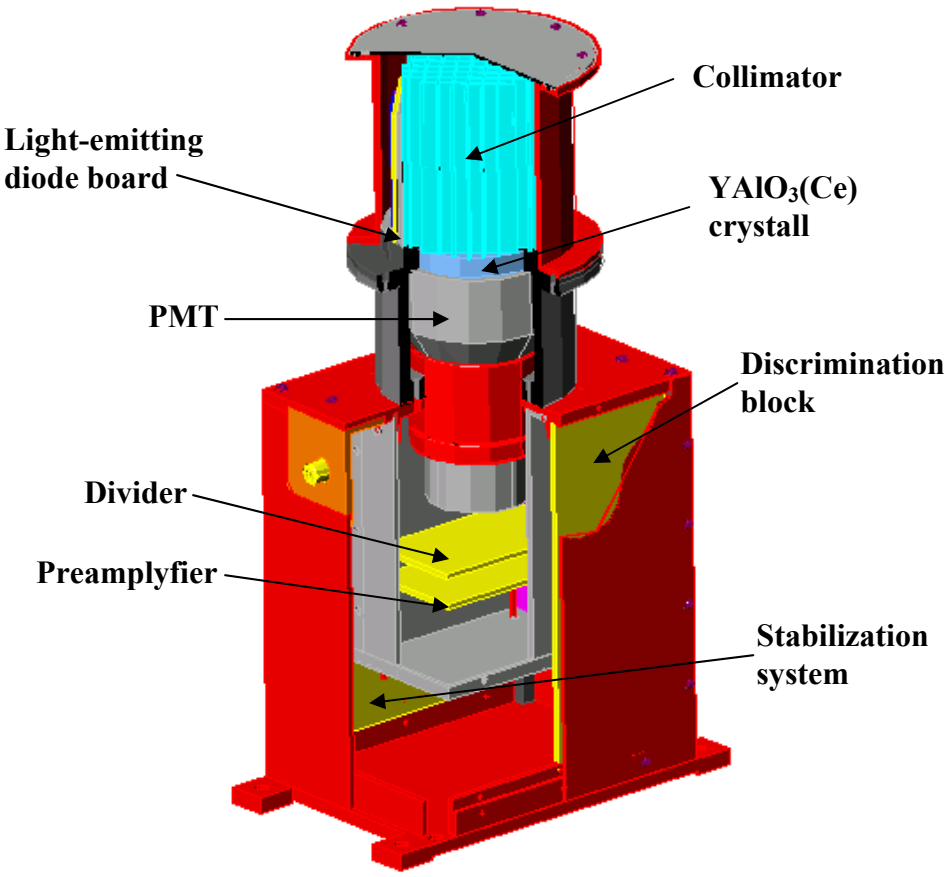

Fig. 6. Detector block BRM-D

Multi-channel monitor of ultraviolet radiation PHOKA

Yu.D. Kotov, A.V. Kochemasov, V.N. Yurov,

Moscow Engineering Physics Institute (State University), Russia

Scientific tasks of the experiment:

- Study of solar flares appearance and evolution mechanisms and variations of solar radiation;
- Research of the Earth upper atmosphere conditions.

Goals of the experiment:

- Monitoring of ultraviolet solar radiation in the range of wavelengths: (1□11) nm; (27□37)nm; 121.6nm;
- Determination of correlation between radiation in XUV/EUV band and in other energy ranges;
- Occultation measurements of ultraviolet solar radiation absorption in the Earth atmosphere at the altitudes of 150 – 500 km.

Main parameters and configuration of the instrument

PHOKA instrument is designed for measurements of soft X-ray and ultraviolet radiation total intensity from the solar disk with time resolution of 0.1s in three pairs of XUV/EUV spectral bands and in visual.

Band number	Spectral window, nm	Main emission lines	Origin of generation
1	< 11		Corona
2	27 – 37	30,4 нм – HeII	Transition region
3	121,6	Ly-α	Chromosphere
4	< 11		Corona
5	27 – 37	30,4 нм – HeII	Transition region
6	121,6	Ly-α	Chromosphere
7	< 1100		Photosphere

When the solar disk is observed through the Earth atmosphere, during occultation, it is possible to obtain temperature and density distributions and to specify theoretical and empirical models of thermosphere and ionosphere.

PHOKA includes the detector block PHOKA-D (Fig. 7) situated on the front frame of the satellite oriented to the Sun and the electronics block PHOKA-E mounted in the hermetic module of the spacecraft.

Each registration channel includes a silicon photodiode AXUV-100 in assembly with a collimator and an appropriate spectral filter, a preamplifier and a voltage-to-frequency converter. The accuracy of absolute intensity measurement is about a few percent of the total flux.

The PHOKA-D weight is 3 kg.

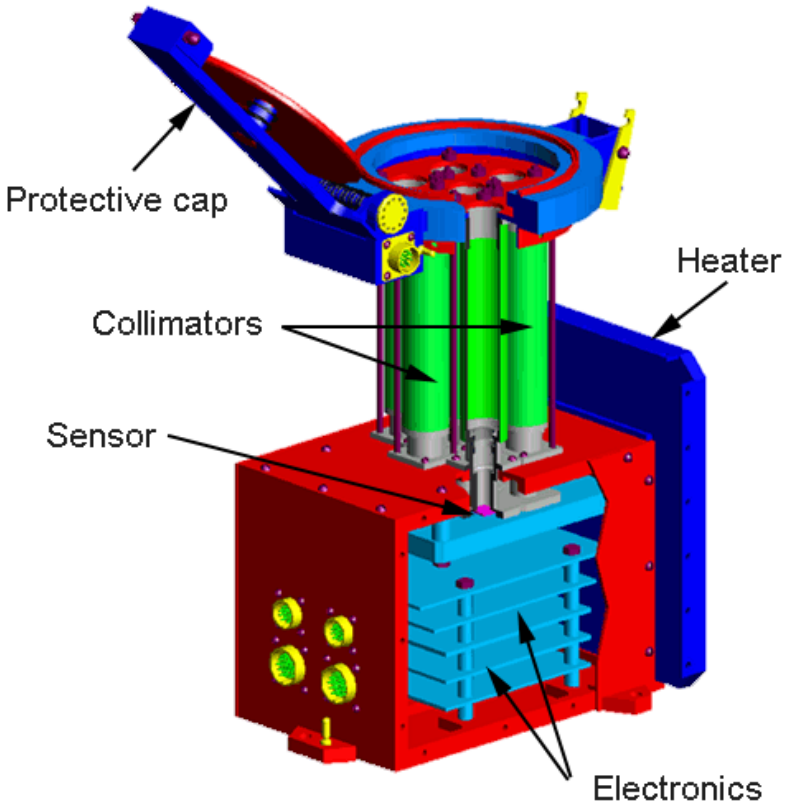

Fig. 7. Scheme of the detector block PHOKA-D

Telescope-spectrometer TESIS for imaging solar spectroscopy in X-rays

S.V. Kuzin, I.A. Zhitnik, O.I. Bugaenko, A.P. Ignat'ev, V.V. Krutov,
A.V. Mitrofanov, S.N. Oparin, A.A. Pertsov, V.A. Slemzin, N.K. Suhodrev
Lebedev Physical Institute of Russian Academy of Sciences, MOSCOW, RUSSIA

Scientific tasks of the experiment:

- Study of transient processes in solar atmosphere and its connections with magnetic fields structure;
- Research of corona heating mechanisms and solar wind acceleration;
- Research of the Earth upper atmosphere parameters.

Goals of the experiment:

- Monitoring of solar activity with high time (up to second) and spatial resolution (1 – 2 arc sec.);
- Research of active areas in the X-ray band on the Sun and their evolution (active areas, coronal holes, bright spots, flares, transients, etc.);
- Observation of the solar corona up to 5 radii from the Sun in XUV band with high spatial resolution;
- Diagnostics of solar plasma by X-ray images of the Sun obtained simultaneously in several spectral channels;
- Study of solar activity impact on the Earth upper atmosphere.

Main parameters and configuration of the instrument

TESIS instrument is designed for registration of solar images in narrow spectral bands and monochromatic emission lines of HeII, SiXI, FeXXI – FeXXIII, MgXII ions in high temperature plasma of transition region and corona.

TESIS consists of detector block TESIS-BD, electronic block TESIS-BE and optical sensor TESIS-OD. The TESIS-BD block includes four independent telescope channels for solar image registration:

- telescope-coronagraph 134 Å – in lines FeXXI – FeXXIII (132 – 136 Å);
- telescope-coronagraph 304 Å – in lines HeII, SiXI (295 – 315 Å);
- telescope-spectrometer Mg1 and Mg2 – in lines MgXII (8.418 – 8.423 Å) in orthogonal plane of dispersion.

The optical sensor (star tracking) is designed for control of telescope three axes orientation with up to 1′ accuracy.

Parameter	Channel		
	134 Å	**304 Å**	**Mg 1,2**
Spectral band, Å	132 – 136	295 – 315	8.418 – 8.423
Field of view	Disk – 35′; Corona – from 2 till 5 R_{Sun} (with mirrors shifting)		45′
Spatial resolution, arc sec	1		2

Spectral resolution, λ/Δλ	10	2×10^{-4} Å/cell
Exposure time, s	0.01-600	
Mirrors effective area, cm^2	100	60

Principle of operation

Images of the Sun are formed on a detector sensitive area by special mirrors (Fig. 8). The multi-element filter system is used for blocking optical solar radiation. This system includes free superthin films on supporting grids and polymeric membranes. CCD detectors with electrical cooling are used in all channels. The received data are processed by onboard computer, archived and transmitted to SSRNI.

Sizes: detector block – 2200×500×300 mm, electronic block – 300×250×236 mm, optical sensor block 450×200×150 mm.

The weight of TESIS is less than 74 kg.

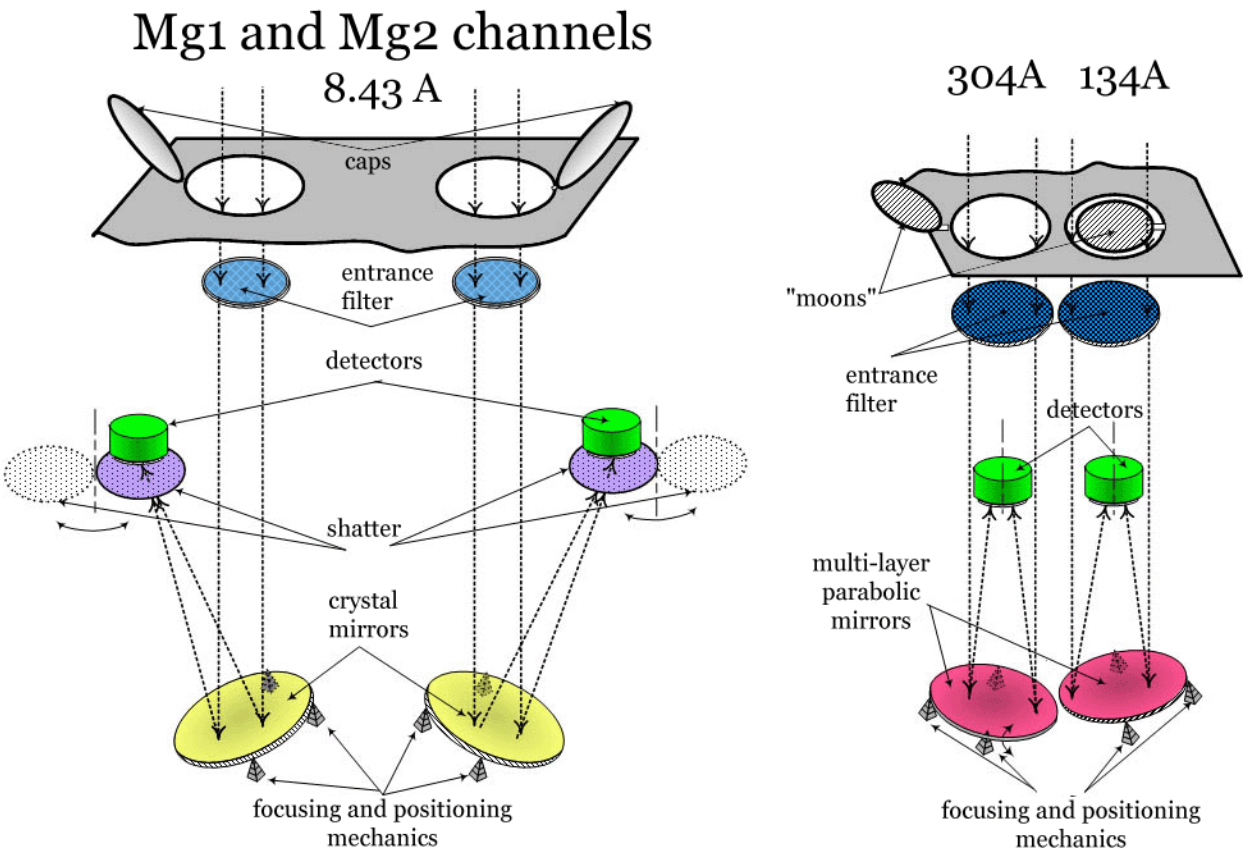

Fig. 8. Optical schemes of the TESIS-BD channels

Multi-channel solar photometer SOKOL

V.D.Kuznetsov, Y.D.Zhugzhda, N.I. Lebedev, N.I., S.I.Boldyrev, I.M. Kopaev,
IZMIRAN, Troitsk, Russia

Scientific tasks of the experiment:

Continuous observations of the solar radiation intensity variations in range 280 - 1500 nm, relative intensity resolution $2x10^{-6}$ of total intensity, observation angle - 2°.

Technical parameters

- radiation intensity is measured simultaneously in 7 optical spectrum bands by 8 photosensors: 280, 350, 500, 650, 850, 1100 and 1500 nanometers with the measuring bandwidth below 10% of the value of central wavelength.
- relative intensity resolution is $2x10^{-6}$ of the total solar radiation intensity.
- temporal resolution of intensity measurements - 30 sec.
- spacial resolution is not available.
- photometer observation angle - 2°.
- precision of the photometer orientation towards the center of the solar disk is 5 arc. min.
- the photometer consists of the photosensors unit PU and electronics unit EU.

Dimensions: PU - 130x130x510 mm.
Weight: 5.2 kg.

Fig.9 SOCOL photosensors unit

Charged particle analyzer «ELECTRON-M-PESCA»

M.I.Panasuk, S.N. Kuznetsov, Yu.I. Denisov, Yu.P. Gordeev, A.S. Chepurnov

Scobeltsyn Institute of Nuclear Physics at Moscow State University, Russia

Scientific tasks of the experiment:

- Study of physical mechanisms and conditions of electrons and protons (nuclei) acceleration in different phases of solar flares;
- Research of cosmic ray anomalous component and radiation trapped by the Earth magnetosphere.

Goals of the experiment:

- Study of energetic spectra, charge and isotope composition of nuclei accelerated during solar flares;
- Registration of solar electron fluxes and spectra of in the energy range of 0.2 – 2 MeV;
- Registration of protons and nuclei fluxes and energy spectra on the satellite orbit.

Main parameters and configuration of the instrument

Registered characteristics	Energy ranges
Spectra and fluxes of protons	1 – 20 MeV
Spectra and fluxes of electrons	0.2 – 2.0 MeV
Fluxes of nuclei with charge number Z < 26	2 – 50 MeV/nucleon

Charge resolution of nuclei isotope composition is 0.5. «ELECTRON-M-PESCA» instrument can register fluxes up to 5×10^7 particles/cm^2·s·str.

The instrument consists of the detector block «ELECTRON-MD-PESCA» and the electronic block «ELECTRON-ME-PESCA».

The main element of the detector block is a telescope. It is the system of four ion-implanted silicon detectors placed in a cylindrical passive aluminium protection.

System geometric factor is 2 – 3 cm^2·str. Field of view is 50°.

Detectors	D1	D2	D3	D4
Effective area, cm^2	9	6	9	12
Thickness, μm	158	509	705	324

Principle of operation

The specific ionization energy of particles during their movement through detectors system (Fig. 10) is used for particle identification and determination of their energy. The pulse amplitude from a charged particle (ΔE) is measured in a counter and particles whose energy release in the *n-p* detector exceeds the predefined threshold are selected for further analysis. Signals from the semiconductor detector pass through multipliers and forming devices to integral discriminators. Each integral discriminator is tuned to trigger when a particle with the energy in a definite energy range passes through the detector. The system of D1 – D2 detectors is used to measure spectra and fluxes of protons. To measure fluxes of electrons the system of D1 – D4

detectors is used. And the system of D1 – D3 detectors is used to measure spectra and fluxes of alpha-particles.

Sizes of the instrument blocks are «ELECTRON-MD-PESCA» – 200×186×140 mm, «ELECTRON-ME-PESCA» – 250×150×284 mm.

Weight of the instrument:
«ELECTRON-MD-PESCA» block – 1.8 kg, «ELECTRON-ME-PESCA» block – 7 kg.

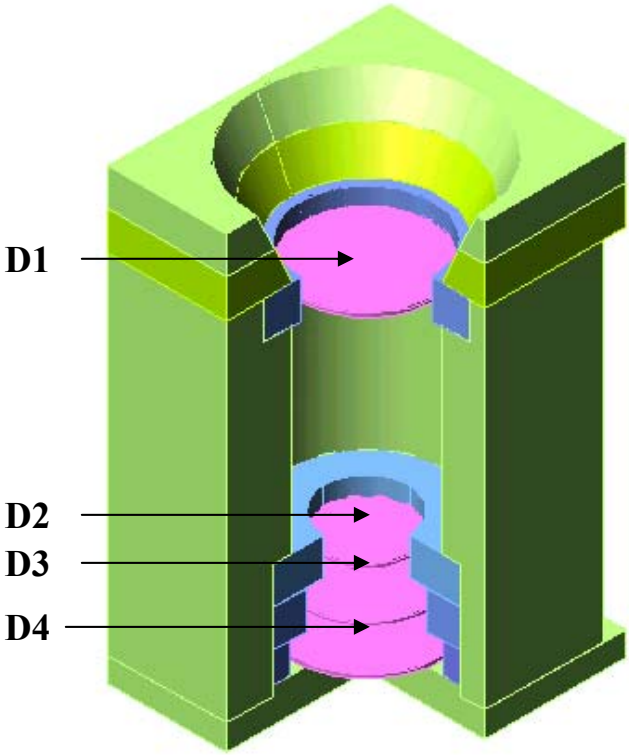

Fig. 10. Telescope of the «ELECTRON-MD-PESCA» block detector

Satellite telescope of electrons and protons STEP-F

A.V. Dudnik, V.K. Persikov
Karazin Kharkov National University, Ukraine

Scientific tasks of the experiment:

- Research of high energy electrons and protons energy spectra and pinch-angle distributions evolution in Earth radiation belts during magnetospheric storms and sub-storms due to high speed solar wind impact on magnetosphere;
- Study of wave processes and dynamics of energetic particles in Earth magnetosphere.

Goals of the experiment:

- Determination of height where electric and magnetic components of Earth magnetic field fluctuations primarily impact the radiation belts particles process of radial diffusion;
- Determination of power-low spectrum degree in pinch-angle distributions of precipitated electrons from values D_{st}, K_p and AU-indexes, which characterizes magnetospheric storm magnitude on different latitudes;
- Search of correlations between bursts in the radio band observed on middle latitude on the Earth surface level and solar, magnetospheric and ionospheric activity;
- Research of micro bursts of high energy electrons below the outer radiation belt;
- Study of connection of captured and precipitated particle fluxes of magnetospheric origin with solar proton events and cosmic rays;
- Test of hypotheses about genetic connection of precipitated high energy electrons fluxes from Earth radiation belts with mechanism of high frequency radio bursts generation.

Main parameters and configuration of the instrument

STEP-F instrument is able to register fluxes of:

- electrons in the energy range of 0.4 – 14.3 MeV;
- protons in the energy range of 9.8 – 61.0 MeV;
- alpha-particles in the energy range of 37.0 – 246.0 MeV.

The instrument consists of detector block STEP-F-D (Fig. 11), installed outside the hermetic module, and digital information processing block STEP-F-E. The detector block includes two identical silicon position-sensitive detectors and two scintillation detectors. Each silicon detector has the size of 45×45 mm and 350 μm thickness. Scintillation detectors are based on CsI(Tl) crystals and viewed by large area photodiodes. The average telescope field of view is 97×97°. The size of each of 36 matrix square elements of semiconductor detector is 7.3×7.3 mm, which allows to receive the average angular resolution in telescope total field of view about 8°. The effective area of each semiconductor detector is 20 cm^2, scintillation detectors is 36 and 49 cm^2. Geometric factor of STEP-F instrument is 20 $cm^2 \cdot strad$.

Weight of STEP-F is about 13 kg.

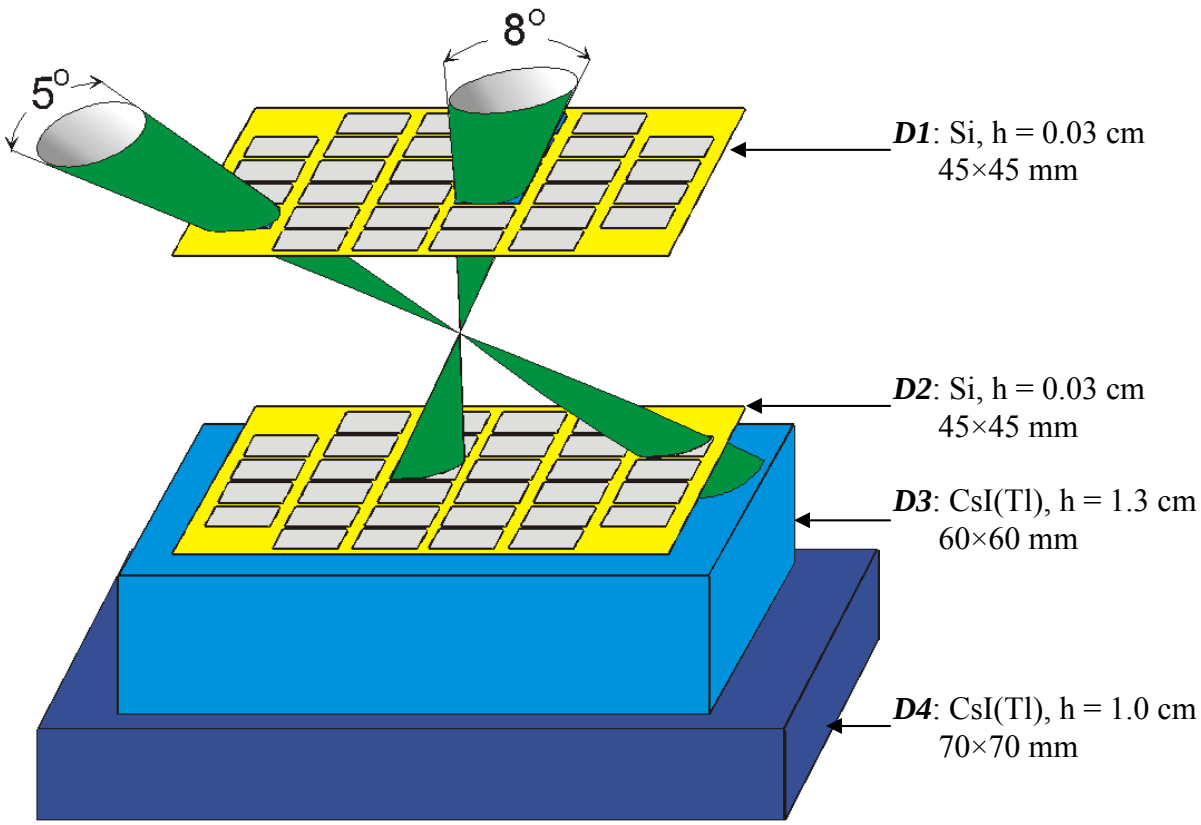

Fig. 11. Detector block STEP-F-D

D1, *D2* – silicon position-sensitive totally depleted pin-detectors;
D3, *D4* – scintillation detectors.

Magnetometer SM-8M

V.V. Averkiev[1], V.N. Yurov[2] K.V. Chavchanidze[1], V.F. Boskalev[1], S.I. Boldyrev[2]
[1]FGU NPP «Geologorazvedka», St-Petersburg, Russia
[2]Moscow Engineering Physics Institute (State University), Russia

Magnetometer allows to measure three perpendicular projections of Earth magnetic field induction vector on orthogonally located magneto-responsive elements (ferro-sondes). It produces signals in form of direct current amplitude proportional to the projections.

It is planning to use the magnetometer in conjunction with charge particle analyzers of "PHOTON" scientific payload.

Magnetometer consists of ferro-sondes block (FSB) and electronic block (EB).

Main parameters of the instrument

Parameter	Value
Measurements dynamic range, nTl	-55000 ... +55000
Type of transformer	Ferro-sonde, three orthogonal sensors
Resolution, nTl	150 – 300
Accuracy of determination of spacecraft axes orientation, arc degree	2 – 3
Calibration field, nTl	10000 – 13000
Error of calibration signal on output	< ± 1% (± 100 nTl)
Type of output signal	Analog
Temperature range, °C	FSB 0 ... + 40 EB - 70 ... + 70
Power consumption, W	< 2.0
Construction	FSB on arm of 2 – 4 m long
Weight EB, g	800 ± 50
FSB, g	320 ± 40

Required accuracy of spacecraft axes position determination relative to the Earth magnetic field induction vector (under undisturbed Earth magnetic field):

«PENGUIN-M» – 6 – 10°;

STEP-F – 2 – 3°.

Spacecraft magnetic field is 100 nTl when orientation system is turned off and 60 nTl otherwise.

Scientific Data Acquisition and Registration System SSRNI

I.V. Chulkov, **K.V.Anufreichik, D.G.Timonin, A.V.Semenov, A.A.Konovalov, A.V.Nikiforov,** M.V. Buntov,

Space Research Institute of Russian Academy of Sciences, Moscow, Russia

Purpose of the system

1. SSRNI acquires data from scientific payload and stores it in the long-term memory. Data are formed in digital arrays of 960 bit long. Data transfer rate is 62.5 or 125 Kbit/s. The number of information sources is up to 24. Memory allocation between digital information sources (DIS) is adjusted by quotes and can be changed by commands.
2. SSRNI receives and stores information from BATS (onboard equipment of telesignals) in long-term memory. Amount of data from BATS is up to 44 MByte per day.
3. SSRNI delivers onboard time code, 1 second labels and operation commands. The number of supported devices is up to 24.
4. SSRNI transmits information in radio channel. The data accumulated in SSRNI are transmitted to the satellite ground station during communication session using two close radio channels from 8.2 GHz band. Data transfer rate is 7.68 MByte/s.

Operation modes

SSRNI has the following operation modes:

- «Record»;
- «Playback» (with data recording);
- «Direct transmission».

In «Record» mode the information received from DIS and BATS is saved in the long-term memory.

In «Playback» mode the data stored in the memory is transmitted to radio channel. During that time SSRNI continues to receive and save incoming information arrays.

In «Direct transmission» mode the information received from DIS and BATS passes directly in the radio channel.

Operation modes are switched by main interchange bus commands and/or by single commands.

Technical characteristics

SSRNI long-term memory total capacity used for data storage is 4 Gbit (512 MByte). Weight of SSRNI is 9 kg.

Control and communications block BUS-FM

S.A. Aust, I.V. Kozlov, A.D. Ryabova
Space Research Institute of Russian Academy of Sciences, Moscow, Russia

BUS-FM block is designed for:

1. Control of scientific equipment “PHOTON” operation modes;
2. Commands generation and distribution between scientific instruments;
3. Connection of scientific instruments and engineering systems of spacecraft.

BUS-FM is a relay-communication block made on relay-diode modules. The block consists of three plates (two with modules and one cross-plate).

BUS-FM block accepts single, programmed and multi-address commands.

Technical characteristics

Command output voltage is + 27 $^{+7}_{-3,5}$ V.

Weight of BUS-FM is less than 11 kg.

Ground segment of recovery and distribution scientific information

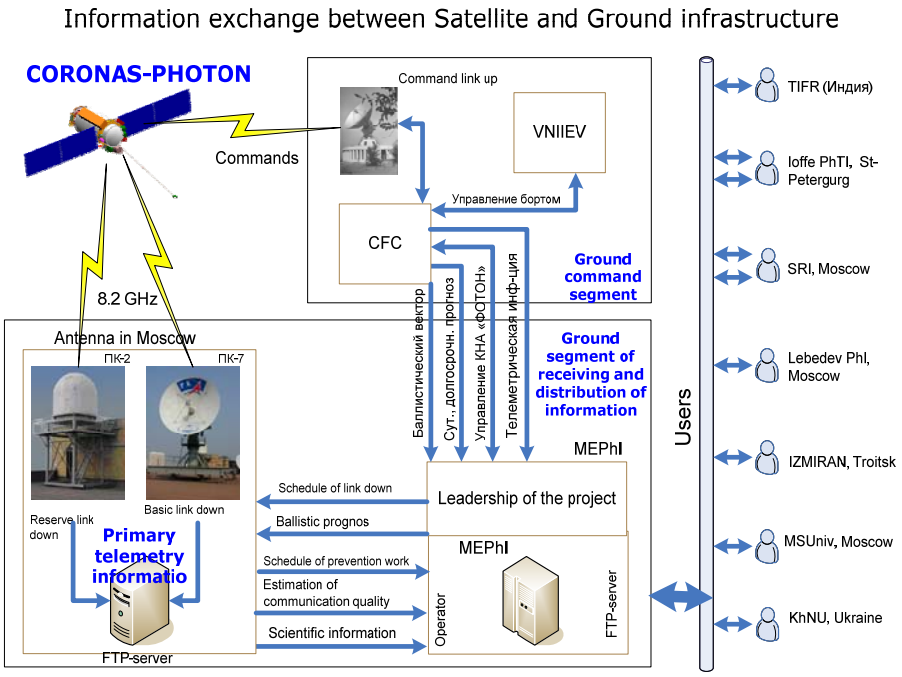

Fig.12. Structure of ground infrastructure to receive and distribute scientific telemetry information, as well as to control thescientific instrument parameters by telecommands.

Operator function of the space complex “CORONAS-PHOTON” is performed by MEPhI.

Preliminary results of observations in period February to November 2009

Onboard scientific instruments were put in operation in February in according with outgassing and switch on procedures. During February-March the in-flight calibration and adjustment to values were performed. All instruments were operated in accordance with requirements specifications. On the end of November 2009 the communication with the satellite "CORONAS-PHOTON" was lost due to failing of onboard power system. All making attempts to restore the power system were ineffective. So, the observation were performed from February to November 2009.

During observational period the solar activity was extremely low. The solar flares of classes C and higher were extremely infrequent. Instrument PINGUIN-M/CORONAS-PHOTON that has detector of soft X-ray radiation with 2keV threshold registered during mentioned period about 200 flares including 101 of class B flares and 13 of class C. Large amount of A class and weaker were observed by SphinX instrument that has good sensitivity in the band (1.0-10) keV.

This period of unique quite Sun was adequate for study of simplest, "elementary" dynamic processes in solar corona in simple configuration of magnetic field.

During mentioned period the team of TESIS/CORONAS-PHOTON have received the next results:

- For the first time the imaging of interim (at distance from 0.5 to 1.5 solar radius) solar corona in shot wave band was observed;
- In conference with Hinode (Japan) have observed the new type of "hot" coronal mass ejection with plasma temperature about 1×10^6 °K;
- For the first time the process of coronal mass "separation" from solar magnetic field was measured in details;
- For the first time the dynamic of hot coronal X-ray spots and chromospheres spicule was measured with cadence 1 sec. The best former measurements made by satellite SOHO (ESA) has cadence 60sec.
- For the first time the new type of event – burst of solar radiation in bright coronal spots and active regions with duration less 1 min was observed. Such temporal activity of Sun was unknown due to absence of observation with so fast cadence.
- For the first time the accurate values of temperature of hot ($T>5\times10^6$ °K) micro structures of solar corona were measured by spectroscope methods (using the spectroscopic line broad). Distributions of instantaneous and average temperature were determined.

Uninterrupted monitoring of EUV flux was performed by PHOKA/CORONAS-PHOTON radiometer in bands 0.5-11 nm, 27-37 nm и 116-125 nm every 0.4 s. Example of performed occultation observation (satellite way out from the Earth shadow) is show in fig.13. From it one can estimate the input of visual band in total signal and influence of radiation absorption by upper earth atmosphere during each come of satellite in shadow and come out from it.

Recalculated fluxes absorption as function of occultation height (km) are presented in Fig.14 for observed radiation both in visual band and after passing different filters. Types of used filters are mentioned in the plot.

Radiation flux in 0.5-7nm band measured by PHOKA on 28.02.2009 is $6.0*10^{-5}$W/m^2. This value was getting from measured photocurrents by using reference spectrum recommended by LASP (Laboratory for Atmospheric and Space Physics, USA) for solar quite period. This value is in

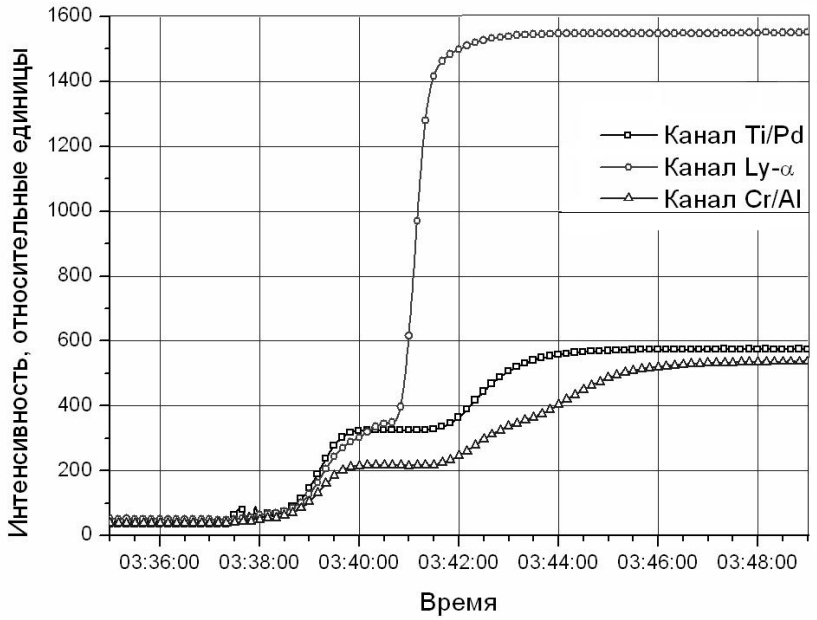

Fig. 13. Intensity of EUV(arbitrary units) in different bands (mentioned at the plot) verses time (UT)

Sunrise in visual band started at 03:38:30. Sun was quite.

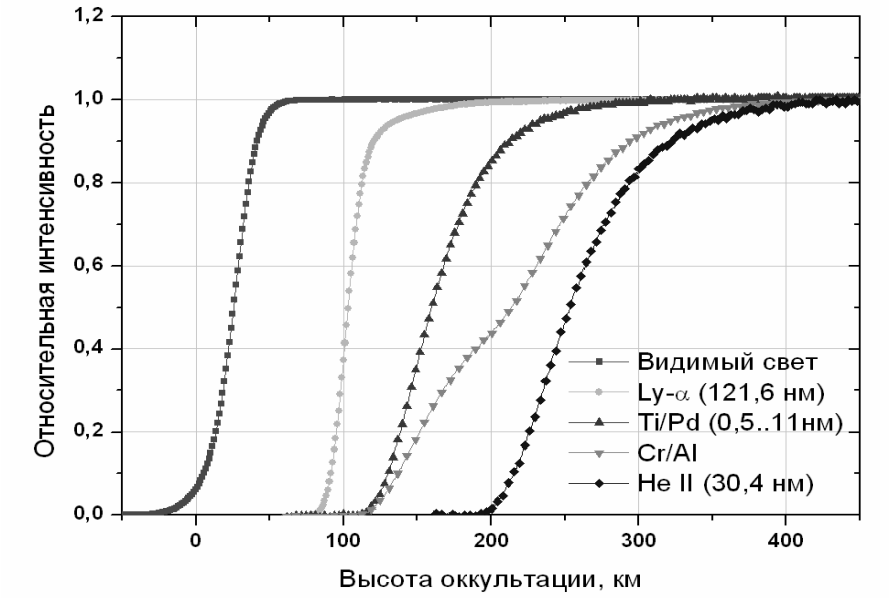

Fig.14. Flux absorption as function of occultation height (km)

agreement with results $7{,}1*10^{-5}$ W/m^2 (with methodic accuracy 12-30%) received for the same band and date by LASP using measurements by XPS (X ray photoelectron spectrometer) onboard of satellite SORCE (Solar Radiation and Climate Experiment).

Flux of Ly-alpha radiation measured by Phoka for 2009.02.28 is $5.7*10^{-3}$ W/m^2 with estimated accuracy about 15%. This figure is in a good agreement with figure $5.77*10^{-3}$ W/m^2 received from SOLSTICE(SOLar STellar Irradiance Comparison Experiment)/SORCE for the same date.

Detector SphinX (Solar Photometer in X-rays), jointly working with TESIS, is a high sensitive and fast spectra-photometer for registration of solar soft X-ray in band 0.85□15keV. Energy resolution is 0.1 keV, temporal resolution is 1 sec. SphinX has sensitivity 100 times higher than radiometers of satellite GOES. As an example the measured solar flux variability is shown in fig. 15. Data are averaged over 5 min observation.

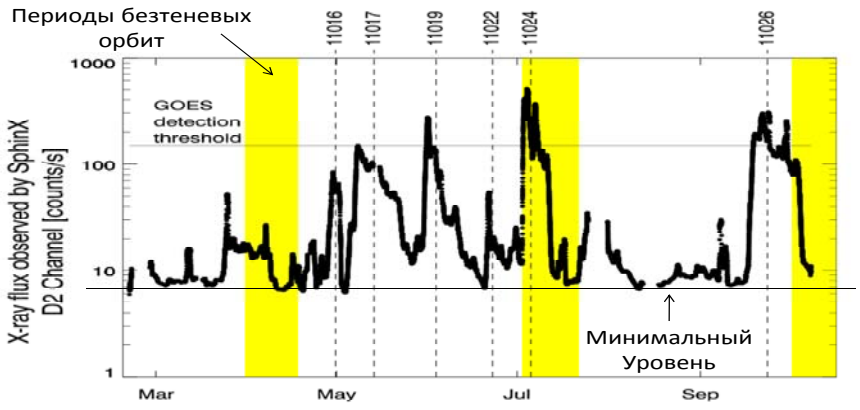

Fig.15. SphinX light curve observations during quite Sun.

According these data the flux of absolutely quite solar corona is 20 times less than GOES threshold. The level of flux and its variability is higher during existence of active regions at the solar disk. The number of active regions is given at top of the plot.

Maximum observational data were received by several instruments of the CORONAS-PHOTON mission for two solar flares: 05 July 2009 (C2.7-class) and 26 Oct2009 (C1.3-class). Temporal dependence of different instrument counts as a function of time is given in fig.16.

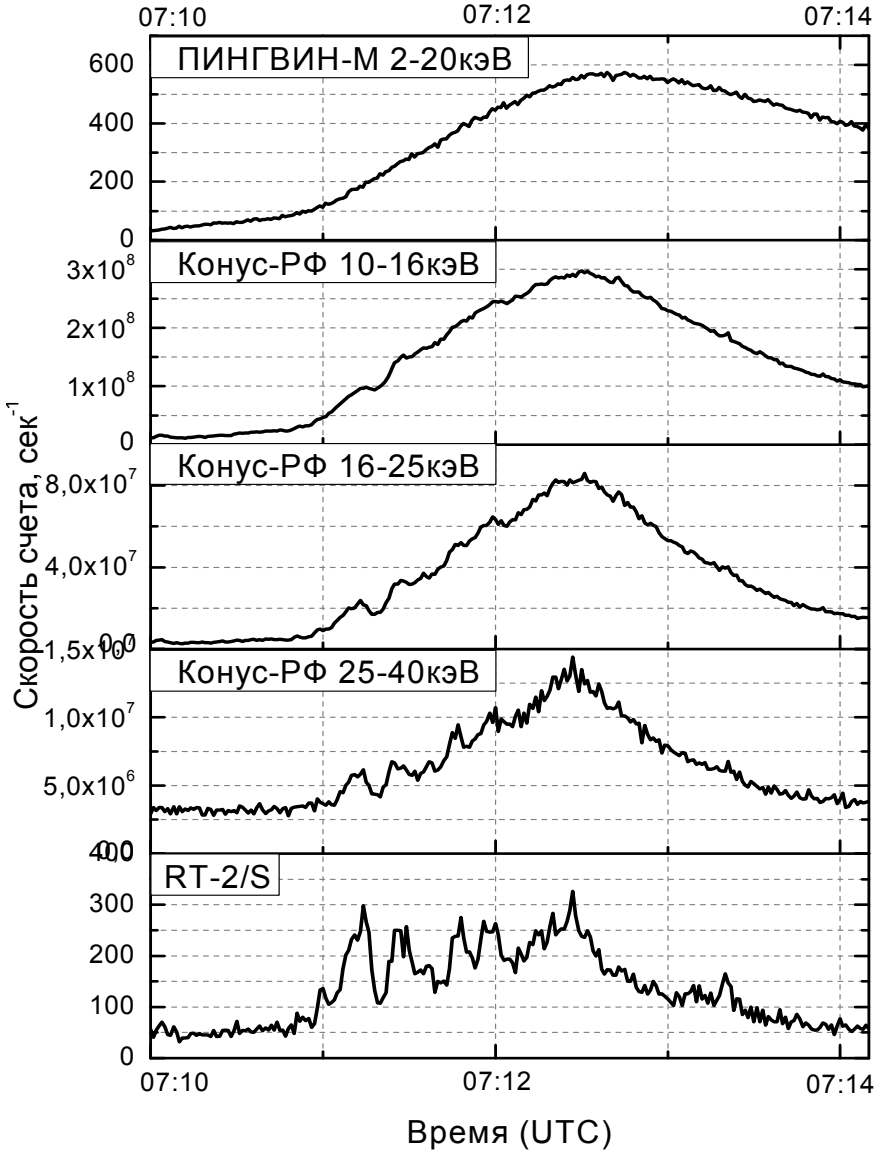

Fig.16. Temporal dependence of soft and hard X-rays (counts/sec) observed by instruments PPINGUIN-M, Konus-RF and RT-2

One can see from the plot the appearance of fine temporal structure as photon energy is higher. The most clear this structure is seen in RT-2 data due to effective suppression of background by using phoswich mode and passive collimator. Analysis of temporal series have shown the 12 and 16 sec periodicities.

Flare 26 Oct 2009 stated in 22:38 UT in disk position N19W35. Development of it in EUV channels (PHOKA data) and in soft X-ray (PINGUIN-M data) are presented in fig. 17 and fig.18.

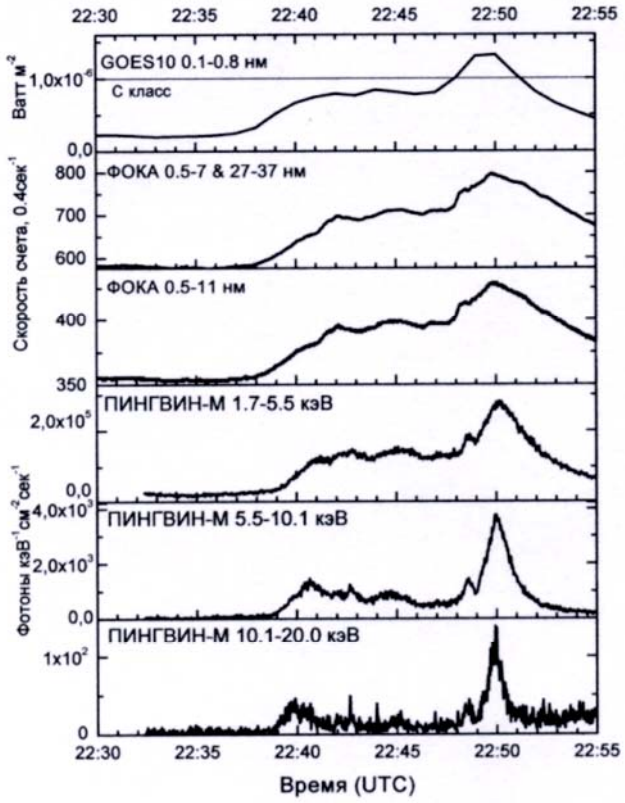

Fig. 17. Light curves in soft X-ray band in flare 26 Oct 2009. Data are from спутником GOES instruments PHOKA and PINGUIN-M of CORONAS-PHOTON mission.

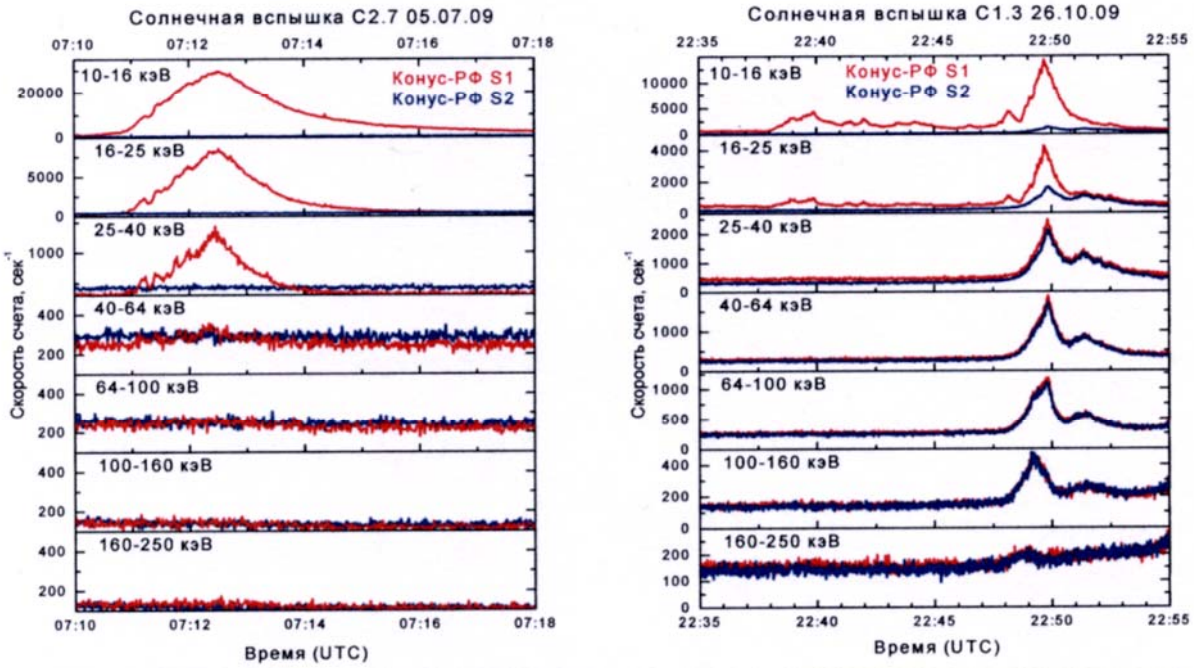

Fig 18. Comparison of hard X-ray curves in two solar flares: 05 July 2009 and 26 Oct 2009 for different energy bands. Red line –solar detector (oriented to the Sun), Blue line-antisolar detector(oriented into opposite direction).

During observation period the next observational results were received by CONUS-RF group:

- Received observational data on activity of anomaly X-ray pulsar AXP/SGR1E1547.0-5408

- On 05 June 2009 was discovery the new soft gamma-repeater SGR 0418+5729 (Fig 19)
- Observe 3 solar flare
- Observed 82 cosmic gamma-rays bursts including very intense burst 8 April 2009

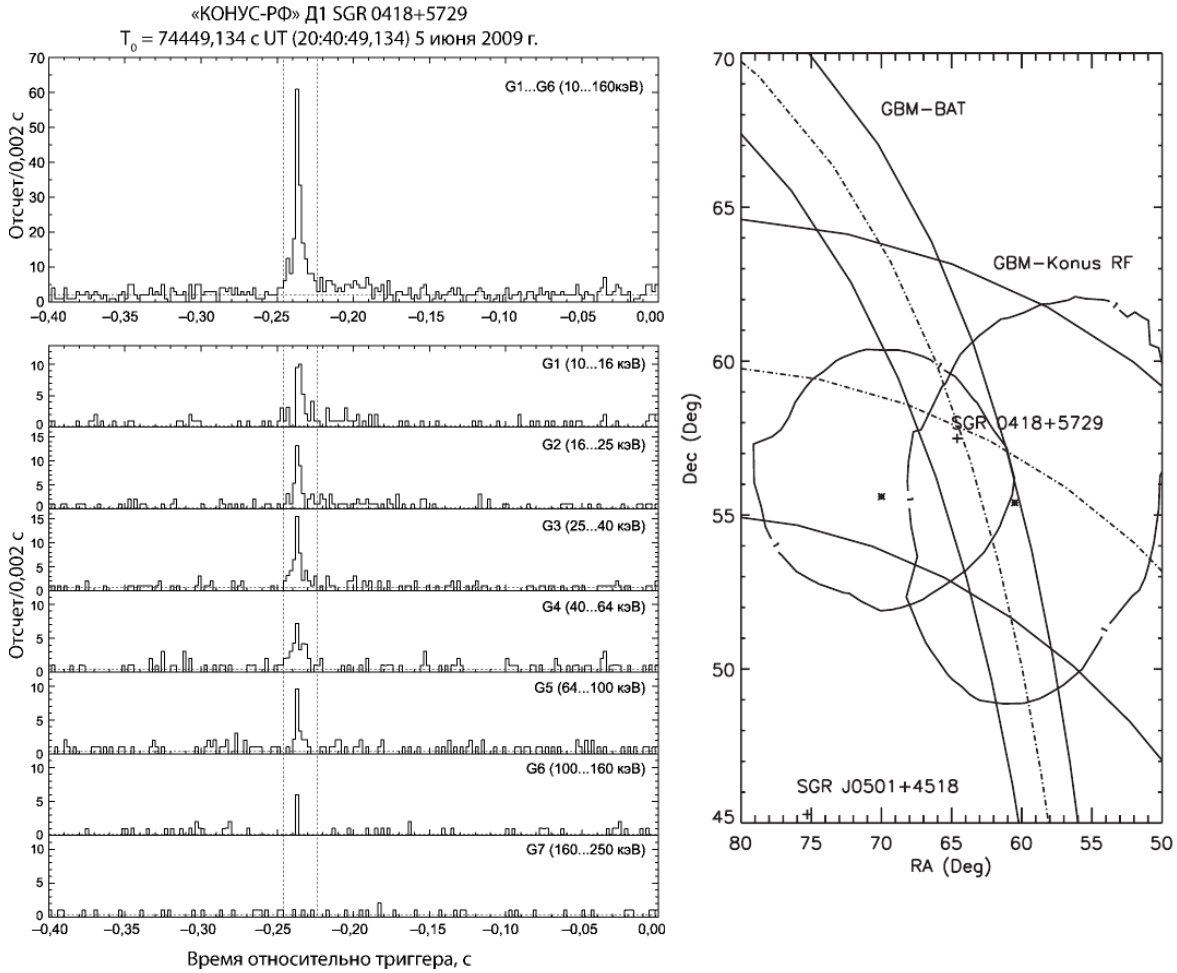

Fig.19. Light curve of soft gamma-repeater SGR 0418+5729 (left panel)
Triangulation measurement of event position (right panel)

Experiment ELECTRON-M-PESKA have observed in 2009 during minimum solar activity essential (more order of value) increase of electrons in outer radiation belt in spite of absence of geomagnetic disturbances. This increasing is correlate with high velocity flux of solar wind.

Similar increasing were observed in March, April, beginning of May, July, August and end of November 2009.

All activity on CORONAS-PHOTON project was sponsored by ROSCOSMOS in the frame of Russian Federal Space Program.

2.1.7. P.N. Lebedev Physical Institute of RAS
Laboratory of X-ray Solar Astronomy

Investigations of the solar corona in the TESIS (CORONAS-Photon) and SPIRIT (CORONAS-F) space experiments

2.1.7.1. The TESIS experiment on-board the CORONAS-Photon satellite

Fig.1. CORONAS-Photon satellite before the launch in Plesetsk

The solar EUV telescope-spectroheliometer TESIS was launched on the Russian CORONAS-Photon satellite on January 31, 2009 (Fig. 1).
The main goal of the TESIS experiment is to study the origin of solar activity and mechanisms of solar flares. To achieve this goal, the following tasks of the experiment have been defined:

- Investigation of processes of energy accumulation, release and transformation;
- Determination of physical condition and plasma parameters of various coronal phenomena and structures (flares, active regions, CMEs et al.);
- Investigation of small-scale and large-scale structure and dynamics of the solar corona.

Structure of the TESIS instrument

- 2 high resolution telescopes for spectral ranges 132|171 and 171/304 A
- Wide-field telescope-coronograph 304 A
- X-ray spectroheliograph Mg XII 8.42 A
- XUV spectroheliograph for 280-330A
- X-ray spectrophotometer SphinX 0.5–15 keV (developed in the Space Center of Polish Academy of Sciences)

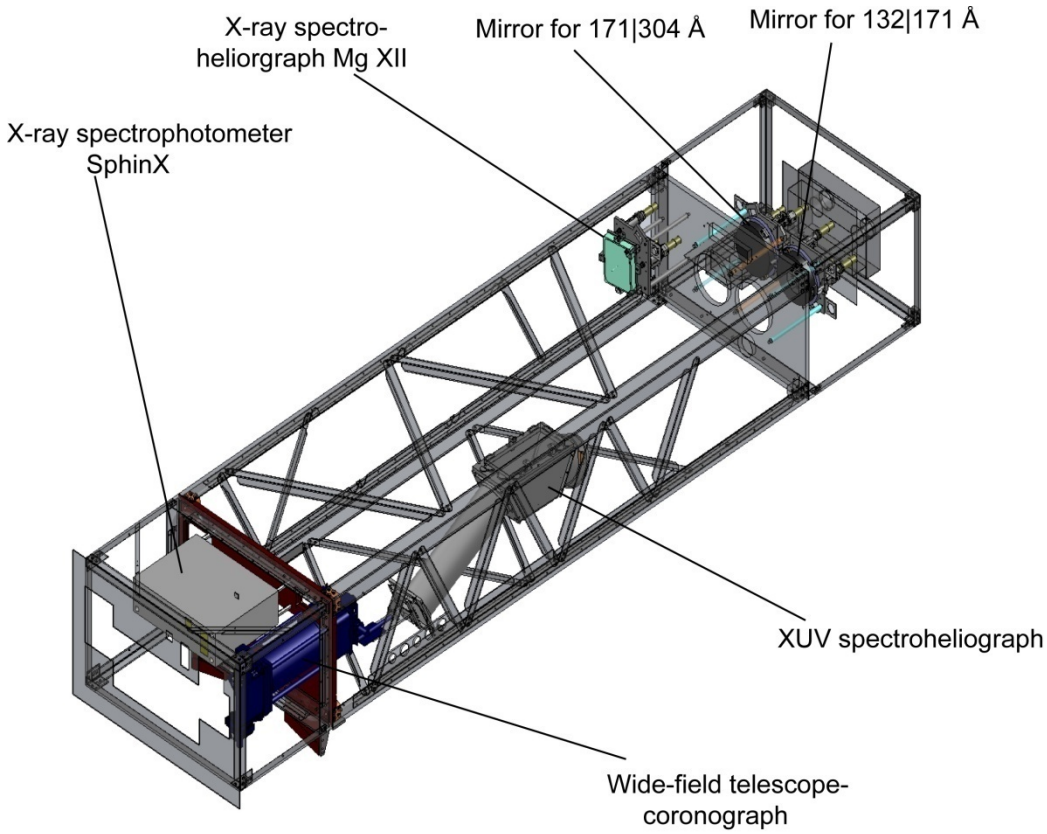

Fig. 2. The TESIS instrument

Comparing with similar existing solar instruments, TESIS has improved angular resolution (1.7”), temporal resolution (several seconds), new wavelength bands (132 A) and wide dynamic range which allows to observe the Sun at low and high solar activity as well.

The site of the TESIS experiment: www.tesis.lebedev.ru (Kuzin et al. 2010)

TESIS images of the Sun in the extremely low activity stage

- During 11 months of operation in orbit from February to November 2010 the instrument was checked out and tuned. The observation modes were optimized according to current solar conditions.
- More than 500 Gbytes of scientific data were obtained which contain new information about solar activity in the period of its minimum and start of growing of the 24th cycle.

- In spite of extremely low solar activity, many solar phenomena have been registered by TESIS:
  - 4 eruptions of giant prominences (16 April, 23 April, 14 June, 26 September);
  - One complex CME event (12 May)
  - 14 flares of the GOES C-class

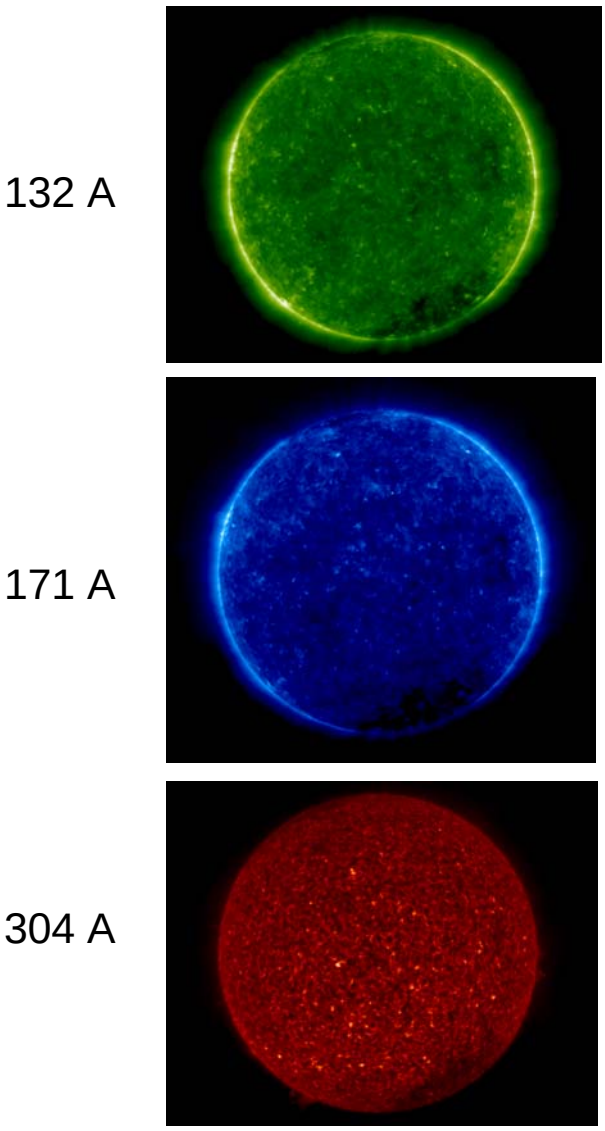

Fig. 3. Images of the Sun obtained by TESIS in the 132, 171 and 304 A bands

TESIS observations of giant prominence eruptions

Prominence eruption of 23 April 2009. He II 304 A

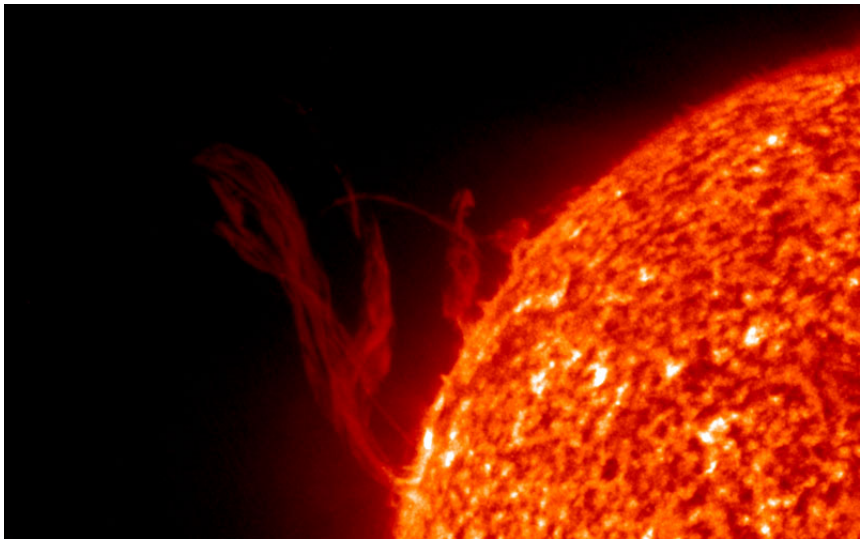

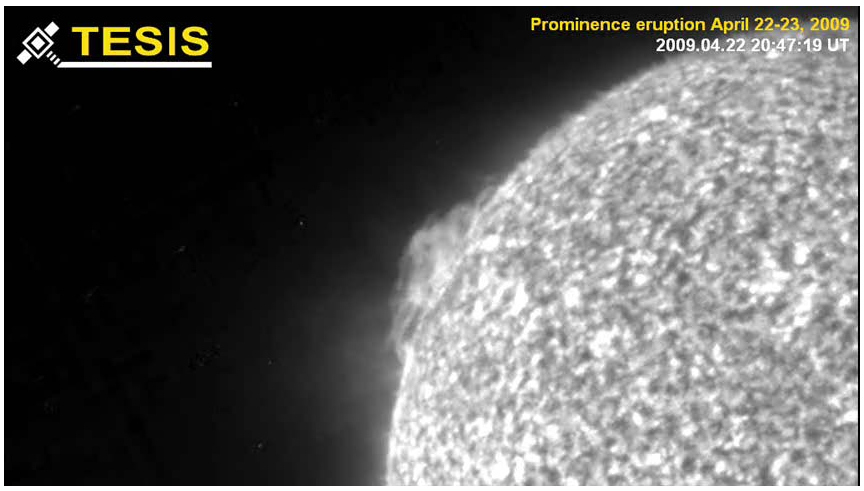

Prominence eruption of 14 July 2009. He II 304 A

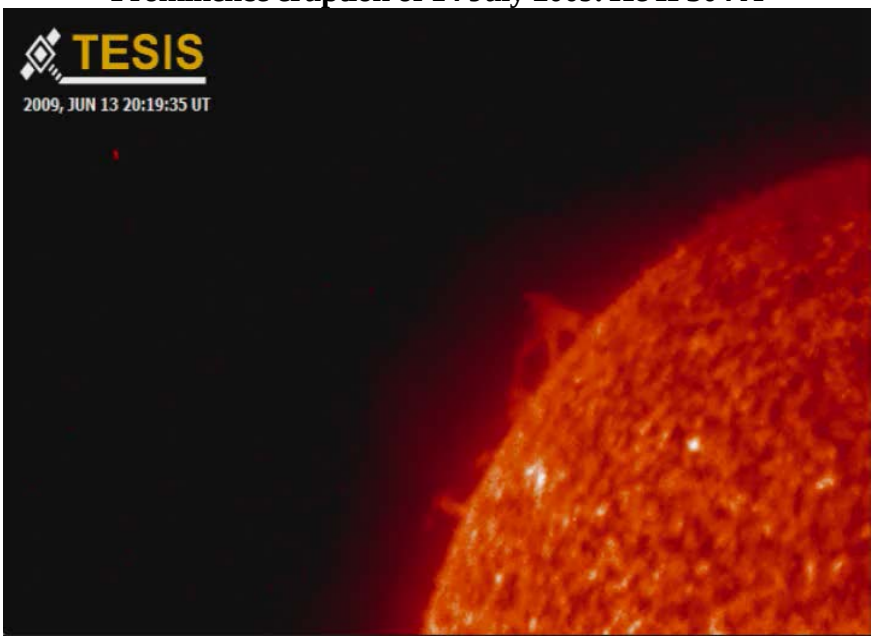

Prominence eruption of 26 September 2009. He II 304 A

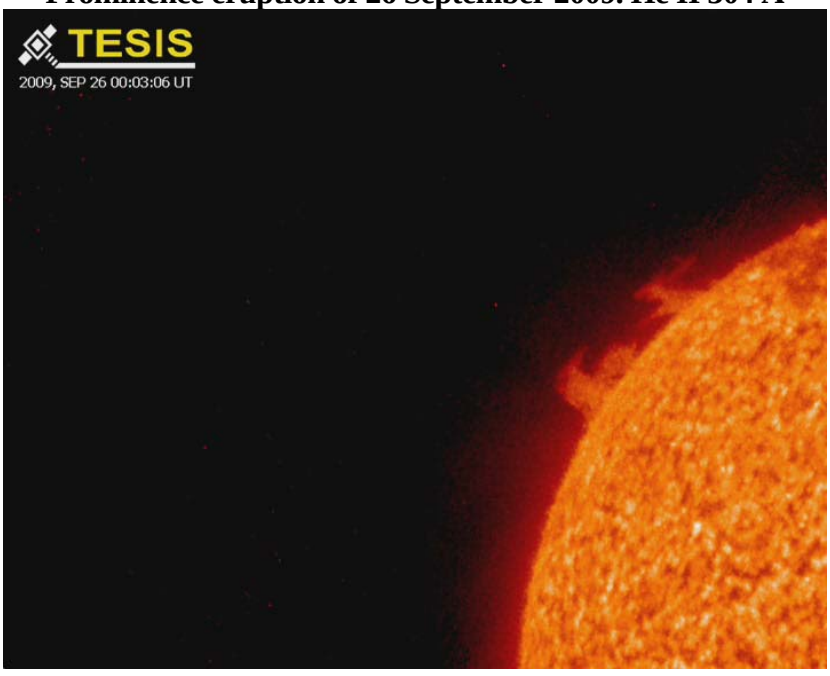

TESIS observations of the inner EUV Corona

Due to its very high sensitivity, TESIS is able to observe the solar EUV corona at large distance above the limb. Observations of quiet corona in the Fe IX line 171 A (T~1 MK) revealed unexpectedly rich fine structure of the magnetic field at low solar activity (Fig. 4). The observed rays point out possible sources of the solar wind.

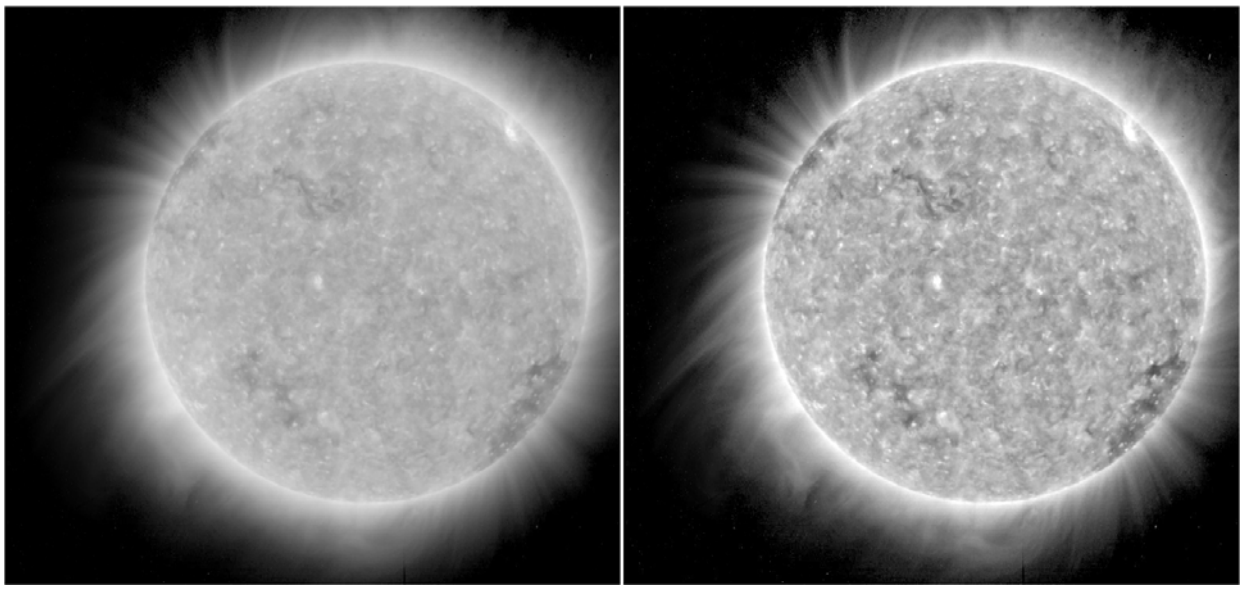

Fig. 4. EUV solar corona at low activity stage observed by TESIS on 30.04.2009

U-type magnetic eruption of May 12, 2009

The movie composed from images taken in the TESIS Fe IX 171 A and He II 304 A bands shows restructuring of the coronal magnetic field during the CME event of May 12-14, 2009.
TESIS observations give a very detailed description of disconnection of U-shaped loop as a result of interaction of closed magnetic lines of inner corona with those of open heliospheric magnetic field. The disconnection occurred in X-point at the height of 0,5 Rsun due to low electric conductivity of the plasma at the place of the moving prominence.

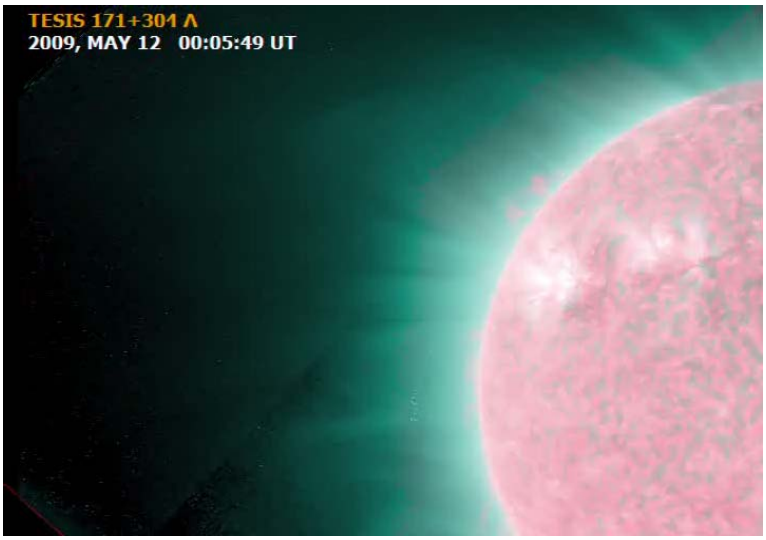

Fig. 5. U-shaped magnetic structure erupted from the Sun on May 12, 2009

TESIS observations of the solar eclipse of July 22, 2009

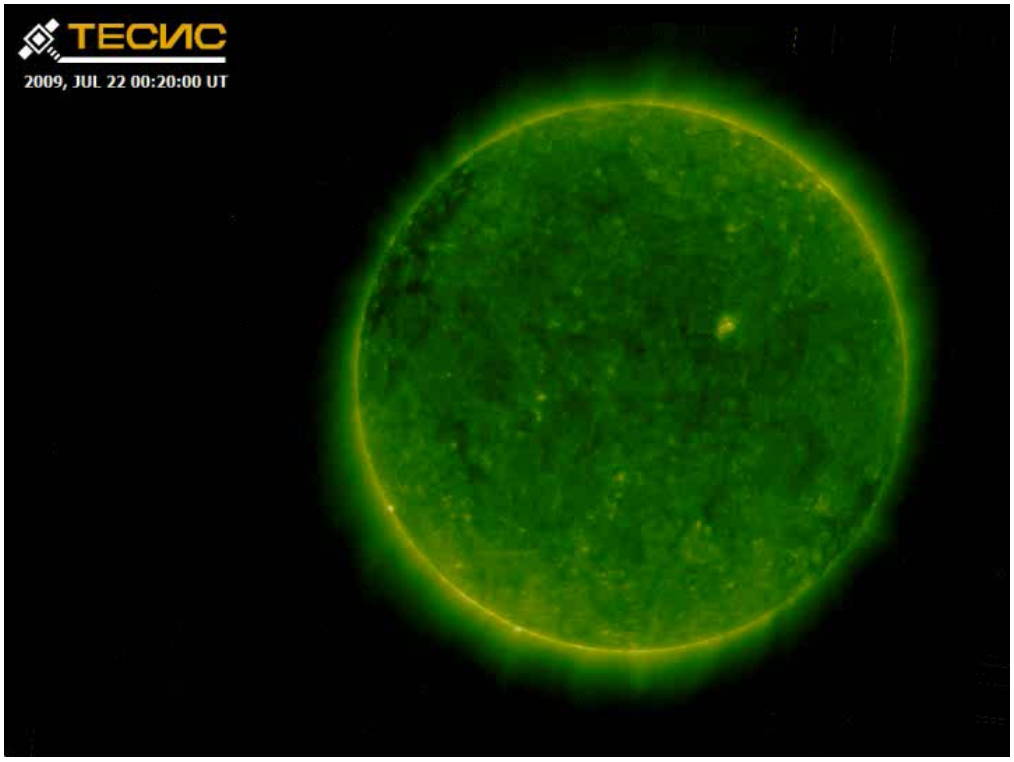

TESIS observations of solar flares

B1.8 flare was recorded by TESIS on March 26, 2009 in the Fe IX 171 Å, Fe 132 Å and 8.42 Å Mg XII spectral bands (Fig. 6).
Using the methods of multi-wavelength diagnostics developed earlier at the Lebedev Institute, it was shown for the first time that the coronal plasma can be heated to high temperature above 10 MK even during the period of low solar activity.

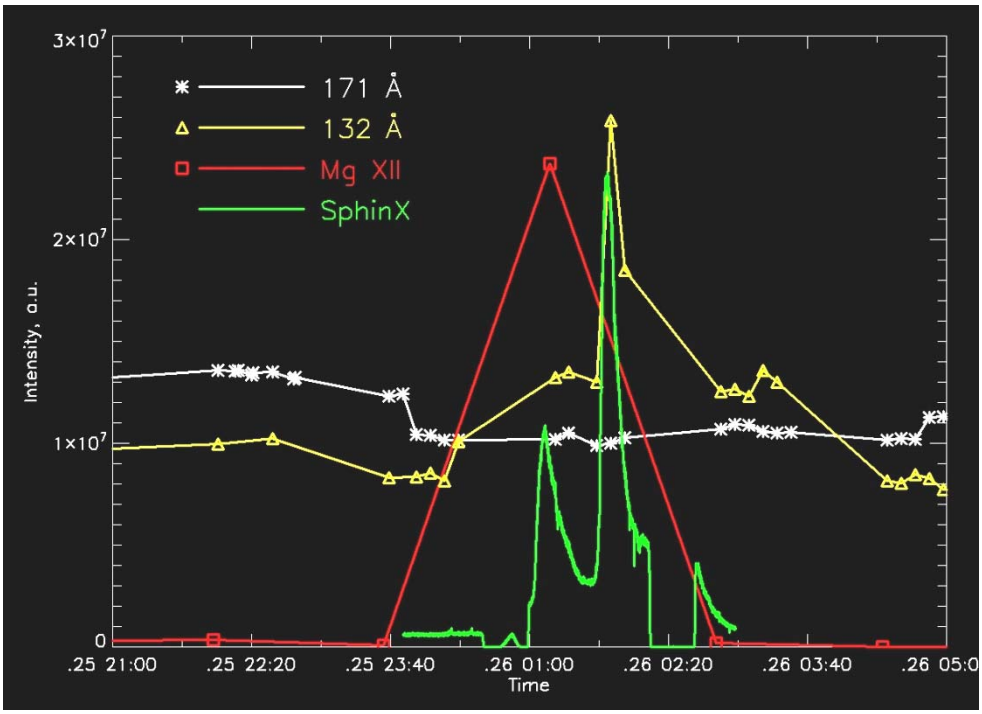

Fig. 6. The flare of March 26, 2009 observed by TESIS in the EUV (171, 132 A) and Mg XII (8.42 A) bands and SphinX in X-rays (0,5-15 KeV).

TESIS observations of non-flaring hot solar plasma

TESIS discovered that hot plasma with temperature above 10 MK can appear in the solar corona even in the absence of flares. Fig. 7 shows a comparison of images in the Mg XII 8.42 A band (T~5-15 MK) and in the Fe IX 171 A band (0.8-1.2 MK).

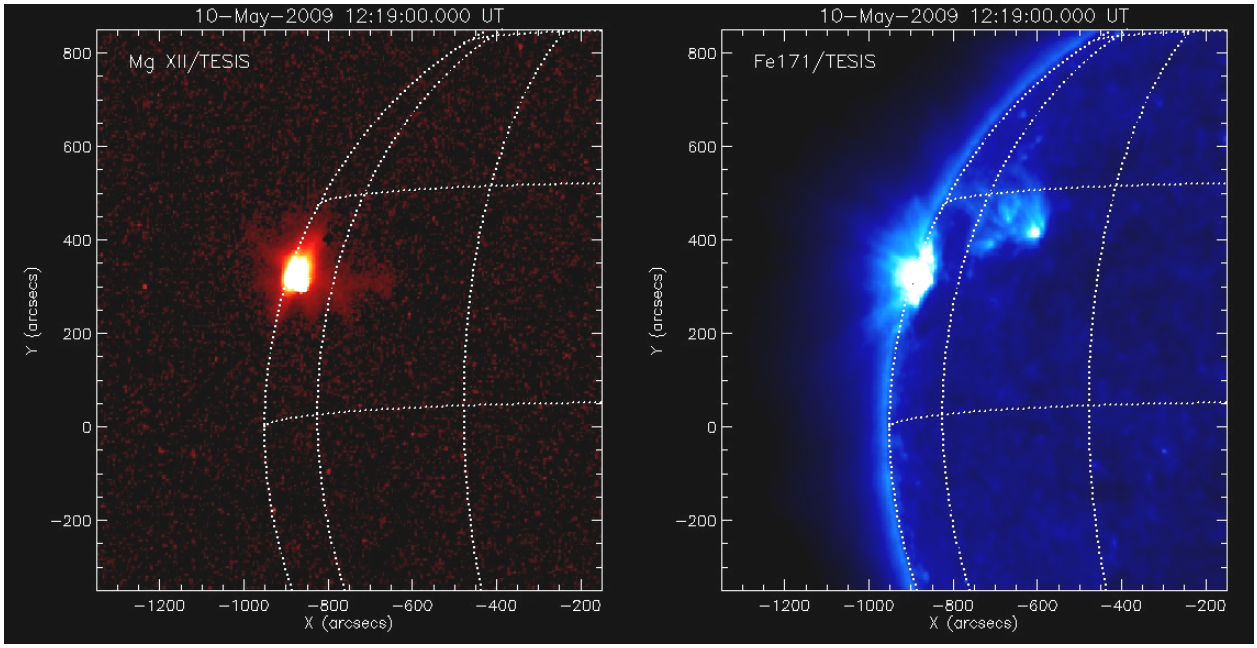

Fig. 7. Images of hot solar plasma in the TESIS Mg XII 8.42 A band and in the Fe IX 171 A band obtained on May 10, 2009 in absence of a flare

TESIS studies of X-ray bright points

X-ray bright points were studied by TESIS in Fe IX 171 A band using high cadence imaging with temporal resolution of 4-10 s. Several types of brightness oscillations with minute periods have been revealed. It was found that for some neighboring points brightness variations were synchronized

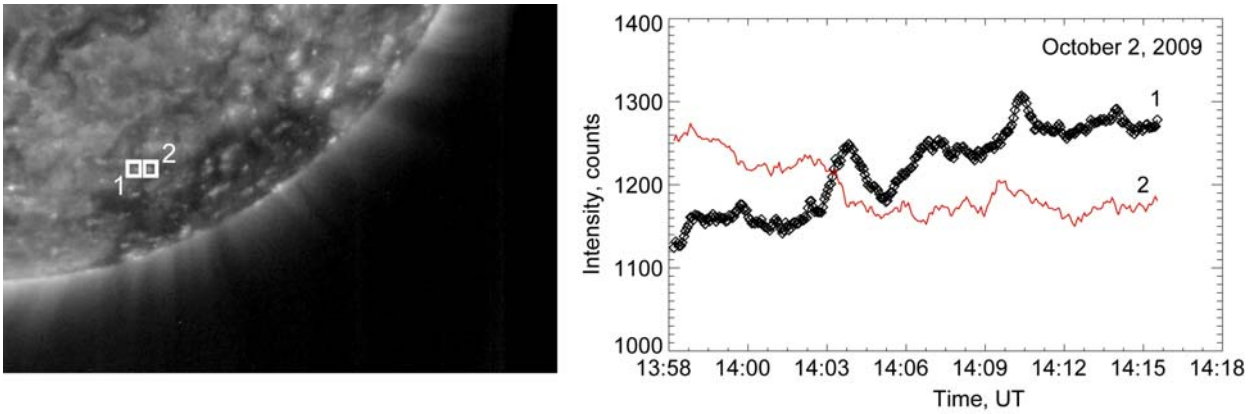

Fig. 8. Light curves of two closely located bright points measured in 171 A with temporal resolution of 10 s.

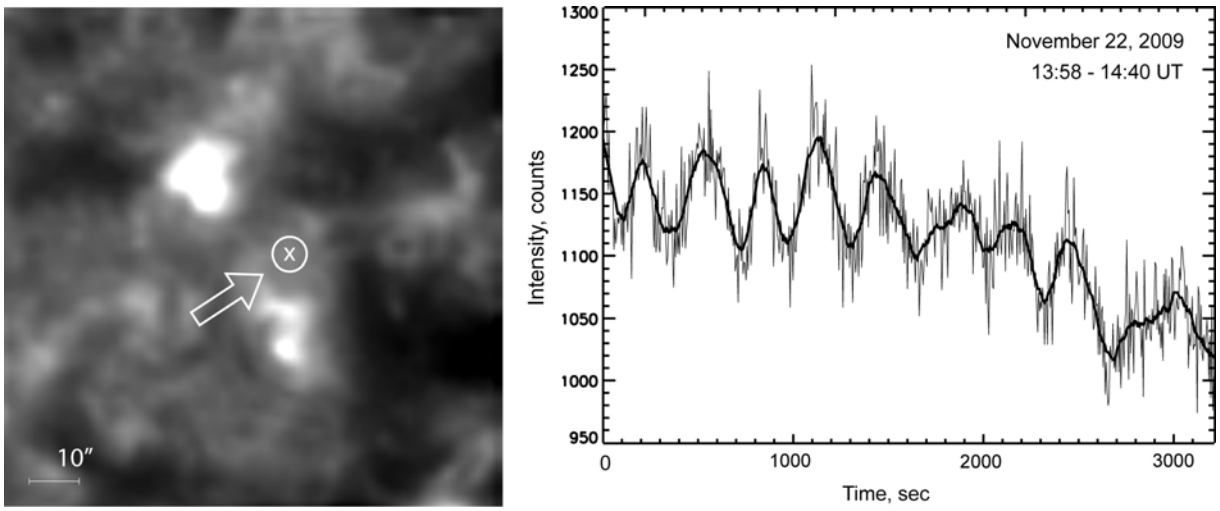

Fig. 9. Light curve of compact region between two bright points measured in 171 Å with 4 s cadence.
Oscillations have a period of 250 s.

II. Study of hot solar corona in the SPIRIT/CORONAS-F experiment

1. Study of hot (5-20 MK) plasma structures observed by SPIRIT in the Mg XII 8.42 A monochromatic solar images

SPIRIT (2001-2005) discovered a new class of hot plasma objects in the solar corona seen in monochromatic Mg XII 8.42 A images characterized by various sizes from 6" through 0.3 solar radius and lifetimes from several minutes to several days -"spiders", clouds, hot x-ray bright points (Fig. 10).
The spiders are shown to be a post-eruptive phenomena, characterized by quasi-static magnetic configurations with high temperature gradients (T=5-20 MK) and a coronal density of order 2·109 cm3 (with slow gradient) and B (of order 10 G).

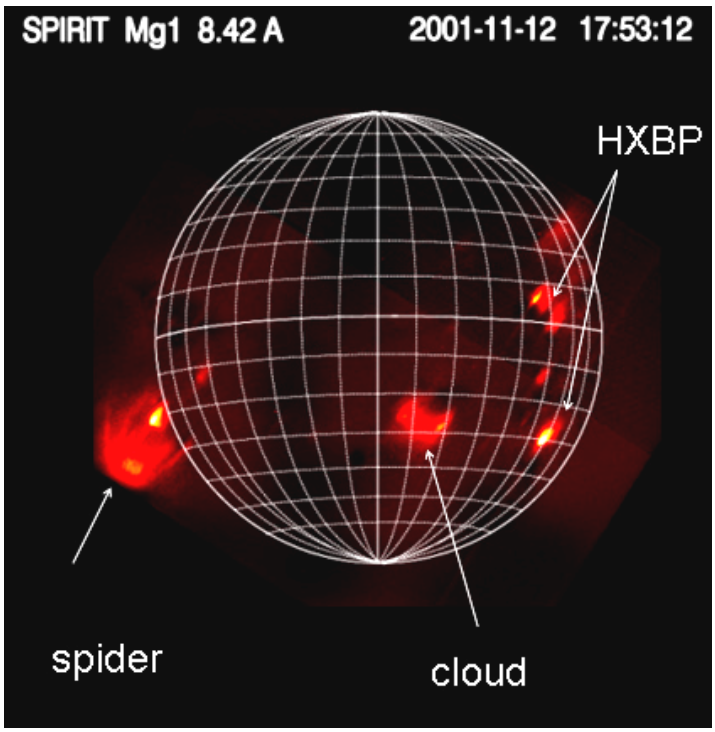

Fig.10. "Spider", cloud and hot X-ray bright points (HXBP)

2. Modeling of “spiders” plasma

A new model of hot plasma structures was proposed based on the exact analytical generalization of well known Chandrasekhar-Prendergast (Ap.J.1956) model.
This model (Fig. 11) uses a sequence of magnetic toroids stabilized within a spherical cover by an external potential magnetic field. The generalized solution allows new possibilities for explanation of dissipative flare-like processes, provides a natural description of their specific features and suggests the approach to the coronal plasma heating alternative to that for impulsive flares.
(A. Solov’ev et al. 2010)

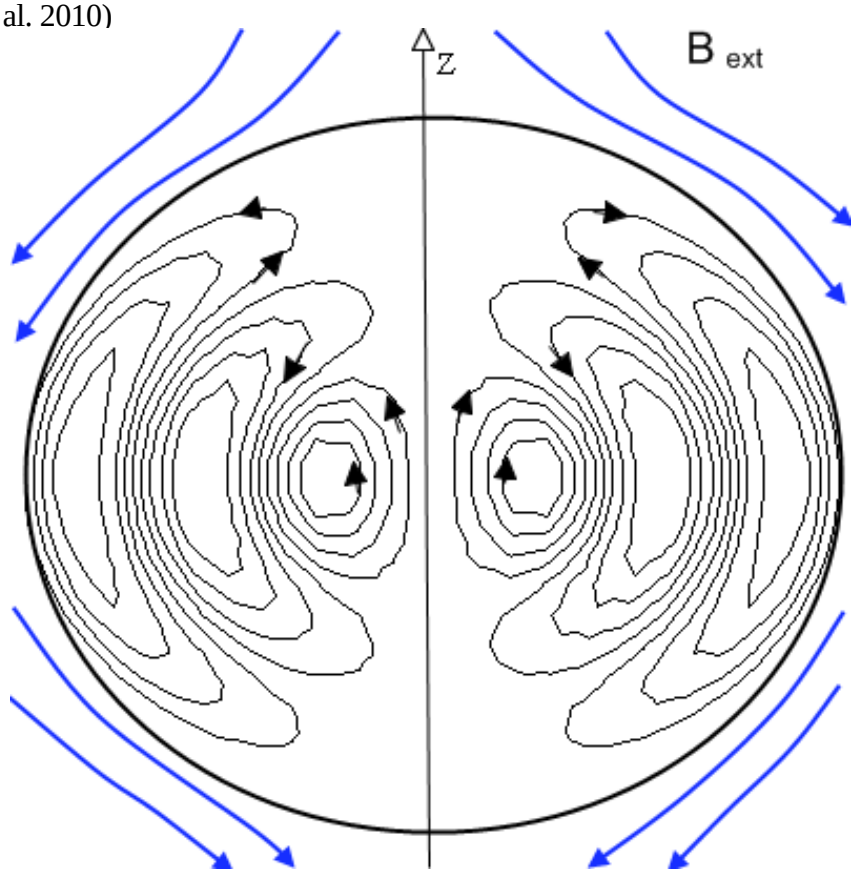

Fig.11

3. Diagnostics of DEM in AR coronal loops and flares using SPIRIT EUV spectral images

The method of determination of the Differential Emission Measure (DEM) function of the solar plasma developed at the Lebedev Institute uses SPIRIT monochromatic solar spectroheliograms (Fig. 12).
DEM function is retrieved from spectral line intensities using the Bayesian iterative algorithm. For more than 9 lines the method provides agreement with experimental data within 20%.

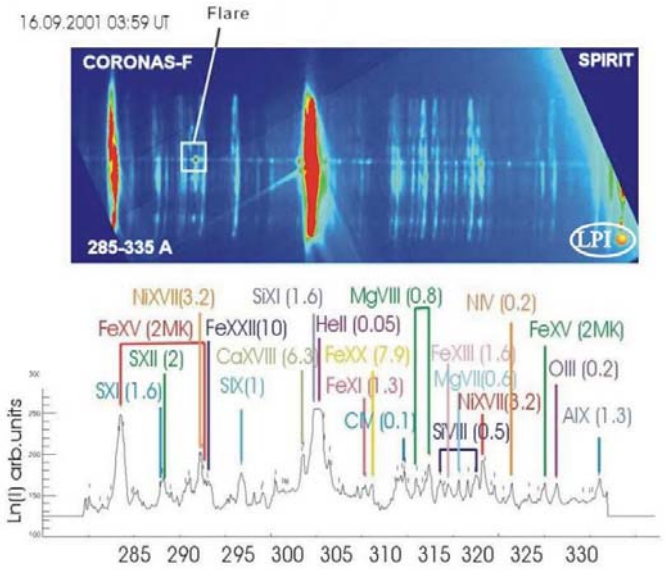

Fig. 12. SPIRIT spectroheliogramms in the 280-330 A band

Recent analysis of DEM for various plasma structures shows that hot plasma with the temperature in the range 8-15 MK may exist in the absence of flares (Fig. 13).
(Shestov et al. 2010)

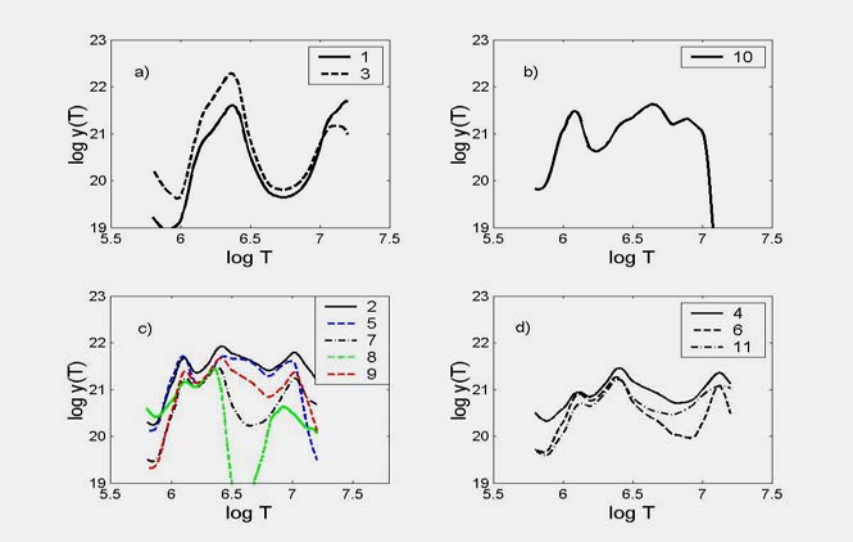

Fig. 13. DEM functions of non-flaring ARs

4. Study of hot plasma structures

Observations of hot plasma structures X-ray emission provide a knowledge of both processes: storage and release of energy. Due to the fact that the heating takes place as a result of recurrent energy release at the same area, hot plasma structures are the “markers” of energy release site (reconnection sites).

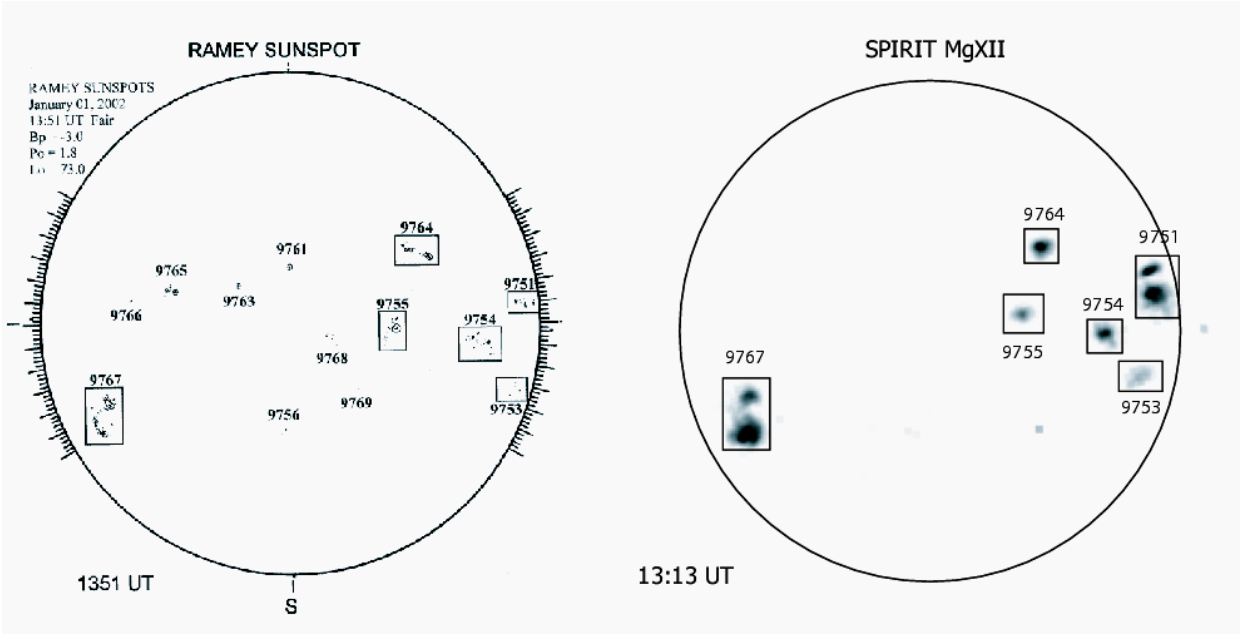

Fig. 14. Position of HXBPs with respect to active regions

The X-ray sources observed by SPIRIT are characterized by complex topology rather than the magnetic field strength, since they are seen only in active region loop systems comprising of more than two spots. (Fig. 14)

(Bogachev et al. 2010)

5. Study of the solar EUV corona at 1-3 Rsun

The structure and dynamics of the solar EUV corona at the distances 1-3 Rsun was studied using the SPIRIT images in 175 and 304 A obtained in June and December 2002 (Movie).

At the distances up to 1.5 Rsun the brightness in the coronal 175 A band correlates with closed loop structures. Above this height it concentrates in rays matched with elements of streamers in white light (LASCO).

In the He II 304 A band the spatial distribution of coronal brightness is caused by resonant scattering of radiation of the underlying solar surface (Fig. 15).

(V. Slemzin,S.Kuzin et al. ANGEO, 26, 2008).

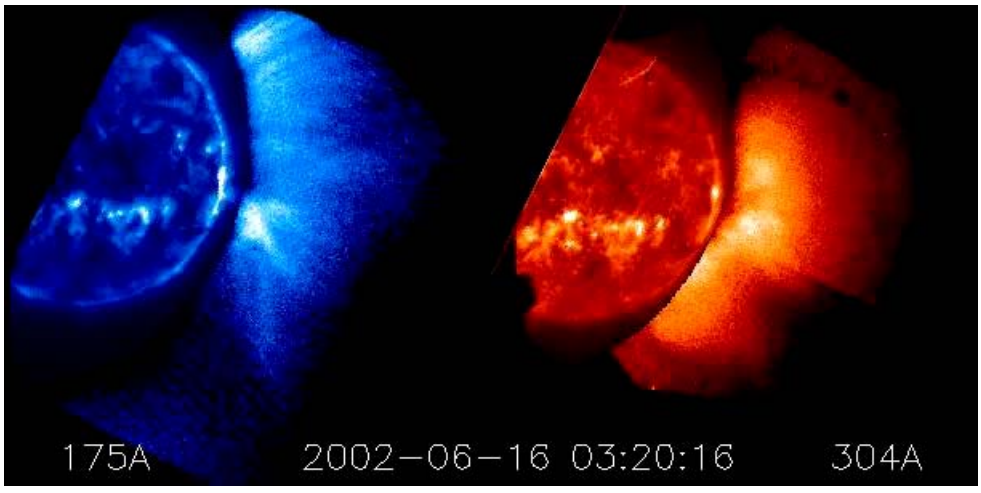

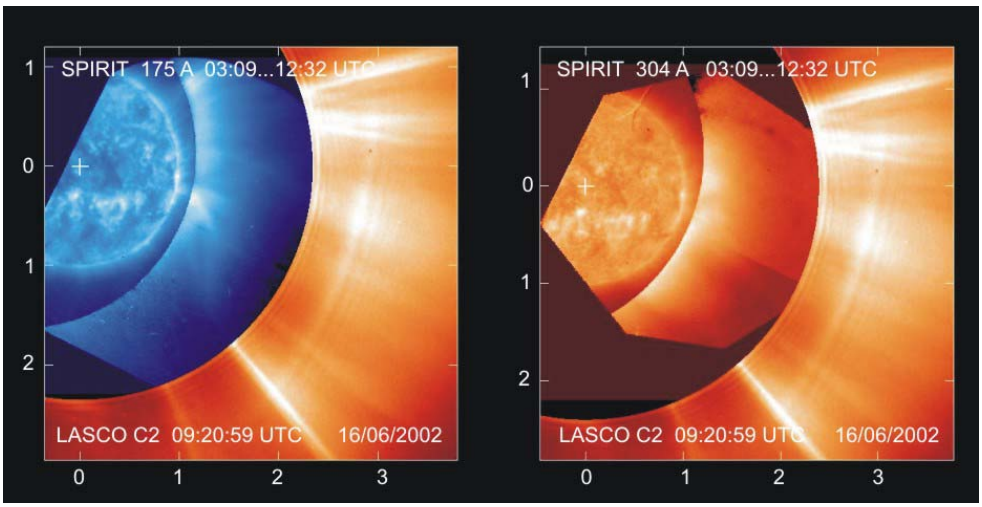

Fig. 15. Comparison of the corona in EUV (SPIRIT) and white light (LASCO) bands

Summary

The main results obtained by the Laboratory of X-ray Solar Astronomy of P.N. Lebedev Physical Institute during 2008-2009 are:

- A new TESIS telescope/spectroheliograph was successfully launched aboard the CORONAS-Photon satellite in January 2009.
- During the 11 months of operation in 2009 TESIS have obtained more than 500 Gb of images, which contain unique information about solar activity in deep minimum period.
- Due to improved spatial and temporal resolution TESIS obtained a detailed information about the solar corona, including solar flares, eruption of giant prominences, bright x-ray points and other active processes.
- It was shown that hot solar plasma may appear not only during flares but also in quiet Sun areas in the form of hot x-ray bright points.
- Studies of the solar EUV corona at 1-3 Rsun using the SPIRIT data in 175 and 304 A bands have shown that it has specific structure associated with active regions at the solar disk which correlate with white light structure of streamers.
- The methods based on multi-temperature model were applied to spectroscopic diagnostics of hot solar plasma structures with T=5-20 MK discovered in previous SPIRIT experiment. In particular, it was found that large-scale structures (“spiders”) have typical densities of electrons of 2.109 cm-3 which is two orders less than in solar flare.
- It was also shown that these X-ray sources are characterized by complex topology rather than by the strength of the magnetic field since they associated only with active region loop systems comprising of more than two spots.
- A theoretical description of the spider phenomena is proposed. This model presents a sequence of magnetic toroidal configurations stabilized within a spherical cover by an external potential magnetic field. The model gives a realistic picture of observable phenomena allowing new possibilities for the generation of dissipative flare-like processes in solar corona.